Chapter 8

Numerical Methods

ABSTRACT
In classical investigations on non-Newtonian fluid problems, the non-Newtonian mechanism is only taken into account in momentum equation while energy equation taken same form as in Newtonian fluid. In this chapter, we present some numerical studies for transport characteristics and mechanism of non-Newtonian fluids. Several modified Fourier's heat conduction laws and modified Darcy's diffusion laws are proposed for power law non-Newtonian fluids and fractional Maxwell viscoelastic fluid subject to various physical regimes and the fractional convection diffusion in a comb-like structure with Cattaneo–Christov flux. The governing equations are formulated and numerical solutions are obtained, the influences of pertinent parameters on the velocity, temperature, and concentration fields transport characteristics are analyzed and discussed in detail.

8.1 REVIEW OF NUMERICAL METHODS

Numerical methods have become important means for solving nonlinear differential equations of fluid problems. Many complex problems that could be solved in the past by analysis methods now can be resolved quickly by numerical simulations. In this chapter, we present some works for solving numerically the heat transfer and fluid flow problems arising in power law non-Newtonian fluids or fractional viscoelastic fluids subject to various nonclassical conditions. In the following, we first review some numerical methods used in this book (Ames, 1977; Ciarlet, 1978; Fletcher, 1988; Samarskii, 2001; Smith, 1985).

8.1.1 Numerical Methods for Linear System of Equations

Linear systems of equations are associated with many problems in engineering and science, as well as with applications of mathematics to the social sciences

Mathematics in Science and Engineering. http://dx.doi.org/10.1016/B978-0-12-811753-8.00008-6

and the quantitative study of business and economic problems. Consider to solve the linear system $AX = B$:

$$A = \begin{bmatrix} a_{11} & a_{12} & \dots & a_{1n} \\ a_{21} & a_{22} & \dots & a_{2n} \\ a_{31} & a_{32} & \dots & a_{3n} \\ \dots & \dots & \dots & \dots \\ a_{n1} & a_{n2} & \dots & a_{nn} \end{bmatrix}, \quad X = \begin{bmatrix} x_1 \\ x_2 \\ x_3 \\ \vdots \\ x_n \end{bmatrix}, \quad B = \begin{bmatrix} b_1 \\ b_2 \\ b_3 \\ \vdots \\ b_n \end{bmatrix}$$

where A is an $n \times n$ matrix, X and B are both $n \times 1$ column vector, respectively. The determinant of A denoted by det$A$ or $|A|$, which provides existence and uniqueness results for linear systems when $|A| \neq 0$.

There are many numerical methods for solving linear systems of equations, such as Gaussian elimination, pivoting strategies, matrix inversion, matrix factorization, iterative techniques, etc. As an example, we present matrix factorization used in this book to illustrate applications, and one can find other methods in any textbook of numerical analysis.

Gaussian elimination is the principal tool in the direct solution of linear systems of equations. From study on the Gaussian elimination element method for $Ax = b$, we know that the essence of the eliminating process is to perform $\frac{n}{2}(n-1)$ times sequential of the elementary row transformation on coefficient matrix A to transform the matrix into an upper triangular matrix. If Gaussian elimination can be performed on the linear system $AX = B$ without row interchanges, then the matrix A can be factored into the product of a lower-triangular matrix L and an upper-triangular matrix U. The factorization is particularly useful when it has the form $A = LU$, where L is lower triangular and U is upper triangular, defined as follows:

$$L = \begin{bmatrix} 1 & & & & \\ l_{21} & 1 & & & \\ l_{31} & l_{32} & 1 & & \\ \dots & \dots & \dots & & \\ l_{n1} & l_{n2} & \dots & \dots & l_{nn-1}\ 1 \end{bmatrix} \text{ and } U = \begin{bmatrix} u_{11} & u_{12} & u_{13} & \dots & u_{1n} \\ & u_{22} & u_{23} & \dots & u_{2n} \\ & & u_{33} & \dots & u_{3n} \\ & & & \dots & \dots \\ & & & & u_{nn} \end{bmatrix},$$

then

$$a_{ij} = \sum_{k=1}^{n} l_{ik}u_{kj} = \begin{cases} \sum_{k=1}^{i-1} l_{ik}u_{kj} + u_{ij} & j \geq i \\ \sum_{k=1}^{j-1} l_{ik}u_{kj} + l_{ij}u_{jj} & j < i \end{cases} \qquad i,j = 1,2,\dots,n \tag{8.1}$$

For $i = 1$, $a_{1j} = u_{1j}$, $j = 1, 2, \dots, n$; and for $j = 1$, $a_{i1} = l_{i1}u_{11}$, $i = 2, 3, \dots, n$

We obtain

$$u_{1j} = a_{1j}, \quad j = 1, 2, \ldots, n, \tag{8.2}$$

$$l_{i1} = a_{i1}/u_{11}, \quad i = 2, 3, \ldots, n, \tag{8.3}$$

$$u_{ij} = a_{ij} - \sum_{k=1}^{i-1} l_{ik}u_{kj}, \quad i \le j, \tag{8.4}$$

$$l_{ij} = \left(a_{ij} - \sum_{k=1}^{j-1} l_{ik}u_{kj}\right) \Big/ u_{jj}, \quad i > j, \tag{8.5}$$

The factorization of the matrix can be divided into two kinds: the present lower triangular matrix is the unit of the triangular matrix, known as the Doolittle decomposition; and when the unit is on the upper triangular matrix it is called Crout decomposition.

8.1.2 Numerical Methods for Ordinary/Partial Differential Equations

Numerical methods for differential equations are used to find numerical approximations to the solutions of ordinary/partial differential equation (ODE/PDE), they are also known as "numerical integration." There are many numerical methods for solving ordinary/partial differential equations. Here, we only present three methods used in this book to illustrate the applications.

8.1.2.1 Runge–Kutta Method

Runge–Kutta method is an effective and widely used method for solving the initial-value problems of differential equations. Runge–Kutta method can be used to construct high order accurate numerical method by functions' self without needing the high order derivatives of functions.

Consider first-order initial-value problem:

$$\begin{cases} y' = f(x,y), \ \ a \le x \le b \\ y(a) = y_0 \end{cases} \tag{8.6}$$

To derive the Runge–Kutta method, we divide the interval $[a,b]$ into N subintervals as $[x_n,x_{n+1}]$ $(n = 0,\ 1,\ldots\ N-1)$, integrating $y' = f(x,y)$ over $[x_n,x_{n+1}]$ and utilizing the mean value theorem for integrals, obtain

$$y(x_{n+1}) - y(x_n) = \int_{x_n}^{x_{n+1}} f(x, y(x))dx = hf(\xi, y(\xi)) \tag{8.7}$$

where $h = x_{n+1} - x_n$, $\xi \in [x_n, x_{n+1}]$, i.e.,

$$y(x_{n+1}) = y(x_n) + hf(\xi, y(\xi)) \tag{8.8}$$

If we approximate $f(\xi,y(\xi))$ by the linear combination values $f(\xi_1,y(\xi_1))$, $f(\xi_2,y(\xi_2))$, …, $f(\xi_m,y(\xi_m))$ of $f(x,y(x))$ on the interval $[x_n,x_{n+1}]$, then arrive at the general form of Runge− Kutta method:

$$y_{n+1} = y_n + h\sum_{i=1}^{m} c_i f(\xi_i, y(\xi_i)) \tag{8.9}$$

Choose different values of parameters m, c_i and ξ_i, we can obtain different form computation formula of Runge−Kutta; one can obtain higher order Runge−Kutta computation formula by choosing suitable values of parameters. The most widely used Runge−Kutta formula is

$$\begin{cases} y_{n+1} = y_n + \dfrac{1}{6}(K_1 + 2K_2 + 2K_3 + K_4) \\ K_1 = hf(x_n, y_n) \\ K_2 = hf\left(x_n + \dfrac{1}{2}h, y_n + \dfrac{1}{2}K_1\right) \\ K_3 = hf\left(x_n + \dfrac{1}{2}h, y_n + \dfrac{1}{2}K_2\right) \\ K_4 = hf(x_n + h, y_n + K_3) \end{cases} \tag{8.10}$$

It needs four values of function in each step iteration, also called four-order Runge−Kutta method.

In the following, we consider the higher order differential equations, for example,

$$\begin{cases} y'' = f(x, y, y') \\ y(x_0) = y_0, y'(x_0) = u_0 \end{cases}. \tag{8.11}$$

Let $y' = u$, Eq. (8.11) is transformed into the system of first-order differential equations:

$$\begin{cases} y' = u \\ u' = f(x, y, u) \\ y(x_0) = y_0, u(x_0) = u_0 \end{cases}. \tag{8.12}$$

Then, we can solve the initial values for the system of first-order differential equations, and the computation formula is written as following:

$$\begin{cases} y_{n+1} = y_n + \dfrac{1}{6}(m_1 + 2m_2 + 2m_3 + m_4) \\ u_{n+1} = u_n + \dfrac{1}{6}(k_1 + 2k_2 + 2k_3 + k_4) \end{cases}. \tag{8.13}$$

with

$$\begin{cases} m_1 = hu_n, \\ m_2 = h\left(u_n + \frac{1}{2}k_1\right), \\ m_3 = h\left(u_n + \frac{1}{2}k_2\right), \\ m_4 = h(u_n + k_3). \end{cases} \quad \begin{cases} k_1 = hf(x_n, y_n, u_n), \\ k_2 = hf\left(x_n + \frac{1}{2}h, y_n + \frac{1}{2}m_1, u_n + \frac{1}{2}k_1\right), \\ k_3 = hf\left(x_n + \frac{1}{2}h, y_n + \frac{1}{2}m_2, u_n + \frac{1}{2}k_2\right), \\ k_4 = hf(x_n + h, y_n + m_3, u_n + k_3). \end{cases} \tag{8.14}$$

8.1.2.2 Shooting Method

Shooting method is a commonly used method for solving nonlinear boundary-value problem of differential equation, which is a method by transforming the boundary-value problem into an initial-value problem. The basic idea of shooting method is to transform the boundary-value problem of differential equations into initial-value problem with initial parameter to be established. This can be performed as follows: firstly, to give an initial value of parameter, one can solve the initial-value problem in terms of the Runge−Kutta method; secondly, to adjust the given initial value of parameter, such that the solution of initial value will satisfy the boundary conditions. For example, we consider the shooting technique for the nonlinear second-order boundary-value problem:

$$\begin{cases} y'' = f(x, y, y'), \quad a < x < b \\ y(a) = \alpha, y(b) = \beta \end{cases}. \tag{8.15}$$

Firstly, to give an initial value, by supposing $y'(a) = S$, we obtain an initial-value problem of differential equation with initial parameter of S:

$$\begin{cases} y'' = f(x, y, y'), \quad a \le x \le b \\ y(a) = \alpha, y'(a) = S \end{cases}. \tag{8.16}$$

Eq. (8.16) can be solved by using Runge−Kutta method, denoting the solution by $y(x; S)$, if the solution satisfies the boundary conditions, i.e., $y(b; S) = \beta$, then $y(x; S)$ is the solution of boundary-value problem (Eq. 8.15). If this is not true, then we approximate the solution to the boundary-value problem by using the solutions to a sequence of initial-value problems involving a parameter S, we do this by choosing the parameters $S = S_k$ and then solve the sequence of initial-value problems as

$$\begin{cases} y'' = f(x, y, y') \quad a \le x \le b \\ y(a) = \alpha, y'(a) = S_k, \quad k = 0, 1, 2, \cdots \end{cases}, \tag{8.17}$$

in a manner to ensure that

$$\lim_{k \to \infty} y(b; S_k) = \beta, \tag{8.18}$$

where $y(x;S_k)$ is the solution of initial-value problem Eq. (8.17).

This technique is called a "shooting" method, by analogy to the procedure of firing objects at a stationary target. We start with a parameter S_0 that determines the initial elevation at which the object is fired from the point (a, α) and along the curve described by the solution to the initial-value problem:

$$\begin{cases} y'' = f(x, y, y') & a \le x \le b \\ y(a) = \alpha, y'(a) = S_0 \end{cases}. \tag{8.19}$$

Denote the solution of Eq. (8.19) by $y(x;S_0)$. If $y(x; S_0)$ satisfies

$$y(b; S_0) = \beta \quad \text{or} \quad |y(b; S_0) - \beta| < \varepsilon \ . \tag{8.20}$$

Then we can take $y(x; S_0)$ as the solution of boundary-value problem Eq. (8.15). Otherwise, if $y(b; S_0)$ is not sufficiently close to β, then we correct our approximation by choosing elevations y_1,y_2 and so on, until $y(b; S_k)$ is sufficiently close to "hitting" β, such that

$$|y(b; S_k) - \beta| < \varepsilon.$$

where ε is a small tolerance constant, usually $\varepsilon = 10^{-6}$.

To determine the parameters S_k, we need to determine the parameter S, such that

$$\varphi(S) = y(b; S) - \beta = 0. \tag{8.21}$$

Eq. (8.21) can be solved by Newtonian iteration method, to generate the sequence $\{S_k\}$, here only one initial approximation S_0 is needed, i.e.,

$$S_{k+1} = S_k - \frac{\varphi(S_k)}{\varphi'(S_k)} = S_k - \frac{y(b; S_k) - \beta}{\partial y(b; S_k)/\partial S} \quad k = 0, 1, 2\ldots \tag{8.22}$$

Until $\varphi(S_k) = 0$. We can stop the iteration processes by $|\varphi(S_k)| \le \varepsilon$ with a given tolerance of parameter ε.

For higher order differential equations, or equations solving boundary-value problems, multiple shooting method is needed. Multiple shooting method is much more complex than a single-parameter shooting method. The method divides the interval over which a solution is sought into several smaller intervals, solves an initial value problem in each of the smaller intervals, and imposes additional matching conditions to form a solution on the whole interval. The method constitutes a significant improvement in distribution of nonlinearity and numerical stability over single shooting methods. Multiple shooting method with "smoothness condition" not only can be used to solve boundary-value problem, but also can be used to calculate multidimensional solutions of nonlinear elliptic boundary-value problems.

8.1.2.3 Control Volume Method

The control volume method is also known as the finite volume method. The basic ideas and methods are: the calculation area is divided into a series of unoverlapping control volume, and each grid point is contained in a control

volume, the differential equation to be solved for each control volume integral, then a set of discrete equations is obtained. The unknown is the dependent variable on the grid points. In order to obtain the integral of the control volume, it is necessary to assume the variation law of the value between the grid points. From the choice of the integral region, the control volume method is a subregion method in the weighted residual method. In short, the subregion method belongs to the basic method of finite volume class. The basic idea of the control volume method is easy to understand, and can get a direct physical interpretation. The physical meaning of the discrete equation is the conservation principle of the finite size of the control volume, which is the same as that of the differential equation. Control volume method is derived from the discrete equations, the integral conservation of the variables and the arbitrary set of control volume are met, so the entire computational area, naturally also be met.

There are some discrete methods, such as finite difference method, where only when the grid is extremely fine, the discrete equations can satisfy the integral conservation. The control volume method, even in the case of rough grid, also shows the exact integral conservation. In the case of the discrete method, the control volume method can be regarded as the intermediate between the finite element method and the finite difference method. The finite element method must assume the variation of the value between the grid points (both interpolation function), and the finite element method is used as the approximate solution. The finite difference method can only consider the numerical value on the grid point without considering the variation of the value between the grid points. The control volume method is only for the numerical value of the nodes, which is similar to the finite difference method. But the control volume method must assume the distribution of the points in the grid, which is similar to the finite element method. In the control volume method, the interpolation function is only used to calculate the integral of the control volume, and the interpolation function is not considered.

The control volume method is the most widely used numerical discretization method in computational fluid dynamics and computational heat transfer. It usually consists of five parts as: (1) grid generation; (2) the discretization of the convection term; (3) discretization of boundary conditions; (4) the coupling of pressure and velocity; and (5) the solution of the discrete equation.

8.1.3 Numerical Methods for Fractional Differential Equations

In recent years, fractional differential equations and its application have gotten extensive attention. The main reason is due to the rapid development of the theory of fractional calculus itself and is widely used in mathematics, physics, chemistry, biology, medicine, mechanics, control theory, signal and image processing, environmental science, financial, and other various disciplines.

Fractional order differential equations are generalized and noninteger order differential equations, which can be obtained in time and space with a power law memory kernel of the nonlocal relationships; they provide a powerful tool to describing the memory of different substances and the nature of the inheritance. All of these studies have a clear physical background, which open up a new field of scientific research, including a new theoretical analysis and numerical methods for fractional order dynamical systems.

The numerical calculation of the fractional differential equations has been successfully applied in many research fields. A list of the key references is given in Refs. (Chen et al., 2010; Liu et al., 2009, 2013a, 2015).

8.2 HEAT TRANSFER OF POWER LAW FLUID IN A TUBE WITH DIFFERENT FLUX MODELS

In this section, we present numerical research on forced convection heat transfer of power law non-Newtonian fluids in a circle duct with different thermal conductivity models. A hydrodynamic entrance length is neglected, which allows establishing a fully developed flow. Four thermal conductivity models are considered: constant thermal conductivity model, linear thermal conductivity varying with temperature, thermal conductivity varying as a function of velocity gradient, and thermal conductivity varying as a function of temperature gradient. The energy equation is solved by using an LU decomposition coupled with control volume technique–based finite difference method. Results are compared and the physical characteristics are also analyzed.

8.2.1 Background of the Problem

For half a century, considerable attention has been paid to predict the transport behavior of non-Newtonian fluid flows. Many constitutive models have been proposed. Among these models, the Ostwaald–de Waele fluid model, i.e., the so-called power law model (Acrivos et al., 1960; Schowalter, 1960), gained much acceptance (Abel et al., 2009; Arunachalam and Rajappa, 1978; Chaim, 1998; Crosan and Pop, 2001; Gorla et al., 1992; Hady, 1995; Hossain et al., 2000a,b; Hossain et al., 2001; Howell et al., 1997; Kays, 1966; Kumari et al., 1997; Rao et al., 1999; Salem, 2007; Wang, 1995a,b). For an incompressible power law non-Newtonian fluid in cylindrical coordinates, its shear stress is characterized as $\tau = K\left(\left|\frac{\partial u}{\partial r}\right|^{n-1}\frac{\partial u}{\partial r}\right)$ and the kinematic viscosity is $\nu = \gamma\left|\frac{\partial u}{\partial r}\right|^{n-1}$ (K and $\gamma = K/\rho$ are positive constants). The case $n = 1$ corresponds to a Newtonian fluid, $0 < n < 1$ is pseudoplastic non-Newtonian fluids while $n > 1$ describes dilatant fluids.

In classical research works for power law non-Newtonian fluids, the influence of power law kinematic viscosity is only considered in momentum transport of velocity field, which has been ignored in energy transfer of temperature field, i.e., the thermal conductivity is treated the same as in Newtonian fluid. Obviously, this is inconsistent with the fact that the changing viscosity should affect both the velocity field and the temperature as well. Some researchers have paid attention to this inconsistency.

Pop et al. (1991) and Pop (1993) had suggested that the thermal conductivity of power law non-Newtonian fluids is a power law dependence on the velocity gradient. Ece and Buyuk (2002) performed a boundary-layer analysis for the free convection flow over a vertical flat plate embedded in a porous medium saturated by a power law non-Newtonian fluid and gave the similarity solution to the classical boundary-layer equations. A modified Fourier's law of heat conduction for power law fluids is proposed. Recently, Zheng et al. (2006', 2008), based on the assumption that the thermal diffusion in temperature field is similar to the viscosity diffusion in velocity field for power law viscosity, proposed a modified Fourier's heat conduction law for power law non-Newtonian fluid in which a constitutive model for thermal conductivity is written as

$$k(T) = \begin{cases} k_0 \left|\dfrac{\partial T}{\partial y}\right|^{,n-1} & \dfrac{\partial T}{\partial y} \neq 0 \\ k_0, & \dfrac{\partial T}{\partial y} = 0 \end{cases},$$

where k_0 is a positive constant. Li et al. (2010a,b,c) presented an investigation on steady conduction of heat and diffusion of power law fluids in a circular duct. In this chapter, we focus our attention on studying the following four types of thermal conductivity constitutive models:

1. Thermal conductivity is a constant.
2. Thermal conductivity is a linear function of temperature.
3. Thermal conductivity is a power law function of velocity gradient.
4. Thermal conductivity is a power law function of temperature gradient (proposed by Zheng).

8.2.2 Formulation of the Problems and Numerical Algorithms

Cases (1) and (2) The thermal conductivity is assumed a constant or a linear function of temperature.

We consider first the Cases (1) and (2), where the thermal conductivity is assumed a constant or a linear function of temperature and the duct wall is maintained at a constant temperature lower than the uniform temperature of the fluid at the entrance, and temperature is symmetrical about the axis. The fluid axial conduction, viscous dissipation, thermal energy sources, and

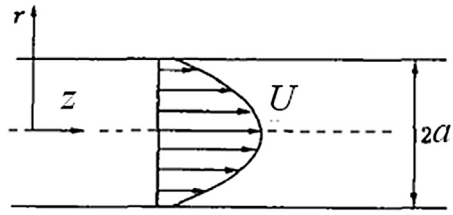

FIGURE 8.1 Physical description of the problem.

conduction in the direction of flow are negligible and laminar. Except for a few kinds of fluids, the hydrodynamic entrance region is much shorter than the thermal entrance one. The last assumption implies that a hydrodynamic entrance length is neglected, which allows establishing a fully developed flow. Take z and r to be coordinate axes parallel and perpendicular to the channel walls, and the axial component of the velocity field is given by (Barletta et al., 1997)

$$U(r) = \frac{3n+1}{n+1} U_m \left[1 - \left(\frac{r}{D_r} \right)^{(n+1)/n} \right] \tag{8.23}$$

U_m and D_r are the mean velocity and the radius of the duct and n is the power law index, the case $n = 1$ corresponds to a Newtonian fluid problem known as the Graetz problem (see Fig. 8.1).

The energy equation becomes:

$$\rho c_p U \frac{\partial T}{\partial z} = \frac{1}{r} \frac{\partial}{\partial r} \left(rk(T) \frac{\partial T}{\partial r} \right) \tag{8.24}$$

ρ and c_p are the density and fluid specific heat, respectively. $k(T)$ is the thermal conductivity and it is of the form $k(T) = k_0 \left[1 + \varepsilon \left(\frac{T - T_w}{T_{in} - T_w} \right) \right]$ with ε as a small parameter and k_0 is positive constant, and T_w and T_{in} are the wall and the inlet temperature, respectively. This research introduces the following dimensionless quantities:

Dimensionless temperature:

$$\Theta = \frac{T - T_w}{T_{in} - T_w}. \tag{8.25}$$

We assume $T_{in} > T_w$ to keep Θ positive.

Dimensionless radial coordinate:

$$R = \frac{r}{D_r} \tag{8.26}$$

Dimensionless velocity:

$$U^* = \frac{U}{4U_m}. \tag{8.27}$$

Dimensionless axial coordinate:

$$Z^* = \frac{k_0 z}{\rho c_p D_r^2 U_m}. \tag{8.28}$$

Applying the dimensionless quantities to the energy equation, the problem under consideration is transformed in dimensionless form as:

$$U^* \frac{\partial \Theta}{\partial Z^*} = \frac{1}{R} \frac{\partial}{\partial R} \left[R(1 + \varepsilon \Theta) \frac{\partial \Theta}{\partial R} \right]. \tag{8.29}$$

The dimensionless velocity profile becomes:

$$U^*(R) = \frac{3n+1}{n+1} \left[1 - R^{(n+1)/n} \right]. \tag{8.30}$$

The corresponding boundary conditions are:

$$\Theta|_{Z^*=0} = 1, \tag{8.31}$$

$$\Theta|_{R=1} = 0, \tag{8.32}$$

$$\left. \frac{\partial \Theta}{\partial R} \right|_{R=0} = 0. \tag{8.33}$$

In order to obtain the numerical solution, we transfer the problem Eqs. (8.29)–(8.33) to a system of algebraic equations. The calculation domain is divided into a few nonoverlapping control volumes each of which surrounds a grid point (shown in Fig. 8.2).

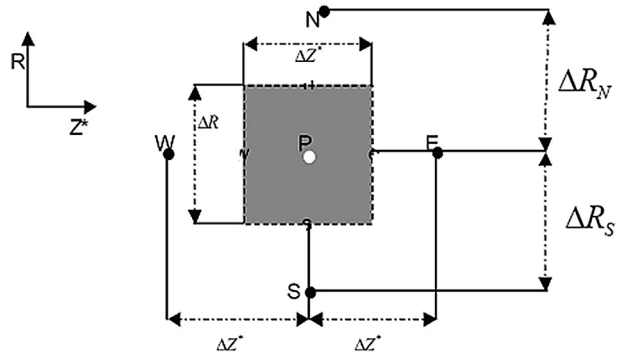

FIGURE 8.2 The sketch of control volume.

The energy Eq. (8.29) is integrated over each control volume. $\frac{\partial \Theta}{\partial R} < 0$, so we have as follows:

$$U^*(\Theta_P - \Theta_W)\frac{R_N^2 - R_S^2}{2} = \left[R_N(1+\varepsilon\Theta_P)\frac{\Theta_N - \Theta_P}{\Delta R_N} - R_S(1+\varepsilon\Theta_P)\frac{\Theta_P - \Theta_S}{\Delta R_S}\right]\Delta Z^* \tag{8.34}$$

Suppose that Θ_P is the P-th nonoverlapping control volume in R direction.

$$\varepsilon\Theta_P = \varepsilon[(\Theta_1 - \Theta_0) + (\Theta_2 - \Theta_1) + \cdots + (\Theta_P - \Theta_{P-1})] = \varepsilon\sum_1^P \Delta\Theta_Q \tag{8.35}$$

Assuming the calculation domain is divided into many control volumes that are small enough, we have

$$\lim_{\Delta\Theta_Q \to 0} \varepsilon \sum_1^P \Delta\Theta_Q = \varepsilon P \Delta\Theta = \varepsilon^* P \tag{8.36}$$

Eq. (8.34) can be written as:

$$U^*(\Theta_P - \Theta_W)\frac{R_N^2 - R_S^2}{2} = \left[R_N(1+\varepsilon^* P)\frac{\Theta_N - \Theta_P}{\Delta R_N} - R_S(1+\varepsilon^* P)\frac{\Theta_P - \Theta_S}{\Delta R_S}\right]\Delta Z^* \tag{8.37}$$

Rearranging the equation in the form as:

$$a_P\Theta_P = a_W\Theta_W + a_N\Theta_N + a_S\Theta_S \tag{8.38}$$

$$a_W = \frac{U^*\left(R_N^2 - R_S^2\right)}{2\Delta Z^*} \tag{8.39}$$

$$a_N = \frac{R_N(1+\varepsilon^* P)}{\Delta R_N} \tag{8.40}$$

$$a_S = \frac{R_S(1+\varepsilon^* P)}{\Delta R_S} \tag{8.41}$$

$$a_P = a_W + a_N + a_S \tag{8.42}$$

Eqs. (8.38)−(8.42) are a linear system of equations that can be solved by using LU decomposition method.

Case (3) The thermal conductivity is a power law function of velocity gradient.

With the same assumptions, we consider laminar power law flow with a neglecting entrance region in which the velocity profile develops. The energy equation is:

$$\rho c_p U\frac{\partial T}{\partial z} = \frac{1}{r}\frac{\partial}{\partial r}\left(rk(T)\frac{\partial T}{\partial r}\right) \tag{8.43}$$

The thermal conductivity is proposed as a form of $k(T) = k_0\left|\frac{\partial U}{\partial r}\right|^{n-1}$ with k_0 as positive constant.

Dimensionless temperature Θ, dimensionless radial coordinate R, and dimensionless velocity U^* are defined as Eqs. (8.25)–(8.27). The dimensionless axial coordinate is introduced as:

$$Z^* = \frac{k_0 U_m^{n-2} z}{\rho c_p D_r^{n+1}} \tag{8.44}$$

Applying the dimensionless quantities to the energy equation, the problem under consideration is given in dimensionless form as:

$$U^*\frac{\partial \Theta}{\partial Z^*} = \frac{1}{R}\frac{\partial}{\partial R}\left(R\left|\frac{\partial U^*}{\partial R}\right|^{n-1}\frac{\partial \Theta}{\partial R}\right) \tag{8.45}$$

The energy Eq. (8.45) is integrated over each control volume, and we have as follows:

$$\begin{aligned} U^*(\Theta_P - \Theta_W)\frac{R_N^2 - R_S^2}{2} = \Bigg[R_N\left(\frac{\Theta_N - \Theta_P}{\Delta R_N}\right)\left|\frac{U_N^* - U_P^*}{\Delta R_N}\right|^{n-1} \\ - R_S\left(\frac{\Theta_P - \Theta_S}{\Delta R_S}\right)\left|\frac{U_P^* - U_S^*}{\Delta R_S}\right|^{n-1}\Bigg]\Delta Z^* \end{aligned} \tag{8.46}$$

Rearranging the equation in the form as:

$$a_P\Theta_P = a_W\Theta_W + a_N\Theta_N + a_S\Theta_S \tag{8.47}$$

$$a_W = \frac{U^*\left(R_N^2 - R_S^2\right)}{2\Delta Z^*} \tag{8.48}$$

$$a_N = \frac{R_N}{\Delta R_N}\left|\frac{U_N^* - U_P^*}{\Delta R_N}\right|^{n-1} \tag{8.49}$$

$$a_S = \frac{R_S}{\Delta R_S}\left|\frac{U_P^* - U_S^*}{\Delta R_S}\right|^{n-1} \tag{8.50}$$

$$a_P = a_W + a_N + a_S \tag{8.51}$$

The linear system of Eqs. (8.47)–(8.51) can be solved by using LU decomposition method.

Case (4) The thermal conductivity is proposed to be a power law function of temperature gradient. The energy equation is:

$$\rho c_p U\frac{\partial T}{\partial z} = \frac{1}{r}\frac{\partial}{\partial r}\left(rk(T)\frac{\partial T}{\partial r}\right) \tag{8.52}$$

We assume that the heat transfer is affected by velocity fields with modified Fourier' law, the thermal conductivity is dependent on gradient of temperature and has the form of $k(T) = k_0\left|\frac{\partial T}{\partial r}\right|^{n-1}$ with k_0 as positive constant. The

dimensionless temperature Θ, dimensionless radial coordinate R, and dimensionless velocity U^* are as Eqs. (8.25)–(8.27) while the dimensionless axial coordinate is:

$$Z^* = \frac{k_0 z}{\rho c_p D_r^2 U_m}\left(\frac{T_{in} - T_w}{D_r}\right)^{n-1} \tag{8.53}$$

Applying the dimensionless quantities to the energy equation, the problem under consideration is given in dimensionless form as:

$$U^*\frac{\partial \Theta}{\partial Z^*} = \frac{1}{R}\frac{\partial}{\partial R}\left(R\frac{\partial \Theta}{\partial R}\left|\frac{\partial \Theta}{\partial R}\right|^{n-1}\right) \tag{8.54}$$

The boundary conditions are stated as before.

The energy Eq. (8.54) is integrated over each control volume, so we have as follows:

$$U^*(\Theta_P - \Theta_W)\frac{R_N^2 - R_S^2}{2} = \left[R_S\left(\frac{\Theta_S - \Theta_P}{\Delta R_S}\right)^n - R_N\left(\frac{\Theta_P - \Theta_N}{\Delta R_N}\right)^n\right]\Delta Z^* \tag{8.55}$$

Suppose the radius of the pipe, which is one in dimensionless form, is divided into M-nodes. We have $\Delta R_S = \Delta R_N = 1/M$. As the fluid flows in the pipe, it gradually becomes cooler. In view of Eqs. (8.31) and (8.32), we get the conclusion that $0 < \frac{\Theta_S - \Theta_P}{\Delta R_S} < \frac{1/M}{1/M} = 1$ and $0 < \frac{\Theta_P - \Theta_N}{\Delta R_N} < \frac{1/M}{1/M} = 1$. Suppose that a linear function $y = \alpha x$ on [0,1] would minimize the error,

$$\int_0^1 \left[\left(\frac{\Theta_S - \Theta_P}{\Delta R_S}\right)^n - \alpha\frac{\Theta_S - \Theta_P}{\Delta R_S}\right]^2 d\left(\frac{\Theta_S - \Theta_P}{\Delta R_S}\right),$$

and

$$\int_0^1 \left[\left(\frac{\Theta_P - \Theta_N}{\Delta R_N}\right)^n - \alpha\frac{\Theta_P - \Theta_N}{\Delta R_N}\right]^2 d\left(\frac{\Theta_P - \Theta_N}{\Delta R_N}\right).$$

$\alpha = \frac{3}{n+2}$ is satisfied. Then, to put $\frac{\alpha\Theta_S - \alpha\Theta_P}{\Delta R_S}$ and $\frac{\alpha\Theta_P - \alpha\Theta_N}{\Delta R_N}$ in the place of $\left(\frac{\Theta_S - \Theta_P}{\Delta R_S}\right)^n$ and $\left(\frac{\Theta_P - \Theta_N}{\Delta R_N}\right)^n$, the problem now is:

$$U^*(\Theta_P - \Theta_W)\frac{R_N^2 - R_S^2}{2} = \left[R_S\frac{\alpha\Theta_S - \alpha\Theta_P}{\Delta R_S} - R_N\frac{\alpha\Theta_P - \alpha\Theta_N}{\Delta R_N}\right]\Delta Z^* \tag{8.56}$$

Rearranging the equation in the form as:

$$a_P\Theta_P = a_W\Theta_W + a_N\Theta_N + a_S\Theta_S \tag{8.57}$$

$$a_W = \frac{U^*\left(R_N^2 - R_S^2\right)}{2\Delta Z^*} \tag{8.58}$$

$$a_N = \frac{R_N \alpha}{\Delta R_N} \tag{8.59}$$

$$a_S = \frac{R_S \alpha}{\Delta R_S} \tag{8.60}$$

$$a_P = a_W + a_N + a_S \tag{8.61}$$

Eqs. (8.57)−(8.61) are solved by using LU decomposition method.

8.2.3 Results and Discussion

Commercial software Compaq Visual FORTRAN Professional Edition 6.6.0 has been used to solve the problem mentioned before. Table 8.1 briefly introduced parameters used in this research. It is worth mentioning that the Reynolds number is not obviously shown in this research as we use the dimensionless form of equations. However, to keep the fluid flow steady in the duct, the Reynolds number should be no more than 2300.

Figs. 8.3 and 8.4 depict the temperature profiles of different dimensionless axial coordinates with linear temperature-dependent thermal conductivity and effects of dimensionless axial coordinate Z^* and power law index n on the temperature profiles Θ with a linear temperature-dependent thermal conductivity model.

Fig. 8.3A displays the dimensionless temperature profiles of different dimensionless axial coordinates. The curves labeled as $n = 0.6$ correspond to shear-thinning non-Newtonian fluid flow. Note in Fig. 8.36A the increase in the dimensionless temperature as the dimensionless axial coordinate decreases. Fig. 8.3B shows the dimensionless temperature profiles versus dimensionless axial coordinate for $n = 1.3$ corresponding to shear-thickening fluid flow. Results indicate that the temperature increases toward the center of the pipe. The thermal wave of the inlet temperature has less penetration near the center with the increasing axial coordinate. It is really interesting to find that Fig. 8.3A seems to be identical to Fig. 8.3B. But we should notice that $\varepsilon^* = -0.001$ in Fig. 8.3A while $\varepsilon^* = 0.001$ in Fig. 8.36B. It is a known fact

TABLE 8.1 The Parameters Covered in This Research

Parameters	Part 2	Part 3	Part 4
Re	<2300	<2300	<2300
n	0.1~2.5	0.6~2.5	0.1~2.5
ε^*	−0.01~0.01	–	–
Z^*	0~0.1	0~0.1	0~0.1

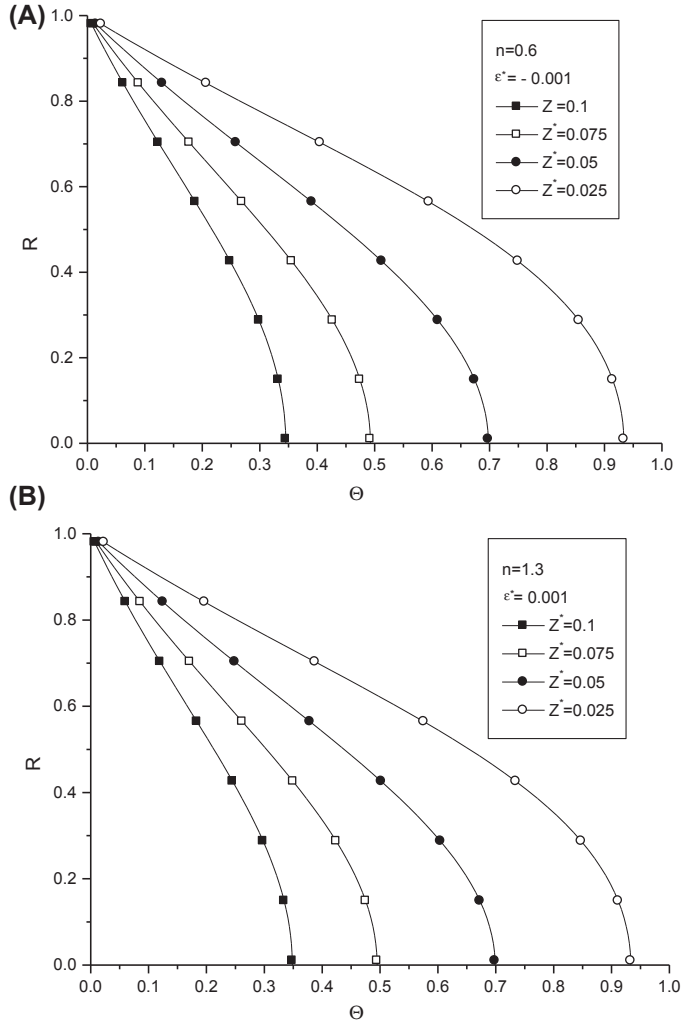

FIGURE 8.3 Temperature profiles of different dimensionless axial coordinates with linear temperature-dependent thermal conductivity. (A) $n = 0.6$ and (B) $n = 1.3$.

that different values of n imply tremendous change in temperature field distribution. The same is reiterated by Fig. 8.4.

Figs. 8.5 and 8.6 show the dimensionless temperature profiles with a velocity-dependent thermal conductivity model. It is found that the behaviors of solutions are remarkably affected by the power law index. Fig. 8.5 indicates the same phenomenon with Fig. 8.3. Fig. 8.6 shows the effects of different power law index on dimensionless temperature profiles; results indicate that, at the center of the pipe, the bigger the power law index, the higher the

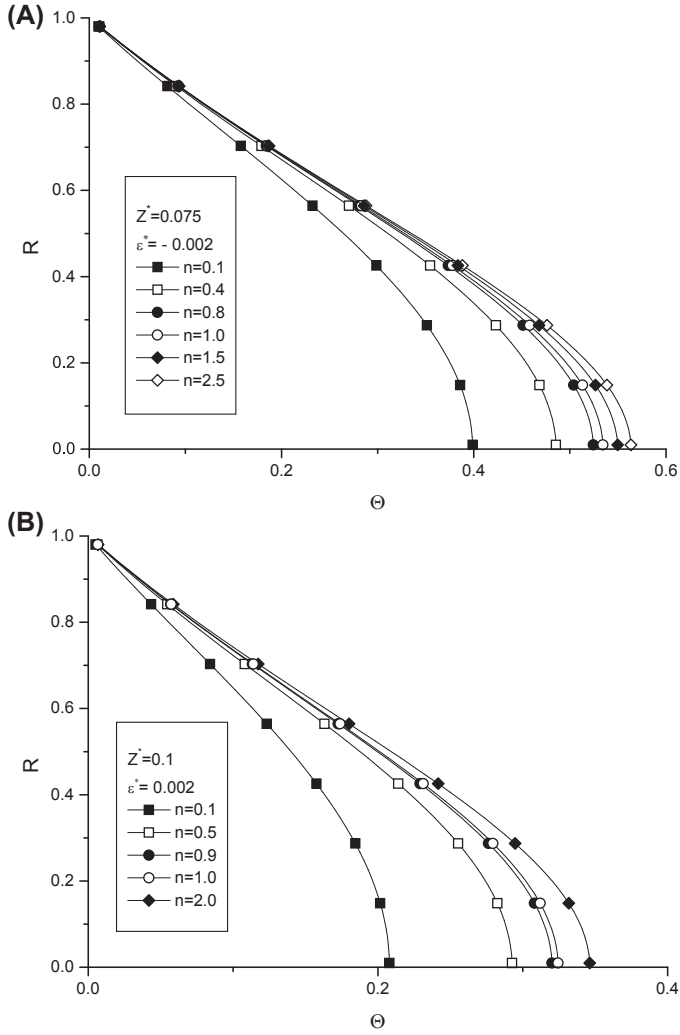

FIGURE 8.4 Temperature profiles of different power law index with linear temperature-dependent thermal conductivity. (A) $Z^* = 0.075$ and (B) $Z^* = 0.1$.

temperature is. '+' presents the Graetz solution in vivid contrast with $n = 1$, which is obtained by using the method mentioned in this research. The results agree well with those obtained by Graetz and the transfer characteristics for values of different parameters correspond to facts, which demonstrates the effectiveness of the model and the robustness of the algorithm.

Figs. 8.7 and 8.8 describe the dimensionless temperature profiles of different axial coordinates for power law index $n = 0.5$ and $n = 1.5$. It is seen that the behaviors of solutions with a power law temperature

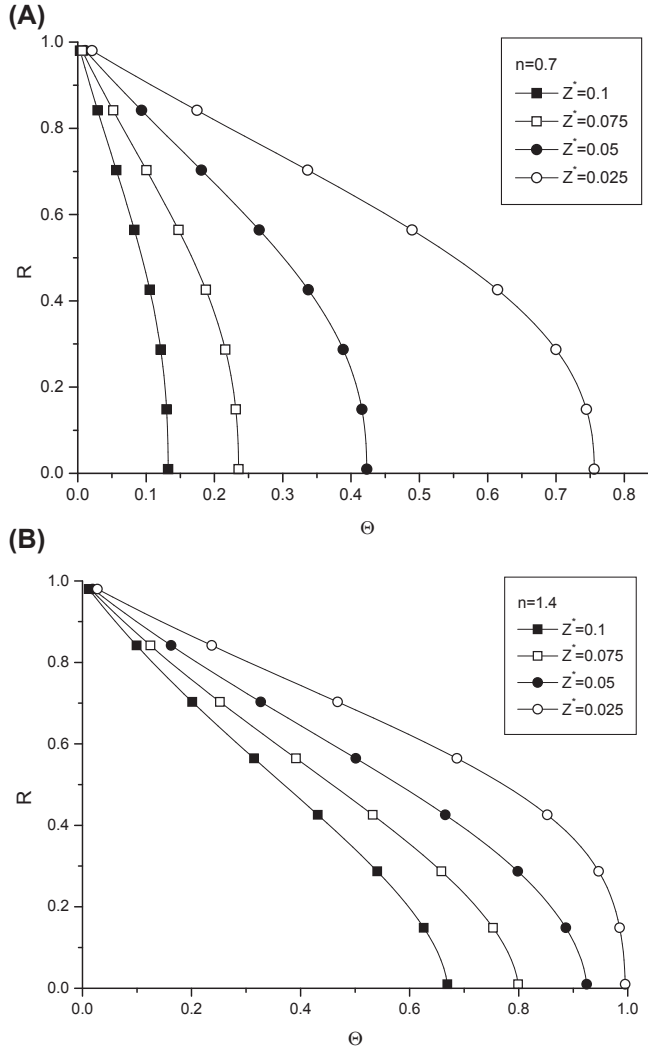

FIGURE 8.5 Temperature profiles of different dimensionless axial coordinate with velocity-dependent thermal conductivity. (A) $n = 0.7$ and (B) $n = 1.4$.

gradient−dependent Fourier's heat conductivity model are very similar with the ones with velocity temperature gradient−dependent Fourier's heat conductivity model.

Fig. 8.7 shows that the flows contribute to reduce heating effects with the increasing axial coordinate. Fig. 8.8 shows the effects of different power law index on dimensionless temperature profiles, and results indicate that, at the center of the pipe, the bigger the power law index is, the higher the

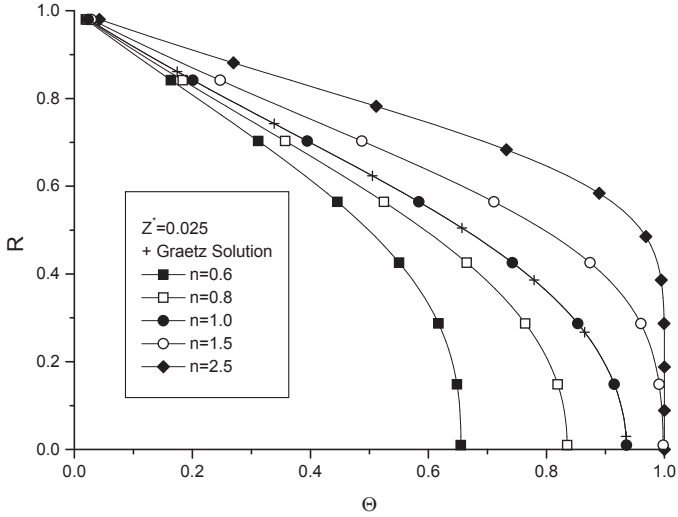

FIGURE 8.6 Temperature profiles of different power law index with velocity-dependent thermal conductivity.

temperature is, which is similar to Fig. 8.6. The temperature profile is flatter as the power law index increases. '+' presents the Graetz solution in vivid contrast with the fluid $n = 1$ which is obtained in the research. Those results also agree well with each other.

Fig. 8.9 shows the effects of linear temperature-dependent thermal conductivity model parameter ε^* on temperature profiles for both shear-thinning ($n = 0.5$) and shear-thickening ($n = 1.5$) fluids. It is observed from these pictures that the increasing values of ε^* result in decreasing the temperature. Fig. 8.10 presents a comparison of different solutions obtained by using the four different Fourier heat conductivity models. The curves with square marks are classical results with a constant thermal conductivity; the profiles with circle marks, with a thermal conductivity assumed to be a function of velocity gradient; the curves with diamond marks; with a power law temperature-dependent thermal conductivity. With the traditional model, the differences of temperature between varying power law index are small; with a temperature-dependent model, the differences are big; with a velocity-dependent model, the differences are biggest.

We now study the effects of pertinent parameters on Nusselt number. The local Nusselt number is defined by

$$Nu = -2\frac{\frac{\partial \Theta}{\partial R}\Big|_{R=1}}{\Theta|_{R=1} - \Theta_b} \tag{8.62}$$

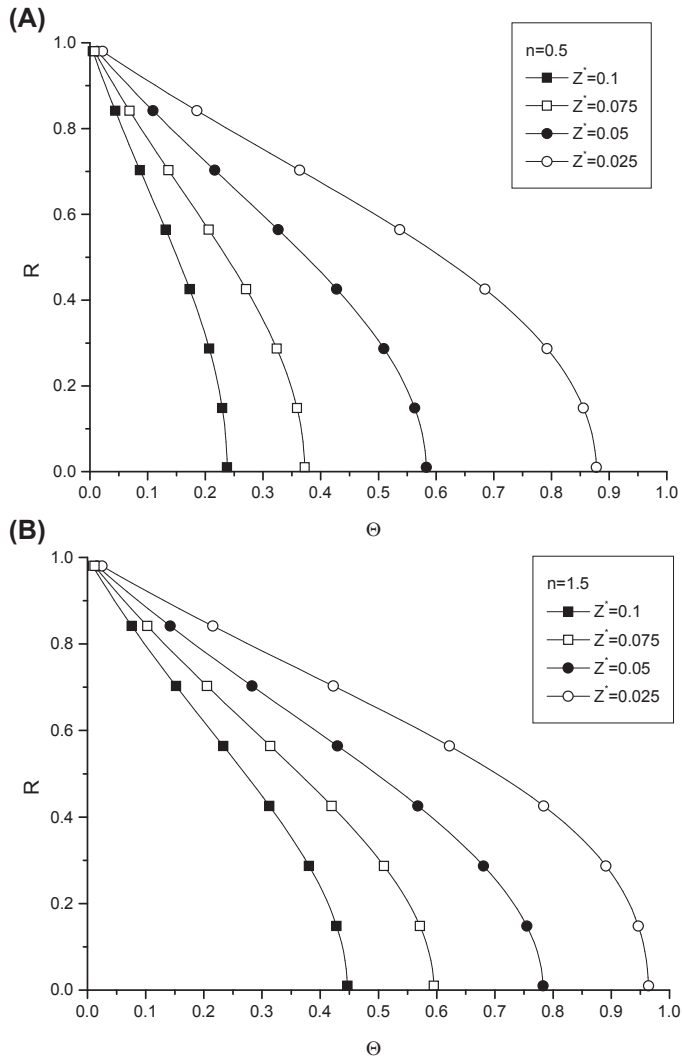

FIGURE 8.7 Temperature profiles of different dimensionless axial coordinate with power law temperature-dependent thermal conductivity. (A) $n = 0.5$ and (B) $n = 1.5$.

where Θ_b is the dimensionless bulk mean temperature, which is defined as

$$\Theta_b = \frac{\int_0^1 U^* \Theta R dR}{\int_0^1 U^* R dR} \tag{8.63}$$

In Table 8.2, local Nusselt numbers in the fully developed region from Irvine et al. (1988) and Kim et al. (1995) are in good agreement with

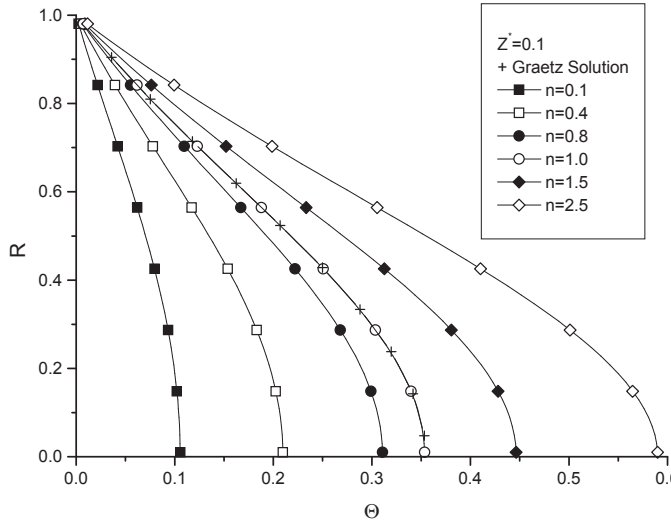

FIGURE 8.8 Temperature profiles of different power law index with power law temperature-dependent thermal conductivity.

calculated values obtained in this research. This comparison with constant model could prove the reliability of the results.

The local Nusselt number increases with the increase in thermal conductivity parameter ε^* as displayed in Fig. 8.11. The local Nusselt number from the entrance to the fully developed region is getting lower, and the Nusselt number of dilatant fluid is smaller than the one of shear-thinning non-Newtonian flow. Fig. 8.12 reveals the difference of local Nusselt number between thermal conductivity models. It shows there is obvious difference between the constant model and the velocity-dependent model. However, Nusselt number varies little from constant model to temperature-dependent model.

From the previous discussion, we can obtain the following conclusions:

1. With traditional constant model, the differences of temperature between varying power law index are small; with a temperature-dependent model, the differences are obviously big; with a velocity gradient-dependent model, the differences are biggest.
2. There is obvious difference in the local Nusselt number between the constant model and the velocity gradient-dependent model. However, Nusselt number varies little from constant model to power law temperature gradient−dependent model.
3. The results show that the heat transfer behaviors strongly depend on the value of the power law index in all the models.
4. The increasing values of thermal conductivity parameter ε^* result in decreasing the temperature and increasing the local Nusselt number when the thermal conductivity is a linear one.

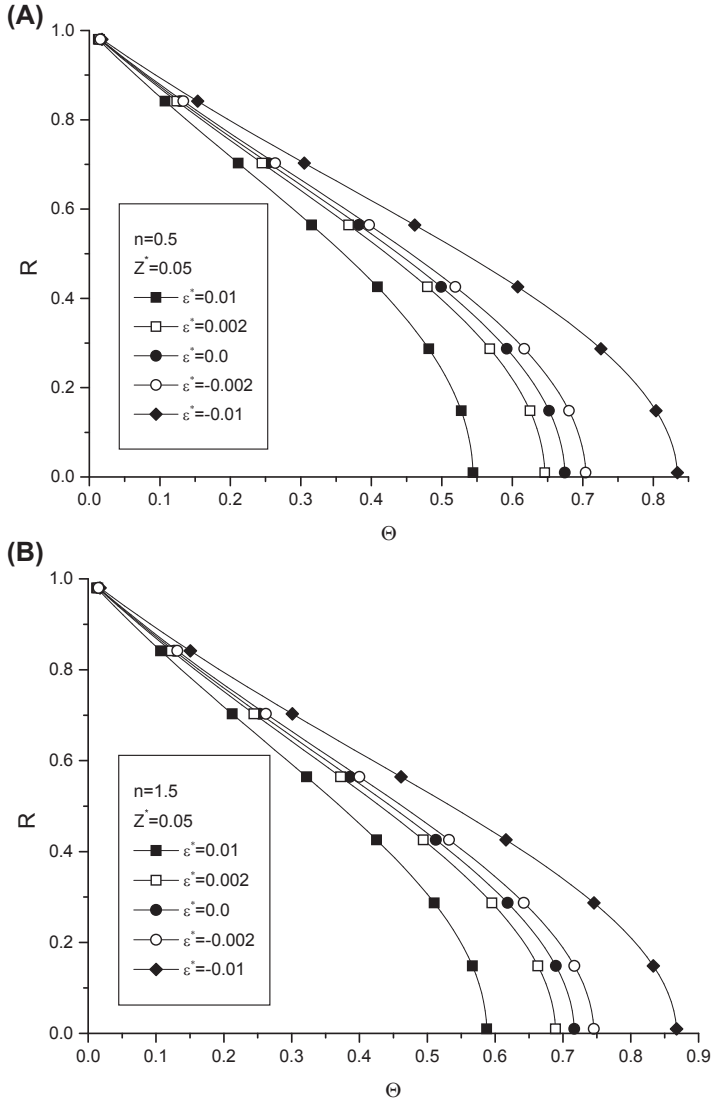

FIGURE 8.9 Effects of thermal conductivity parameter ε^* on temperature profiles in a linear temperature-dependent thermal conductivity model. (A) $n = 0.5$ and (B) $n = 1.5$.

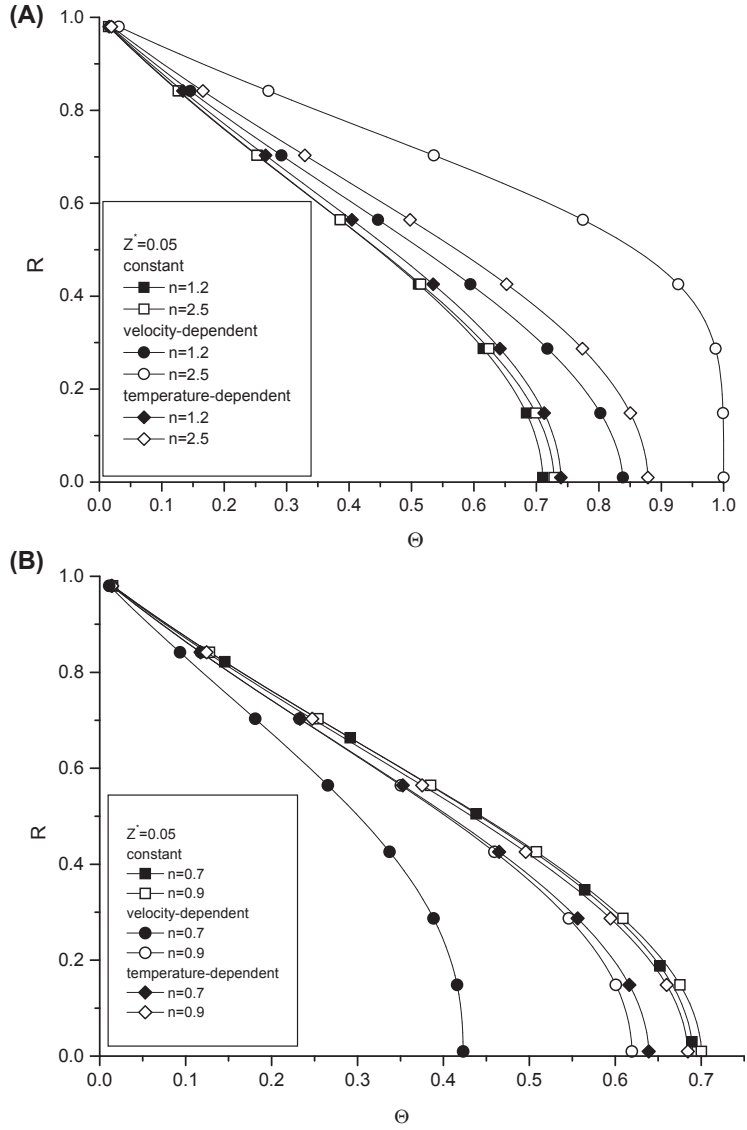

FIGURE 8.10 Comparison of solutions obtained by four heat conductivity models. (A) $n = 0.5$ and (B) $n = 1.5$.

TABLE 8.2 Comparison of Calculated Fully Developed Nusselt Numbers With Constant Model

n	Previous Works	Present Results	Differences
1.4	3.5564 (Kim, 1995)	3.558571	0.061%
1.2	3.5993 (Kim, 1995)	3.600869	0.044%
1.0	3.6568 (Irvine et al., 1988)	3.657589	0.022%
0.9	3.6934 (Irvine et al., 1988)	3.693878	0.013%
0.8	3.7377 (Irvine et al., 1988)	3.731622	0.002%
0.7	3.7921 (Irvine et al., 1988)	3.791383	0.019%
0.6	3.8605 (Irvine et al., 1988)	3.859031	0.038%
0.5	3.9494 (Irvine et al., 1988)	3.946730	0.068%

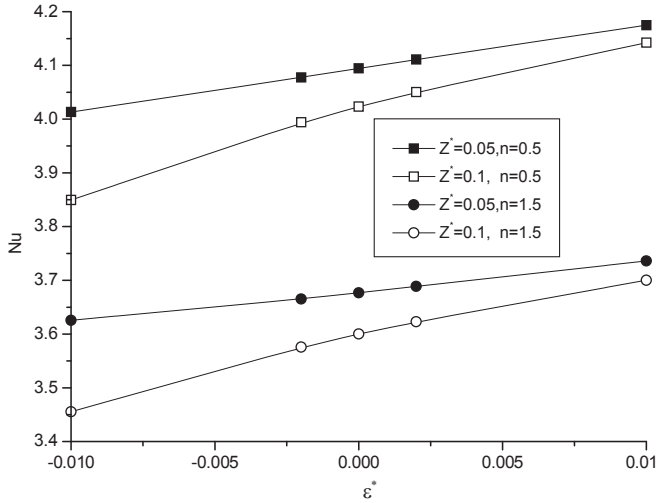

FIGURE 8.11 Effects of thermal conductivity parameter ε^* on local Nusselt number in a linear temperature-dependent thermal conductivity model.

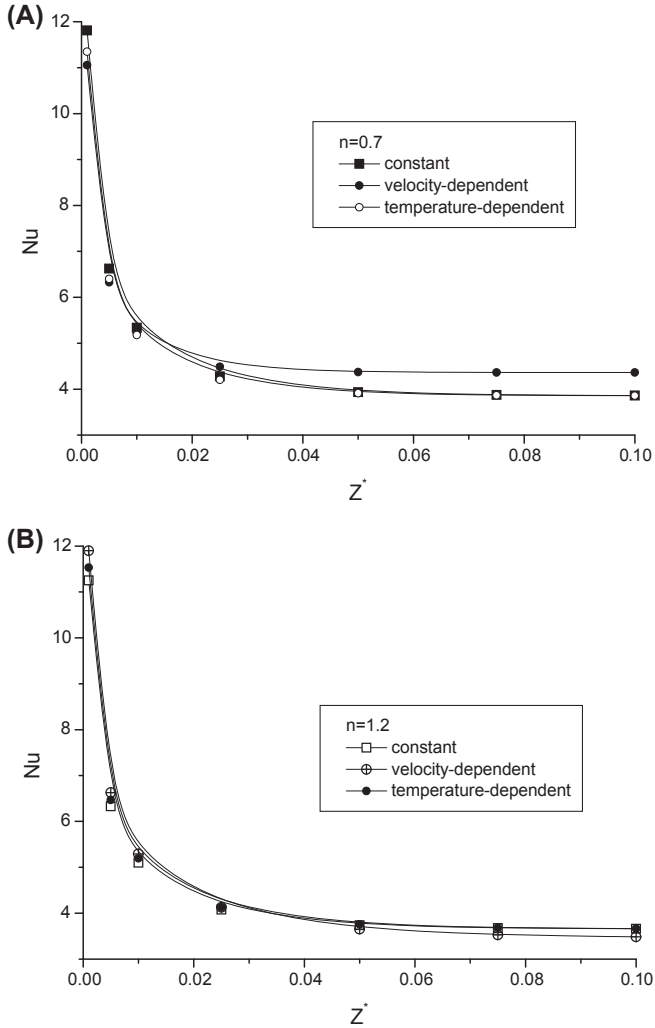

FIGURE 8.12 Comparison of local Nusselt number between models. (A) $n = 0.7$ and (B) $n = 1.2$.

8.3 HEAT TRANSFER OF THE POWER LAW FLUID OVER A ROTATING DISK

8.3.1 Background of the Problem

The fluid flow, heat, and mass transfer over rotating bodies have been studied in many industrial, geothermal, geophysical, technological, and engineering. For the complex of real machines, this type of flow and heat transfer can be modeled by the rotating disk system. The steady flow of Newtonian fluid over rotating disk was first discussed by von Kármán in 1921. Von Kármán introduced an elegant transformation of reducing the Navier–Stokes equations to a set of ordinary differential equations (ODEs), the approximate solution was obtained by using momentum integral method. In 1934, Cochran and Goldstein (1934) calculated more accurate values by numerical integration of the ODEs. Rogers and Lance (1960) and Benton (1966) obtained improved solutions. The problem of heat transfer over a rotating disk maintained at a constant temperature was firstly considered by Millsaps and Pohlhausen (1952) with a variety of Prandtl numbers in the range of $0.5 < (c_v/c_p)\mathrm{Pr} < 10$. Sparrow and Gregg (1959) obtained the results for any values of Prandtl numbers. Since the pioneering work of Von Kármán, the flow and heat transfer problems due to a rotating disk have attracted increasing attentions. A comprehensive review of the problem was reported in 1987 by Zandbergen and Dijkstra (1987).

Recently, the study of flow and heat transfer of non-Newtonian fluid over rotating disk has attracted a great deal of attention due to its many applications. In 1964, Mitschka generalized the Von Kármán's similarity transformation to power law fluid. In 2001, Andersson et al. analyzed the flow in the boundary layer of the power law fluid systematically for power law index in range of $1.5 < n < 2.0$. Attia (2008) studied rotating disk flow and heat transfer through a porous medium of a non-Newtonian fluid with suction and injection. Sahoo (2009) investigated effects of partial slip, viscous dissipation and Joule heating on Von Kármán flow, and heat transfer of an electrically conducting non-Newtonian fluid. Osalusi et al. (2007) considered viscous dissipation and Joule heating on steady MHD flow and heat transfer of a Bingham fluid over a porous rotating disk in the presence of Hall and ion-slip currents. Rashaida (2005) studied the flow of a non-Newtonian Bingham plastic fluid over a rotating disk.

We discuss in this section the steady flow and heat transfer of power law fluid over a free rotating disk. A modified Fourier's heat conduction law for power law fluids is introduced by assuming that the heat diffusion of temperature is affected by velocity field power law viscosity of non-Newtonian fluid. Suitable similarity transformation is introduced to reduce the coupled governing equations into ODEs, which is solved numerically by using multishooting method technique.

8.3.2 Formulation of the Problem and Governing Equations

Let us consider the laminar flow driven solely by an infinite disk rotating steadily with angular velocity Ω about the z-axis. The fluid occupies the infinite region on one side of the disk ($z > 0$) and the motion is rotationally symmetric. The cylindrical polar coordinate system is (r,φ,z), where r is the radial axis, φ is the tangential axis, and z is the vertical axis. The fluid near the disk surface is thrown outward radically, and this in turn induces an axial flow. u,v and w are velocity components in the directions of increasing r,φ and z, respectively. The surface of the rotating disk is maintained at a uniform temperature T_w, and the free stream is kept at a constant temperature T_∞.

The physical model and geometrical coordinates are shown in Fig. 8.13. Unless we give special interpretation, throughout this chapter we make the following assumptions:

1. The density of the fluid ρ is constant.
2. The flow is steady and axial-symmetric, that is, $\frac{\partial}{\partial\varphi} = 0, \frac{\partial}{\partial t} = 0$.
3. The motion and heat transfer of the fluid are all boundary problems (at sufficiently high Reynolds, not very slow flow).
4. The viscosity μ obeys the power law $\mu = \mu_0 \left\{ \left(\frac{\partial u}{\partial z}\right)^2 + \left(\frac{\partial v}{\partial z}\right)^2 \right\}^{(n-1)/2}$,

where μ_0 is the consistency coefficient of the fluid, n is the power law index. Particularly $n = 1$ is for Newtonian fluid and $\mu = \mu_0$.

From the assumptions and the conservation theory, we have $\frac{\partial p}{\partial z} = 0, \frac{\partial p}{\partial r} = 0, \frac{\partial p}{\partial \varphi} = 0,$ which imply that the pressure p is a constant. So the conservation equations for mass and momentum and energy are written as follows:

$$\frac{\partial u}{\partial r} + \frac{u}{r} + \frac{\partial w}{\partial z} = 0, \tag{8.64}$$

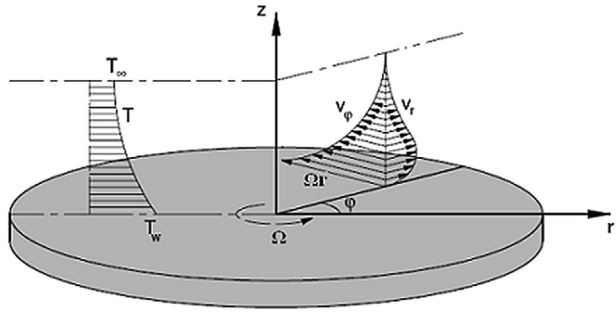

FIGURE 8.13 The sketch model of rotating disk.

$$\rho\left(u\frac{\partial u}{\partial r}-\frac{v^2}{r}+w\frac{\partial u}{\partial z}\right)=\frac{\partial}{\partial z}\left(\mu\frac{\partial u}{\partial z}\right), \tag{8.65}$$

$$\rho\left(u\frac{\partial v}{\partial r}+\frac{uv}{r}+w\frac{\partial u}{\partial z}\right)=\frac{\partial}{\partial z}\left(\mu\frac{\partial v}{\partial z}\right), \tag{8.66}$$

$$\rho c_p\left(u\frac{\partial T}{\partial r}+w\frac{\partial T}{\partial z}\right)=\frac{\partial}{\partial z}\left(\kappa\frac{\partial T}{\partial z}\right), \tag{8.67}$$

where T is the temperature of fluid over the disk, c_p is the specific heat at constant pressure, μ is the viscosity, κ is the thermal conductivity of the power law non-Newtonian fluid with modified Fourier heat conduction law chosen as $\kappa=\kappa_0\left\{\left(\frac{\partial u}{\partial z}\right)^2+\left(\frac{\partial v}{\partial z}\right)^2\right\}^{(n-1)/2}$ (Ming et al., 2009; Zheng et al., 2008). $\mathrm{Pr}=\mu c_p/\kappa=\mu_0 c_p/\kappa_0$ is the Prandtl number.

The corresponding boundary conditions are:

$$z=0: \quad u=0, \quad v=\Omega r, \quad w=0, \quad T=T_w; \tag{8.68a}$$

$$z\to\infty: \quad u=0, \quad v=0, \quad T=T_\infty, \tag{8.68b}$$

where $u=0$, $v=\Omega r$ present the no-slip boundary condition, and $w=0$ presents no suction or induction boundary condition at $z=0$.

8.3.3 Generalized Karman Transformation

Mitschka focused on the boundary layer equations of power law fluid and proposed a generalized dimensionless Karman similarity variable defined as

$$\xi=z\left(\frac{\Omega^{2-n}}{\mu_0/\rho}\right)^{\frac{1}{n+1}}r^{\frac{1-n}{n+1}}. \tag{8.69}$$

The motion of the fluid in radial and azimuthal direction are aroused by the rotation of the disk, so let

$$u=\Omega r\cdot F(\xi), \quad v=\Omega r\cdot G(\xi), \quad w=\left(\frac{\Omega^{1-2n}}{\mu_0/\rho}\right)^{-\frac{1}{n+1}}\cdot r^{\frac{n-1}{n+1}}\cdot H(\xi), \tag{8.70}$$

and here F, G and H denote the nondimensional velocity components in the direction of radial, azimuthal and axial, respectively.

In addition, a dimensionless temperature is defined as

$$\Theta(\xi) = (T - T_\infty)/(T_w - T_\infty) \tag{8.71}$$

where T_w and T_∞, respectively, represent the surface temperature (a constant) and the temperature of the fluid far from the disk.

Since,

$$\frac{\partial \xi}{\partial r} = \frac{1-n}{n+1} z \left(\frac{\Omega^{2-n}}{\mu_0/\rho}\right)^{\frac{1}{n+1}} r^{\frac{1-n}{n+1}-1} = \frac{1-n}{n+1}\frac{\xi}{r}, \tag{8.72}$$

$$\frac{\partial \xi}{\partial z} = \left(\frac{\Omega^{2-n}}{\mu_0/\rho}\right)^{\frac{1}{n+1}} r^{\frac{1-n}{n+1}} = \frac{\xi}{z}, \tag{8.73}$$

$$\frac{\partial u}{\partial r} = \frac{\partial(\Omega r F(\xi))}{\partial r} = \Omega F(\xi) + \Omega r F'(\xi)\frac{\partial \xi}{\partial r} = \Omega\left(F(\xi) + \frac{1-n}{n+1}\xi F'(\xi)\right), \tag{8.74}$$

$$\frac{\partial u}{\partial z} = \frac{\partial(\Omega r F(\xi))}{\partial z} = \Omega r F'(\xi)\frac{\partial \xi}{\partial z} = \Omega r \frac{\xi}{z} F'(\xi), \tag{8.75}$$

$$\frac{\partial v}{\partial r} = \frac{\partial(\Omega r G(\xi))}{\partial r} = \Omega G(\xi) + \Omega r G'(\xi)\frac{\partial \xi}{\partial r} = \Omega\left(G(\xi) + \frac{1-n}{n+1}\xi G'(\xi)\right), \tag{8.76}$$

$$\frac{\partial v}{\partial z} = \frac{\partial(\Omega r G(\xi))}{\partial z} = \Omega r G'(\xi)\frac{\partial \xi}{\partial z} = \Omega r \frac{\xi}{z} G'(\xi), \tag{8.77}$$

$$\frac{\partial w}{\partial z} = \left(\frac{\Omega^{1-2n}}{\mu_0/\rho}\right)^{-\frac{1}{n+1}} \cdot r^{\frac{n-1}{n+1}} \cdot H'(\xi)\frac{\partial \xi}{\partial z} = \Omega H'(\xi), \tag{8.78}$$

$$\frac{\partial T}{\partial r} = \frac{\partial \Theta}{\partial \xi}\cdot\frac{\partial \xi}{\partial r} = (T_w - T_\infty)\frac{1-n}{1+n}\left(\frac{\xi}{r}\right)\Theta'(\xi), \tag{8.79}$$

$$\frac{\partial T}{\partial z} = \frac{\partial \Theta}{\partial \xi}\cdot\frac{\partial \xi}{\partial z} = (T_w - T_\infty)\frac{\xi}{z}\Theta'(\xi). \tag{8.80}$$

Then

$$\mu = \mu_0 \Omega^{n-1} r^{n-1}\left(\frac{\xi}{z}\right)^{n-1}\left[(F'(\xi))^2 + (G'(\xi))^2\right]^{(n-1)/2}, \tag{8.81}$$

$$\kappa = \kappa_0 \Omega^{n-1} r^{n-1}\left(\frac{\xi}{z}\right)^{n-1}\left[(F'(\xi))^2 + (G'(\xi))^2\right]^{(n-1)/2}, \tag{8.82}$$

and

$$\frac{\partial}{\partial z}\left[\mu\frac{\partial u}{\partial z}\right] = \rho\Omega^2 r\left\{F'(\xi)\left[(F'(\xi))^2 + (G'(\xi))^2\right]^{(n-1)/2}\right\}'_{\xi}, \tag{8.83}$$

$$\frac{\partial}{\partial z}\left[\mu\frac{\partial v}{\partial z}\right] = \rho\Omega^2 r\left\{G'(\xi)\left[(F'(\xi))^2 + (G'(\xi))^2\right]^{(n-1)/2}\right\}'_{\xi}, \tag{8.84}$$

$$\frac{\partial}{\partial z}\left[\kappa\frac{\partial T}{\partial z}\right] = \rho\frac{\kappa_0}{\mu_0}\Omega(T_w - T_\infty)\left\{\Theta'(\xi)\left[(F'(\xi))^2 + (G'(\xi))^2\right]^{(n-1)/2}\right\}'_{\xi}. \tag{8.85}$$

Therefore, the partial differential Eqs. (8.64)–(8.67) become the following ordinary differential equations:

$$H' = -2F - \frac{1-n}{1+n}\xi F', \tag{8.86a}$$

$$F^2 - G^2 + \left(H + \frac{1-n}{1+n}\xi F\right)F' = \left\{\left[(F')^2 + (G')^2\right]^{(n-1)/2}F'\right\}', \tag{8.86b}$$

$$2FG + \left(H + \frac{1-n}{1+n}\xi F\right)G' = \left\{\left[(F')^2 + (G')^2\right]^{(n-1)/2}G'\right\}', \tag{8.86c}$$

$$\left(\frac{1-n}{1+n}\xi F + H\right)\Theta' = \frac{1}{\mathrm{Pr}}\left\{\left[(F')^2 + (G')^2\right]^{(n-1)/2}\Theta'\right\}'. \tag{8.86d}$$

The prime symbol denotes differentiation with respect to ξ and Pr is the Prandtl number of the fluid defined as $\mathrm{Pr} = \frac{\mu_0 c_p}{\kappa_0}$. The transformed boundary conditions are given by:

$$\xi = 0: \quad F(0) = 0, G(0) = 1, H(0) = 0, \quad \Theta(0) = 0; \tag{8.87a}$$

$$\xi \to \infty : F = 0, \quad G = 0, \quad \Theta = 1. \tag{8.87b}$$

8.3.4 Multiple Shooting Method

In order to solve the two-point boundary-value problem, finite difference and shooting method are applied by many researchers. In this research, the multishooting method is adopted to solve the two-point boundary-value problem, Eqs. (8.86a–d) and (8.87a and b). Firstly, we transform the equations to first-order system of ordinary differential equations. Let

$$y_1 = F, y_2 = F', y_3 = G, y_4 = G', y_5 = H, y_6 = \Theta, y_7 = \Theta',$$

then

$$
\begin{aligned}
y_1' &= y_2,\\
y_2' &= \frac{1}{n}\cdot\left(y_2^2+y_4^2\right)^{\frac{1-n}{2}}\cdot\left\{\left[1+(n-1)\left(y_2^2+y_4^2\right)^{-1}y_4^2\right]\left[y_1^2-y_3^2+\left(y_5+\frac{1-n}{1+n}\xi y_1\right)y_2\right]\right.\\
&\quad\left.-(n-1)\left(y_2^2+y_4^2\right)^{-1}y_2y_4\left[2y_1y_3+\left(y_5+\frac{1-n}{1+n}\xi y_1\right)y_4\right]\right.,\\
y_3' &= y_4,\\
y_4' &= \frac{1}{n}\cdot\left(y_2^2+y_4^2\right)^{\frac{1-n}{2}}\cdot\left\{\left[1+(n-1)\left(y_2^2+y_4^2\right)^{-1}y_2^2\right]\left[2y_1y_3+\left(y_5+\frac{1-n}{1+n}\xi y_1\right)y_4\right]\right.\\
&\quad\left.-(n-1)\left(y_2^2+y_4^2\right)^{-1}y_2y_4\left[y_1^2-y_3^2+\left(y_5+\frac{1-n}{1+n}\xi y_1\right)y_2\right]\right.,\\
y_5' &= -2y_1-\frac{1-n}{1+n}\xi y_2,\\
y_6' &= y_7,\\
y_7' &= \left(y_2^2+y_4^2\right)^{\frac{1-n}{2}}y_7\left\{\left(\mathrm{Pr}-\frac{n-1}{n}\right)\left(y_5+\frac{1-n}{1+n}\xi y_1\right)-\frac{n-1}{n}\left(y_2^2+y_4^2\right)^{-1}\right.\\
&\quad\left.\times\left(y_1^2y_2-y_2y_3^2+2y_1y_3y_4\right)\right\}.
\end{aligned}
\tag{8.88}
$$

Boundary conditions are:

$$
y_1(0)=0,\ \ y_3(0)=1,\ \ y_5(0)=0,\ \ y_6(0)=1;\ \ y_1(\infty)=0,\ \ y_3(\infty)=0,\ \ y_6(\infty)=0,
\tag{8.89}
$$

where the value of ξ_∞ is affected by the parameters n and Pr. Set $y_2(0)=a$, $y_4(0)=b$, and $y_7(0)=c$, where a, b, c are adjusted by the shooting technique to satisfy the right boundary conditions $y_1(\infty)=0$, $y_3(\infty)=0$, $y_6(\infty)=0$. Thus the boundary-value problem turns into initial-value problem and can be numerically integrated by using Runge−Kutta method.

8.3.5 Results and Discussion

Numerical results are as follows:

Fig. 8.14 shows the distribution of the velocity and temperature with the variable ξ at $n=0.2$ and $\mathrm{Pr}=1.0$ satisfying the right boundary conditions $F(\infty)=0.01$, $G(\infty)=0.01$, $H(\infty)=0.01$, $\Theta(\infty)=0.01$. F represents the component of radial velocity, G represents the component of azimuthal velocity, and H represents the axial velocity. It is indicated that the magnitude of F and H are very small for shear-thinning fluid.

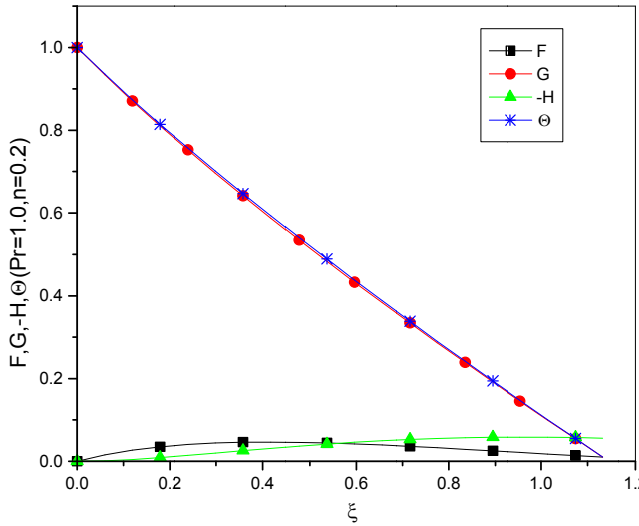

FIGURE 8.14 Velocity components and temperature for a shear-thinning fluid with $n = 0.2$ and $\mathrm{Pr} = 1.0$. Radial (F), azimuthal (G), axial (H), and temperature (Θ).

Fig. 8.15 shows the distribution of the velocity and temperature with the variable ξ at $n = 1.0$ and $\mathrm{Pr} = 1.0$ satisfying the right boundary conditions $F(\infty) = 0.01$, $G(\infty) = 0.01$, $H(\infty) = 0.01$, $\Theta(\infty) = 0.01$, where the fluid is Newtonian fluid. Fig. 8.16 shows the distribution of the velocity and temperature with the variable ξ at $n = 10$ and $\mathrm{Pr} = 1.0$ satisfying the right

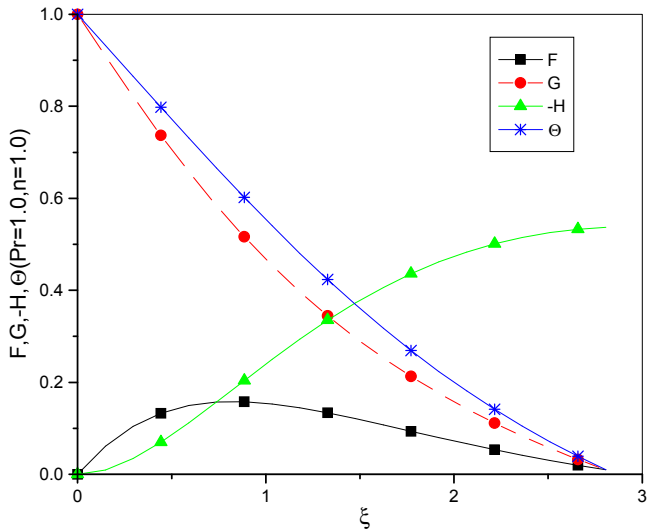

FIGURE 8.15 Velocity components and temperature for Newtonian fluid with $n = 1$ and $\mathrm{Pr} = 1.0$. Radial (F), azimuthal (G), axial (H), and temperature (Θ).

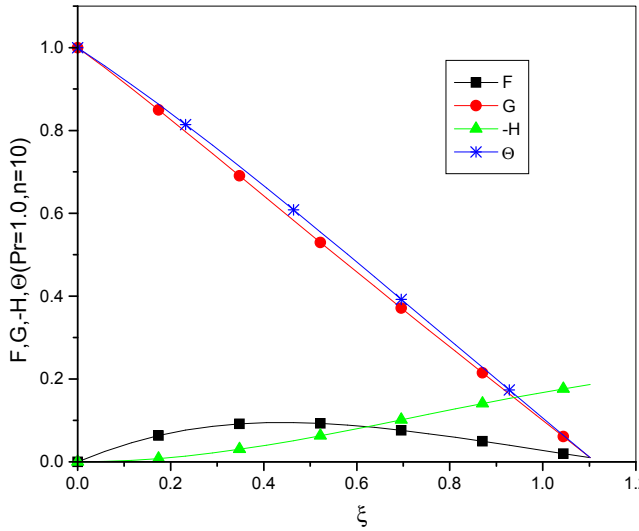

FIGURE 8.16 Velocity components and temperature for a shear-thickening fluid with $n = 10$ and $n = 10$, Pr = 1.0. Radial (F), azimuthal (G), axial (H), and temperature (Θ).

boundary conditions $F(\infty) = 0.01$, $G(\infty) = 0.01$, $H(\infty) = 0.01$, $\Theta(\infty) = 0.01$. The fluid is shear-thickening fluid.

Fig. 8.17A shows the component F and the thickness of the boundary layer increase with n for $0.2 < n < 1.0$, Pr = 1.0. Fig. 8.17B shows the maximum of F increases with n, but the thickness of boundary layer decreases for $1.0 < n < 2.0$, Pr = 1.0, and Fig. 8.17C shows that the component F and the thickness of the boundary layer decreases with n for $2.0 < n < 5.0$, Pr = 1.0. Fig. 8.18A shows that the component G and the thickness of the boundary layer increase with n when $0.2 < n < 1.0$, Pr = 1.0. Fig. 8.18B and C show G decreases with n for $n > 1.0$, Pr = 1.0.

Fig. 8.19A shows that the magnitude of axial velocity increases with n for $0.2 < n < 1.0$. Fig. 8.19B shows that the magnitude of axial velocity vibrates with n for $1.0 < n < 2.0$ and Fig. 8.19C shows that the magnitude of axial velocity decreases with n for $2.0 < n < 5.0$. Fig. 8.20A shows that the temperature increases with n for $0.2 < n < 1.0$. Fig. 8.20B and C show that the temperature decreases with n for $2.0 < n < 5.0$ (Table 8.3). It indicates that the ability of thermal conduction is much stronger for the thickening fluid (Figs. 8.21–8.23).

In this section, the effects of power law index n and Pr on velocity and temperature fields are studied. The boundary layer thickness obtains the maximum value for $n = 1.0$ and decreases with the increase of Pr. The purpose of the present research is to investigate the temperature and velocity distributions and gain a better understanding of the behavior of power law fluid in the laminar boundary layer on a rotating disk.

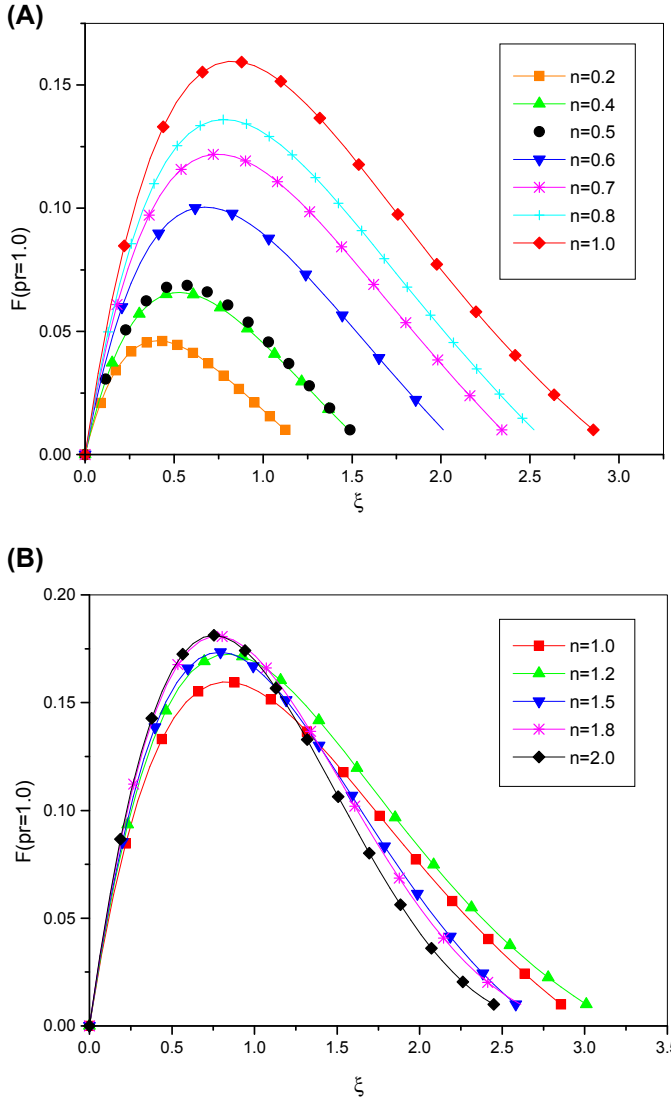

FIGURE 8.17 Cont'd

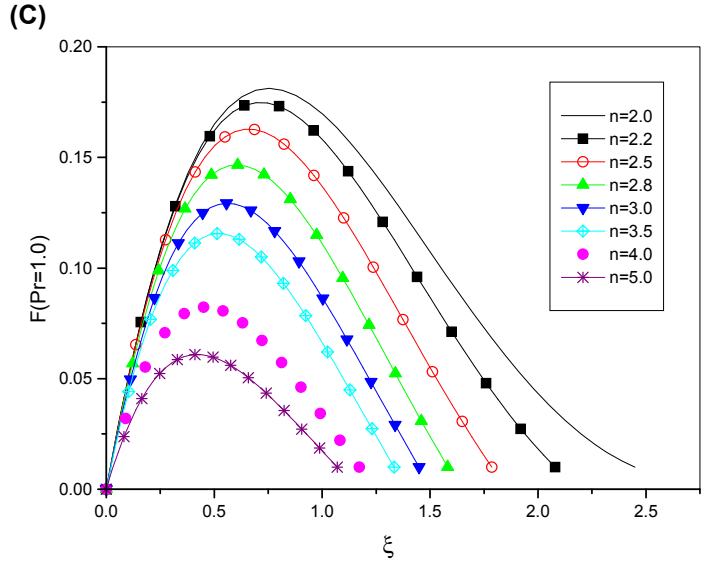

FIGURE 8.17 The distribution of velocity component F for $\mathrm{Pr} = 1.0$ (A) $0.2 < n < 1.0$, (B) $1.0 < n < 2.0$, (C) $2.0 < n < 5.0$.

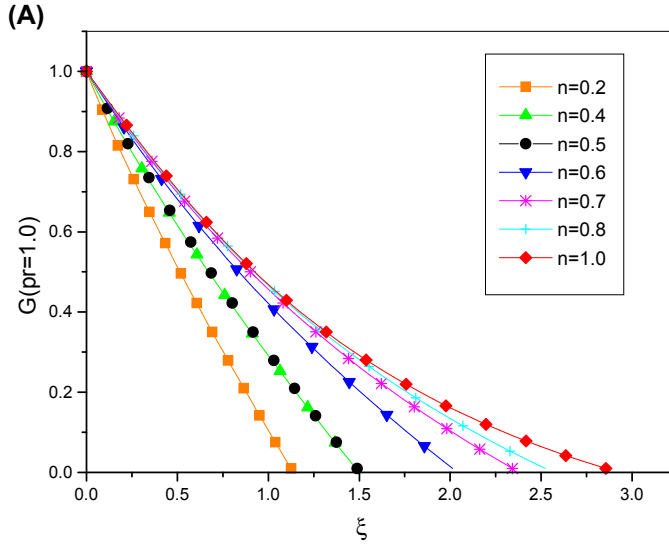

FIGURE 8.18 Cont'd

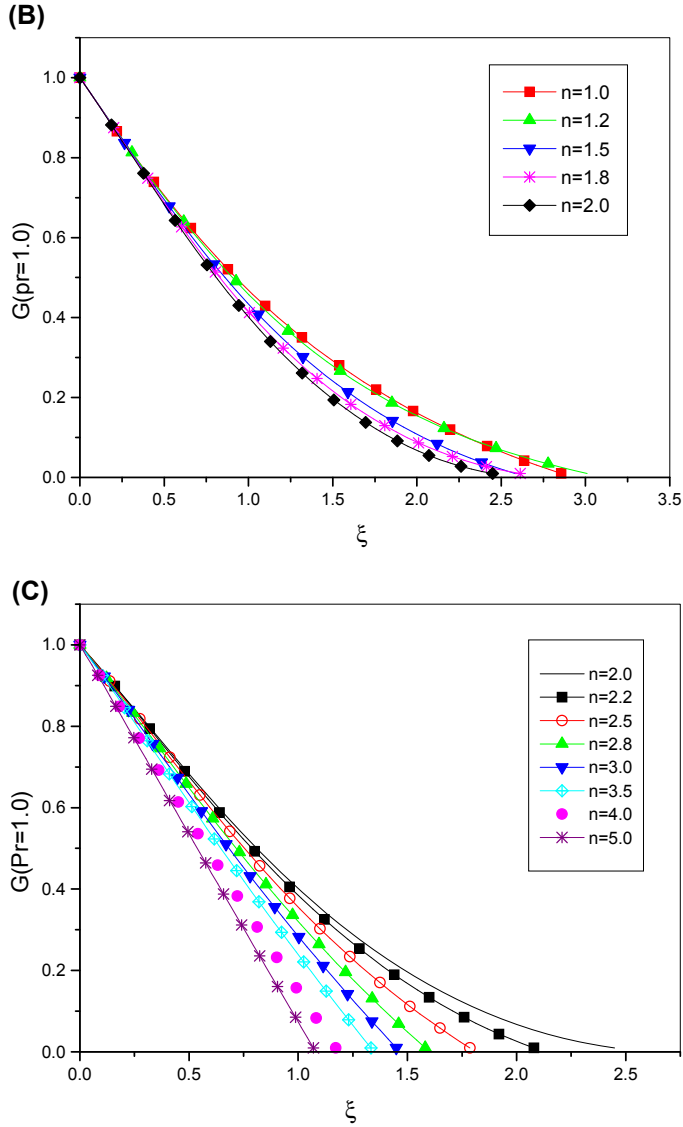

FIGURE 8.18 The distribution of velocity components G with values of power law exponent n for Pr = 1.0. (A) $0.2 < n < 1.0$, (B) $1.0 < n < 2.0$, (C) $2.0 < n < 5.0$.

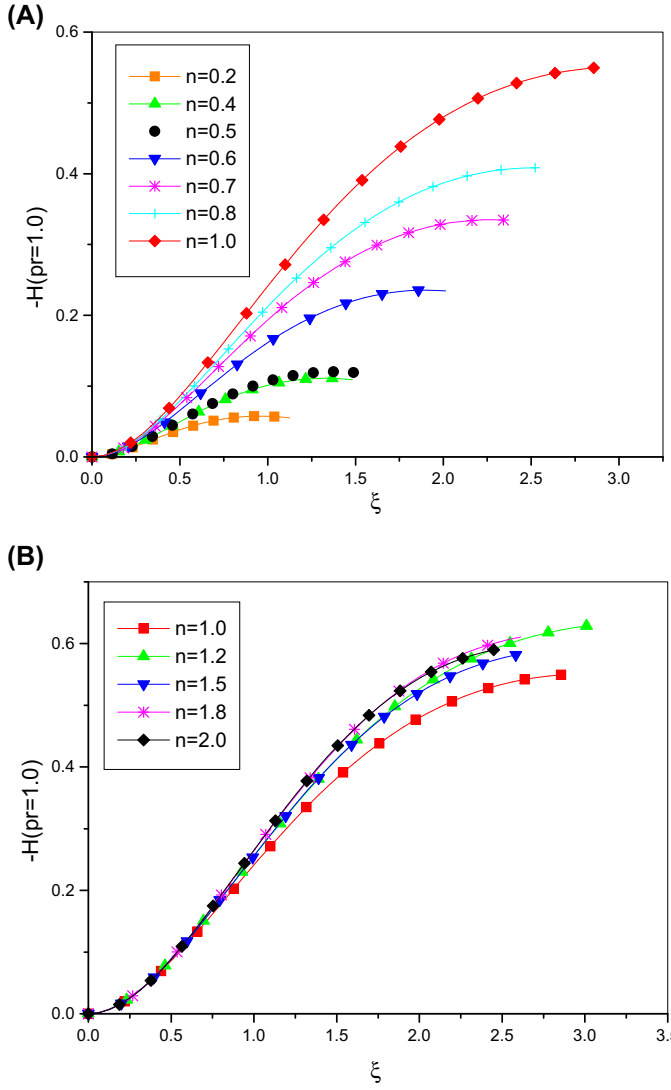

FIGURE 8.19 Cont'd

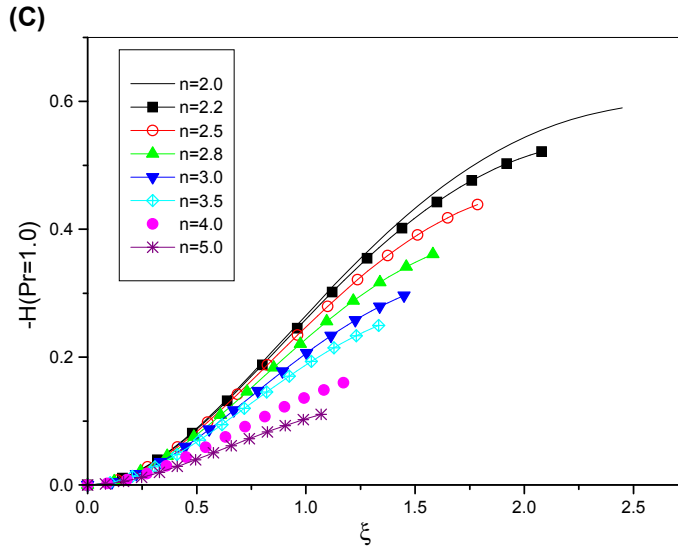

FIGURE 8.19 The distribution of axial velocity H with values of power law exponent n for Pr = 1.0. (A) $0.2 < n < 1.0$, (B) $1.0 < n < 2.0$, (C) $2.0 < n < 5.0$.

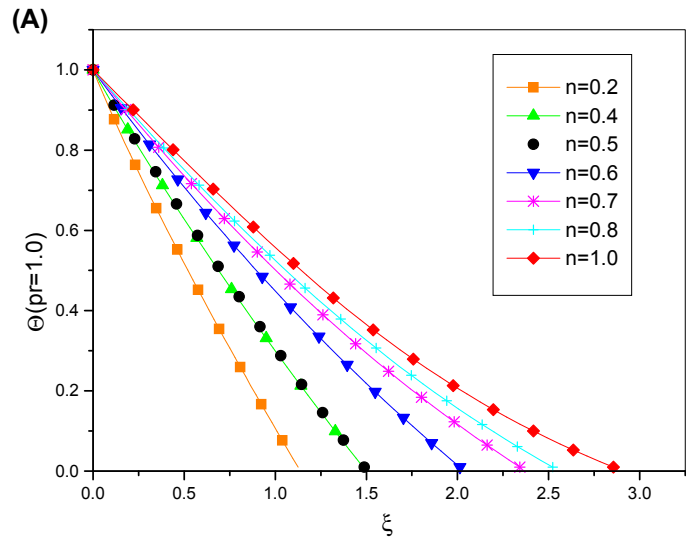

FIGURE 8.20 Cont'd

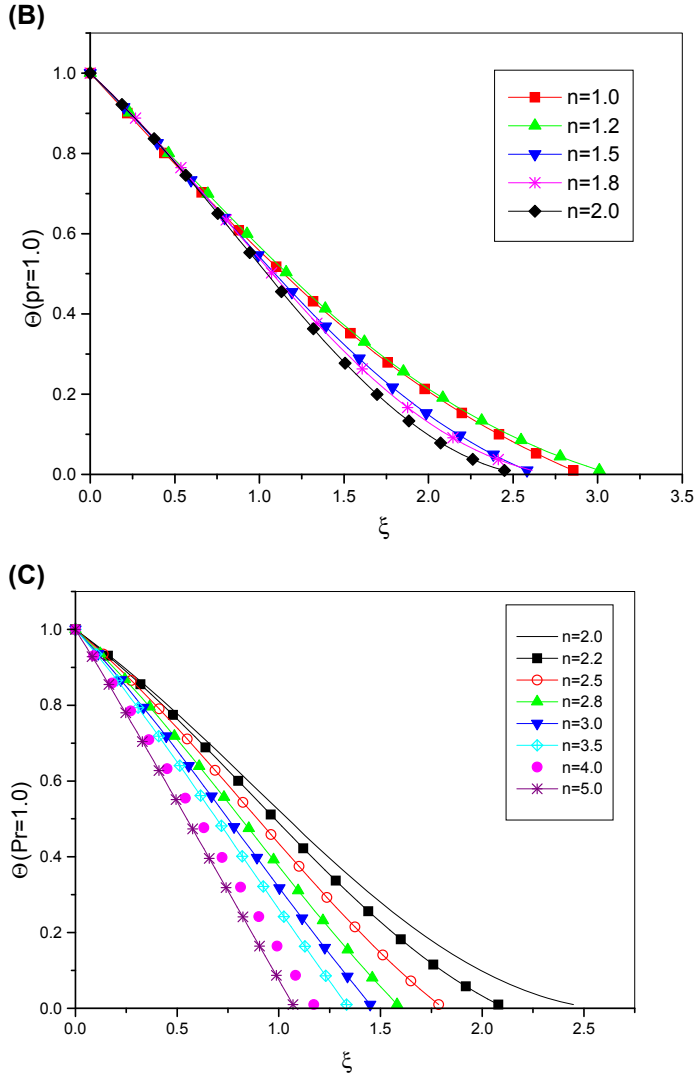

FIGURE 8.20 The distribution of temperature with power law exponent n for Pr = 1.0. (A) $0.2 < n < 1.0$, (B) $1.0 < n < 2.0$, (C) $2.0 < n < 5.0$.

TABLE 8.3 The Numerical Solutions for $n = 1.0$, $\mathrm{Pr} = 1.0$

ξ	F	F'	G	G'	$-H$	Θ	Θ'
0.000	0.000	0.482	1.000	−0.616	0.000	1.000	−0.457
0.146	0.061	0.349	0.910	−0.607	0.009	0.933	−0.456
0.293	0.103	0.239	0.823	−0.584	0.034	0.866	−0.455
0.439	0.132	0.150	0.739	−0.553	0.068	0.800	−0.452
0.586	0.148	0.080	0.661	−0.517	0.110	0.734	−0.446
0.732	0.156	0.025	0.588	−0.480	0.154	0.669	−0.437
0.879	0.156	−0.016	0.520	−0.442	0.200	0.606	−0.426
1.025	0.151	−0.047	0.458	−0.407	0.245	0.545	−0.412
1.172	0.143	−0.068	0.401	−0.373	0.289	0.485	−0.397
1.318	0.132	−0.083	0.349	−0.341	0.329	0.429	−0.379
1.465	0.119	−0.091	0.301	−0.313	0.366	0.374	−0.360
1.758	0.091	−0.097	0.217	−0.263	0.427	0.275	−0.321
1.904	0.077	−0.095	0.180	−0.242	0.452	0.229	−0.301
2.051	0.063	−0.092	0.146	−0.223	0.472	0.187	−0.281
2.197	0.050	−0.088	0.114	−0.206	0.489	0.147	−0.262
2.343	0.038	−0.083	0.085	−0.190	0.502	0.110	−0.243
2.490	0.026	−0.077	0.059	−0.176	0.511	0.075	−0.226
2.636	0.015	−0.072	0.034	−0.163	0.517	0.044	−0.210
2.783	0.005	−0.067	0.011	−0.151	0.520	0.014	−0.194
2.856	0.000	−0.064	0.000	−0.145	0.520	0.000	−0.187

TABLE 8.4 Comparison of Present Solutions With the Results of Andersson et al. (2001).

	$F'(0)$		$-G'(0)$		$-H(\infty)$		$\Theta'(0)$
Power Law Index n	Present	Andersson	Present	Andersson	Present	Andersson	Present
2.5	0.54318	–	0.62184	–	0.44030	–	−0.44752
2.2	0.54563	–	0.60927	–	0.51105	–	−0.41677
2.0	0.54571	0.547	0.60360	0.603	0.57695	0.586	−0.39699
1.7	0.53301	0.537	0.60165	0.600	0.59417	0.633	−0.40002
1.5	0.51832	0.529	0.60319	0.601	0.56188	0.676	−0.41661
1.3	0.50494	0.522	0.60577	0.603	0.54938	0.735	−0.42921
1.1	0.49592	0.514	0.61001	0.610	0.57219	0.822	−0.43502
1.0	0.48234	0.510	0.61619	0.616	0.52038	0.883	−0.45668
0.8	0.44282	0.504	0.64014	0.636	0.38118	1.089	−0.52028

From Table 8.4 we can see that the difference of component of $G'(0)$ is less than 0.002 compared with the result of Andersson's. And the $F'(0)$ and $H(\infty)$ is less than 0.01 near $n = 2.0$).

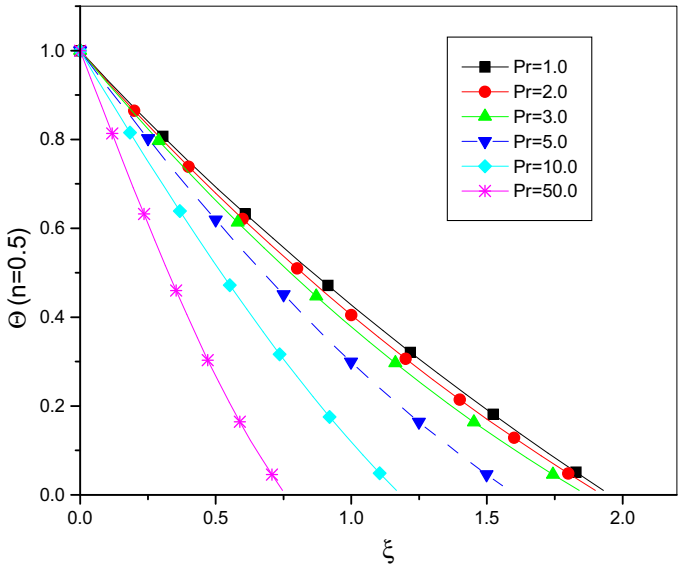

FIGURE 8.21 The variation of the temperature Θ with Pr: 1.0~50 for shear-thinning fluid $n = 0.5$.

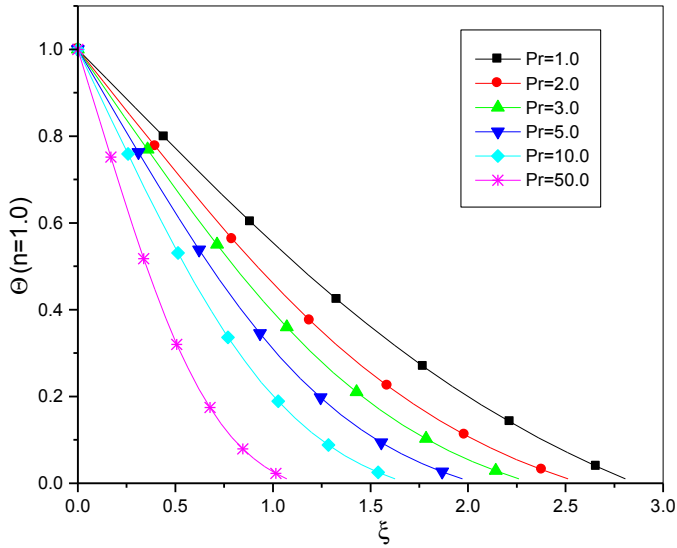

FIGURE 8.22 The variation of the temperature Θ with Pr: 1.0~50 for Newtonian fluid $n = 1.0$.

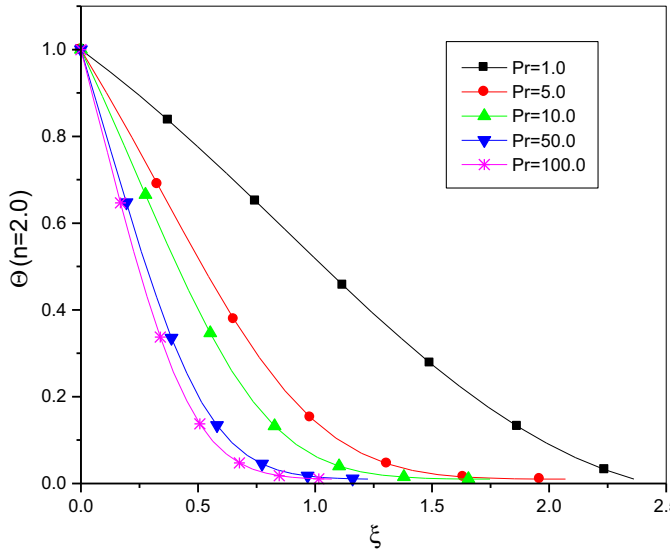

FIGURE 8.23 The variation of the temperature Θ with Pr: 1.0~50 for shear-thickening fluid $n = 2.0$.

8.4 MAXWELL FLUID WITH MODIFIED FRACTIONAL FOURIER'S LAW AND DARCY'S LAW

8.4.1 Background of the Problem

Recently, considerable attention has been devoted to study the transport behavior of fractional viscoelastic fluids. Governing equations are derived from the classical equations by replacing the derivatives of integer-order with noninteger-order integrals or derivatives. Exact analytical solutions of fractional equations are usually obtained by using Laplace transforms, Fourier transforms, and Hankel transforms and presented in terms of Green functions, Fox functions, or H-functions. In doing so, for all of these investigations, the physical property parameters of non-Newtonian fluids are assumed constants (Fetecau et al., 2009; Iomin, 2006; Jamil et al., 2012; Khan et al., 2009, 2012; Nazar et al., 2010; Vieru et al., 2008; Zheng et al., 2011, 2012).

However, experiments had indicated that the assumptions that the physical property parameters of non-Newtonian fluids are constants can only hold if temperature does not change rapidly or impulsively in any particular way (Makinde and Onyejekwe, 2011). Along this line, Seddeek (2002), Jayanthi and Kumari (2007), Cheng (2009), Malekzadeh et al. (2011), and Srinivasa and Eswara (2013) considered the variable viscosity problems for Newtonian fluids, they assumed that the viscosity varied as a linear function of temperature. Later, Malik et al. (2013) and Rundora and Makinde (2013) investigated

that the viscosity is an exponential function that decreases with the temperature.

For the flow and heat transfer of non-Newtonian fluids, the generalized Fourier's law with fractional derivative was taken into consideration by many researchers. Ezzat (2010) derived a new constitutive relation for heat conduction with time fractional derivative of order α for generalized thermoelectric MHD fluid, where the boundary layer theory was applied to Stocks' first problem of an electroconducting viscoelastic flow over an infinite plate with heat source and in the presence of a transverse magnetic field. Li el al. (2012) presented an investigation for helical flows of a heated generalized Oldroyd-B fluid subject to a time-dependent shear stress in porous medium. It is well known that in the flows of viscous Newtonian fluid at low speed through a porous medium, the pressure drop caused by the frictional drag is proportional to the velocity.

Based on a modified Darcy's law for viscoelastic fluid, Tan and Masuoka (2005a,b, 2007) extended Stokes' first problem to that of a second grade fluid, Oldroyd-B fluid and Maxwell fluid in a porous half-space with a heated boundary. Xue and Nie (2009) investigated the Rayleigh−Stokes problem for a heated generalized second grade fluid in a porous half-space with a heated flat plate, and the exact solutions were obtained by using the Fourier sine transform and the fractional Laplace transform.

The purpose of the current work is to present an investigation for coupled flow and heat transfer of a generalized fractional Maxwell fluid in a porous medium between two infinite parallel plates. Unlike most classical works, the temperature-dependent fluid properties (variable fluid viscosity and thermal conductivity) are taken into account by modified fractional Fourier's law and Darcy's law to describe the constitutive relations in highly coupled velocity and temperature fields in porous medium, where the fluid viscosity is assumed to decrease exponentially with temperature. The fractional governing equations are solved numerically using implicit finite difference method based on nonshifted Grünwald formula. The effects of pertinent physical parameters on the velocity and temperature fields are presented graphically and analyzed.

8.4.2 Mathematical Formulation and Governing Equations

The conservation, constitutive, and energy equations of an incompressible fluid are given by (Zheng et al., 2012):

$$\mathbf{T}1 = -P\mathbf{I} + \mathbf{S}, \quad \mathbf{S} + \lambda \frac{\mathrm{D}\mathbf{S}}{\mathrm{D}t} = \mu \mathbf{A}, \tag{8.90}$$

$$\rho c \frac{D\mathbf{T}}{Dt} = -div\mathbf{q} - \mathbf{p} div \overrightarrow{V} + Q_T, \tag{8.91}$$

where $\mathbf{T}1$ is the Cauchy stress tensor, $\mathbf{V}$ is the velocity vector, $\mathbf{S}$ is the extra-stress tensor, ρ is the constant density of the fluid, $\mathbf{T}$ is the temperature, $\mathbf{q}$ is the heat flux, $\mathbf{p}$ is the surface tensor, Q_T is the heat source, μ is the dynamic viscosity of the fluid, and λ is relaxation times. Assuming the velocity and shear stress of the form

$$\mathbf{V} = u(y,t)e_x, \quad \mathbf{S} = \mathbf{S}(y,t), \tag{8.92}$$

where e_x is the unit vector in the x-axis.

Consider the initial condition $\mathbf{S}(y,0) = \mathbf{0}$, the coefficient of variable viscosity and the Fourier's law with fractional derivative, we obtain the constitutive relations with temperature-dependent variable fluid properties for the shear stress equation of generalized Maxwell fluid and the generalized Fourier's law for heat transport:

$$\left(1 + \lambda \mathrm{D}_t^{\alpha}\right)\tau_{xy} = \mu(T)\frac{\partial u}{\partial y}, \tag{8.93}$$

$$\left(1 + \lambda_r D_t^{\beta}\right)\mathbf{q} = -\lambda_0 \frac{\partial T}{\partial y}, \tag{8.94}$$

where, $\tau(y,t) = S_{xy}(y,t)$ is the shear stress, $\mu(T)$ is the dynamic viscosity of the fluid, the fractional differential operators D_t^{α} and D_t^{β} based on Riemann−Liouville's are defined as (Podlubny, 1999):

$$\mathrm{D}_t^{*} f(t) = \frac{1}{\Gamma(1-*)}\frac{d}{dt}\int_0^t \frac{f(\tau)}{(t-\tau)^{*}}d\tau, \quad 0 < * < 1, \tag{8.95}$$

and $\Gamma(\cdot)$ denotes the Gamma function.

In this research, we introduce the modified Darcy's law of the generalized viscoelastic flow in the porous medium. The phenomenological model can be described as:

$$\left(1 + \lambda D_t^{\alpha}\right)\nabla \mathbf{P} = -\frac{\mu\phi}{K}\left(1 + \lambda_r D_t^{\beta}\right)\mathbf{V}, \tag{8.96}$$

where K is the permeability and ϕ is the porosity of the porous medium (Xue and Nie, 2009).

In the absence of body forces in the axial direction and the pressure gradient, the balance of the linear momentum leads to the relevant and meaningful equation,

$$\rho\frac{D\mathbf{V}}{Dt} = -\nabla \mathbf{P} + div\mathbf{S} + \mathbf{r}. \tag{8.97}$$

Therefore

$$\left(1 + \lambda D_t^{\alpha}\right)\mathbf{r} = -\frac{\mu\phi}{K}\mathbf{V}, \tag{8.98}$$

and

$$\rho\left(1+\lambda D_t^{\alpha}\right)\frac{D\mathbf{V}}{Dt}=-\left(1+\lambda D_t^{\alpha}\right)\nabla\mathbf{P}+\left(1+\lambda D_t^{\alpha}\right)div\mathbf{S}-\frac{\mu\phi}{K}\mathbf{V}. \tag{8.99}$$

Then, we get the following governing equation of generalized Maxwell fluid:

$$\left(1+\lambda D_t^{\alpha}\right)\frac{\partial u}{\partial t}=\frac{1}{\rho}\frac{\partial}{\partial y}\left(\mu(T)\frac{\partial u}{\partial y}\right)-\frac{\mu(T)\phi}{\rho K}u, \tag{8.100}$$

$$\left(1+\lambda_T \mathrm{D}_t^{\beta}\right)\frac{\partial \mathrm{T}}{\partial t}=\frac{\lambda_0}{\rho c}\frac{\partial^2 \mathrm{T}}{\partial y^2}+\frac{\mu(T)\phi^2}{\rho c K}\left(1+\lambda_T \mathrm{D}_t^{\beta}\right)u^2. \tag{8.101}$$

In this section, we consider dynamic viscosity of the fluid to be the form

$$\mu(T)=\mu_0\exp\left(\frac{-b}{T_0-T_\infty}T+\frac{bT_\infty}{T_0-T_\infty}\right). \tag{8.102}$$

Assume that the fluid is at rest between two infinite parallel plates. At time $t=0^+$, the one plate is suddenly moved by a time-dependent velocity in x axial direction. In this plate, we consider continuous heating with cosine function. The associated initial and boundary conditions are

$$u(y,0)=\frac{\partial u(y,0)}{\partial t}=0, \tag{8.103}$$

$$u(0,t)=U,\ \ u(L,t)=0, \tag{8.104}$$

$$T(y,0)=T_\infty,\frac{\partial T(y,0)}{\partial t}=0, \tag{8.105}$$

$$T(0,t)=T_\infty+A\cos(\omega t),\ \ T(L,t)=T_\infty, \tag{8.106}$$

where U, A, and ω are constants, T_∞ is the temperature of environment.

We assume that the term u^2 can be expressed as a linear function of u, in view of the best square approximation in the interval of [0,U], we obtain

$$u^2\approx\frac{3}{4}Uu. \tag{8.107}$$

Employing the nondimensional quantities,

$$y^*=\frac{\rho U}{\mu_0}y,\ \ t^*=\frac{U^2\rho}{\mu_0}t,\ \ u^*=\frac{u}{U},\ \ \lambda^*=\left(\frac{U^3\rho}{\mu_0}\right)^{\alpha}\lambda,\ \ \theta=\frac{T-T_\infty}{T_0-T_\infty},\ \ \lambda_T^*=\left(\frac{U^2\rho}{\mu_0}\right)^{\beta}\lambda_T,$$

$$\mathrm{Pr}=\frac{\mu_0 c}{\lambda_0},\ \ \omega^*=\frac{\mu_0}{\rho U^2}\omega,\ \ Da=\left(\frac{\rho U}{\mu_0}\right)^2\cdot K,\ \ \theta_0=\frac{A}{T_0-T_\infty},\ \ L^*=\frac{\rho U}{\mu_0}L,$$

where T_0 is fluid initial temperature. Omit the dimensionless mark "*" and we obtain the dimensionless motion equation as follows:

$$\left(1+\lambda D_t^{\alpha}\right)\frac{\partial u}{\partial t}=\frac{\partial}{\partial y}\left(e^{-b\theta}\frac{\partial u}{\partial y}\right)-\frac{\phi}{Da}e^{-b\theta}u, \tag{8.108}$$

$$\mathrm{Pr}\left(1+\lambda_r \mathrm{D}_t^{\beta}\right)\frac{\partial \theta}{\partial t}=\frac{\partial^2\theta}{\partial y^2}+\frac{M\phi^2}{\mathrm{Pr}Da}e^{-b\theta}\left(1+\lambda_r \mathrm{D}_t^{\beta}\right)u. \tag{8.109}$$

Initial and boundary conditions become:

$$u(y,0)=\frac{\partial u(y,0)}{\partial t}=0, \tag{8.110}$$

$$u(0,t)=1,\quad u(L,t)=0, \tag{8.111}$$

$$\theta(y,0)=\frac{\partial \theta(y,0)}{\partial t}=0, \tag{8.112}$$

$$\theta(0,t)=\theta_0\cos(\omega t),\quad \theta(L,t)=0. \tag{8.113}$$

8.4.3 Numerical Algorithms

In this section, the Grünwald–Letnikov approximation, which is based on a numerical approximation of noninteger derivative operator, is used to describe the solutions. Divide the time interval subintervals of equal size h (also called the step size). Approximate $\mathrm{D}_t^{\alpha}f(t)$ at node k as

$$\mathrm{D}_t^{\alpha}f(t)\approx h^{-\alpha}\sum_{k=0}^{\left[\frac{t}{h}\right]}w_k^{(\alpha)}f(t-kh), \tag{8.114}$$

where the normalized Grünwald weights coefficients are $w_k^{(\alpha)}=(-1)^j\binom{\alpha}{k}$, $k=0,1,2,\cdots$ and are defined by

$$w_0^{(\alpha)}=1,\quad w_k^{(\alpha)}=\left(1-\frac{\alpha+1}{k}\right)w_{k-1}^{(\alpha)},\quad k=1,2,3,\cdots. \tag{8.115}$$

Define $\Delta t=h$ to be a grid size in time dimension where $h=t/M$, $t_i=ih$ for $i=0,\ldots,M$, $y_j=j\Delta y$ where $\Delta y=L/N$ for $j=0,\ldots,N$. Let $\theta_{i,j}$ and $u_{i,j}$ be the numerical approximation to $\theta(t_i,y_j)$ and $u(t_i,y_j)$, respectively.

A universal numerical discretization method, the explicit finite difference method, is used for Eqs. (8.108) and (8.109), yielding:

$$\frac{u_{i+1,j}-u_{i,j}}{h}+\lambda h^{-(\alpha+1)}\sum_{k=0}^{i}\omega_k^{(\alpha+1)}u_{i-k+1,j}=e^{-b\theta_{i,j}}\frac{u_{i+1,j+1}-2u_{i+1,j}+u_{i+1,j-1}}{\Delta y^2} \tag{8.116}$$
$$-be^{-b\theta_{i,j}}\frac{\theta_{i,j+1}-\theta_{i,j}}{\Delta y}\frac{u_{i+1,j+1}-u_{i+1,j}}{\Delta y}-\frac{\phi}{Da}e^{-b\theta_{i,j}}u_{i+1,j}$$

$$\mathrm{Pr}\frac{\theta_{i+1,j}-\theta_{i,j}}{h}+\mathrm{Pr}\lambda_T h^{-(\beta+1)}\sum_{k=0}^{i}\omega_k^{(\beta+1)}\theta_{i-k+1,j}$$
$$=\frac{\theta_{i+1,j+1}-2\theta_{i+1,j}+\theta_{i+1,j-1}}{\Delta y^2}+Me^{-b\theta_{i,j}}\left(u_{i+1,j}+\lambda_T h^{-\beta}\sum_{k=0}^{i}\omega_k^{(\beta)}\theta_{i-k+1,j}\right) \tag{8.117}$$

In view of Eqs. (8.116) and (8.117), we obtain:

$$\frac{e^{-b\theta_{i,j}}\left(b\theta_{i,j+1}-b\theta_{i,j}-1\right)}{\Delta y^2}u_{i+1,j+1}$$
$$+\left(\frac{1}{h}+\lambda h^{-(\alpha+1)}+\frac{e^{-b\theta_{i,j}}\left(2-b\theta_{i,j+1}+b\theta_{i,j}+\frac{\phi}{Da}\Delta y^2\right)}{\Delta y^2}\right)u_{i+1,j} \tag{8.118}$$
$$-\frac{e^{-b\theta_{i,j}}}{\Delta y^2}u_{i+1,j-1}=\frac{1}{h}u_{i,j}-\lambda h^{-(\alpha+1)}\sum_{k=1}^{i}\omega_k^{(\alpha+1)}u_{i-k+1,j}$$

$$-\frac{1}{\Delta y^2}\theta_{i+1,j+1}+\left(\frac{\mathrm{Pr}}{h}+\mathrm{Pr}\lambda_T h^{-(\beta+1)}\omega_0^{(\beta+1)}+\frac{2}{\Delta y^2}\right)\theta_{i+1,j}-\frac{1}{\Delta y^2}\theta_{i+1,j-1}$$
$$=\frac{\mathrm{Pr}}{h}\theta_{i,j}-\mathrm{Pr}\lambda_T h^{-(\beta+1)}\sum_{k=1}^{i}\omega_k^{(\beta+1)}\theta_{i-k+1,j}+Me^{-b\theta_{i,j}}\left(u_{i+1,j}+\lambda_T h^{-\beta}\sum_{k=0}^{i}\omega_k^{(\beta)}\theta_{i-k+1,j}\right), \tag{8.119}$$

where $\alpha=0.5$, $\beta=0.7$, $\omega=3$, $\mathrm{Pr}=15$, $\lambda=5$, $\lambda_T=3$, $\theta_0=5$, $b=0.1$, $M=450$, $\phi=0.1$, $Da=5$ subject to the initial and boundary conditions:

$$u_{0,j}=0,\quad \theta_{0,j}=0\quad \text{for}\quad j=0,\ldots,N, \tag{8.120}$$

$$u_{i,0}=1,\quad u_{i,N}=0,\quad \text{for}\quad i=0,\ldots,M, \tag{8.121}$$

$$\theta_{i,0}=\theta_0\cos(\omega\cdot hi),\quad \theta_{i,N}=0,\quad \text{for}\ i=0,\ldots,M. \tag{8.122}$$

8.4.4 Results and Discussion

The coupled governing nonlinear partial differential equations of the flow and heat transfer of a generalized fractional Maxwell fluid in porous medium are investigated. The motion is due to the longitudinal speed and the energy transmission is due to oscillating boundary condition. The modified Fourier's law, modified Darcy's law, and temperature-dependent variable fluid viscosity are taken into account in coupled velocity and temperature fields. Numerical computations are performed by using an efficient implicit finite difference method based on nonshifted Grünwald formula. In order to study the characteristics of velocity and temperature fields, some numerical results are plotted and presented in Figs. 8.24−8.33.

Fig. 8.24 shows the effects of variable viscosity parameter b on velocity and temperature fields distributions. The results indicate that, for all other parameters fixed, increasing b reduces fluid viscosity, which in turn results in an increasing fluid flow (Fig. 8.24A). In the same periods of fluctuation interval, the fluid viscosity is low if the initial temperature is positive, and therefore the drag effect from lower layer to the upper fluid is low. The difference of speed is very large in the internal close to the left end point, such as in the range of about 0−0.02. On the contrary, the viscosity is relatively large when the initial temperature is negative, the drag effects from lower layer to the upper fluid are high, and therefore the difference of speed is not too large, the flow rate is relatively stable near the position of the left end point, such as for internal of 0.3−0.4. As b increases, the performance of this phenomenon will be more obvious. Fig. 8.24B shows the heat transfer slows down with increasing viscosity effects.

Fig. 8.25 indicates temperature and velocity fields characteristics with increasing time. In this research, we consider the cycle is $2\pi/3$ in the boundary of temperature equation. The initial values of temperature are positive when $t = 2, 6, 10$, which belongs to $[3\pi/2 + 2k\pi, 2\pi + 2k\pi]$. It can be seen from Fig. 8.25A, the velocity increases as time increases, which satisfies the boundary conditions. In Fig. 8.25B, the heat transfer is oscillatory attenuated with the increase of time.

Fig. 8.26 shows the effects of different values of fractional parameter α on the velocity field and temperature field distributions. It is seen that the velocity profile decreases rapidly at the position close to $y = 0$ where the influence of temperature is strong. But, the fluid velocity decreases slowly as α increases when the fluid is away from $y = 0$. Fig. 8.27 displays the effects of fractional parameter β on temperature and velocity profiles. It indicates that the amplitude of fluctuation of temperature profile increases with increasing β in Fig. 8.27B. Meanwhile, the velocity shows a jump decreasing trend due to the increase of temperature oscillation amplitude. When the temperature is negative, the fluid viscosity is strong and the velocity tends to decrease slightly for the upper fluid can move with the

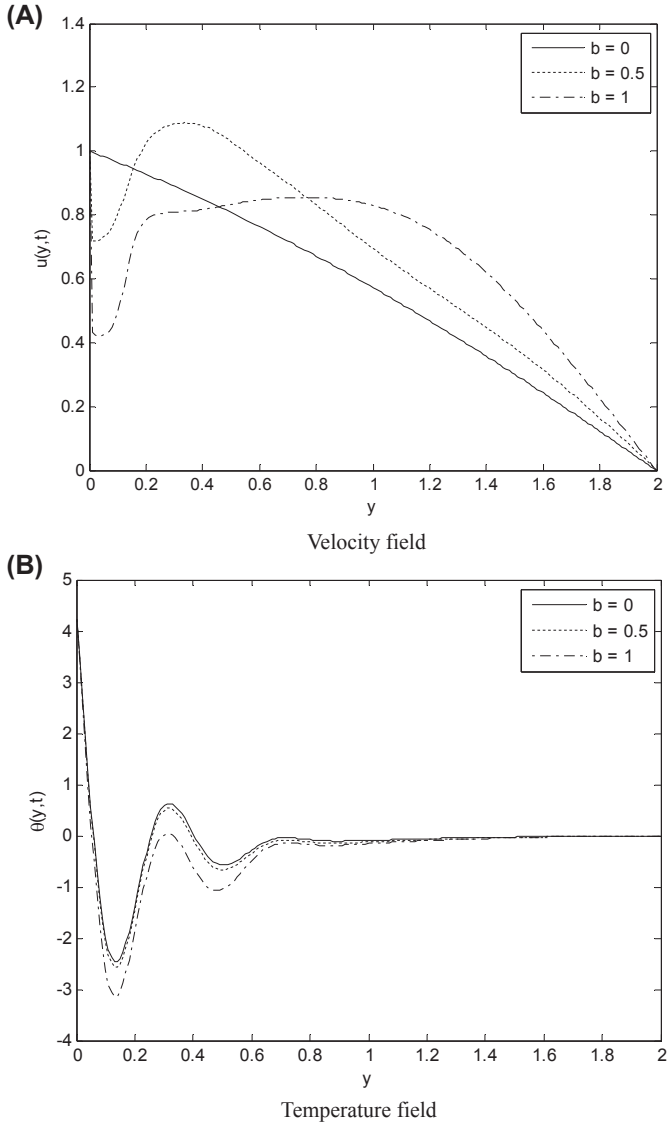

FIGURE 8.24 (A and B) Velocity and temperature profiles for different values of parameter *b*.

lower fluid. Whereas, it is obvious that when the temperature is positive, the fluid viscosity decreases and the velocity tends to increase with the temperature.

The effects of material constant λ and λ_T on the coupled velocity and temperature fields are presented in Figs. 8.28 and 8.29. It is seen from the

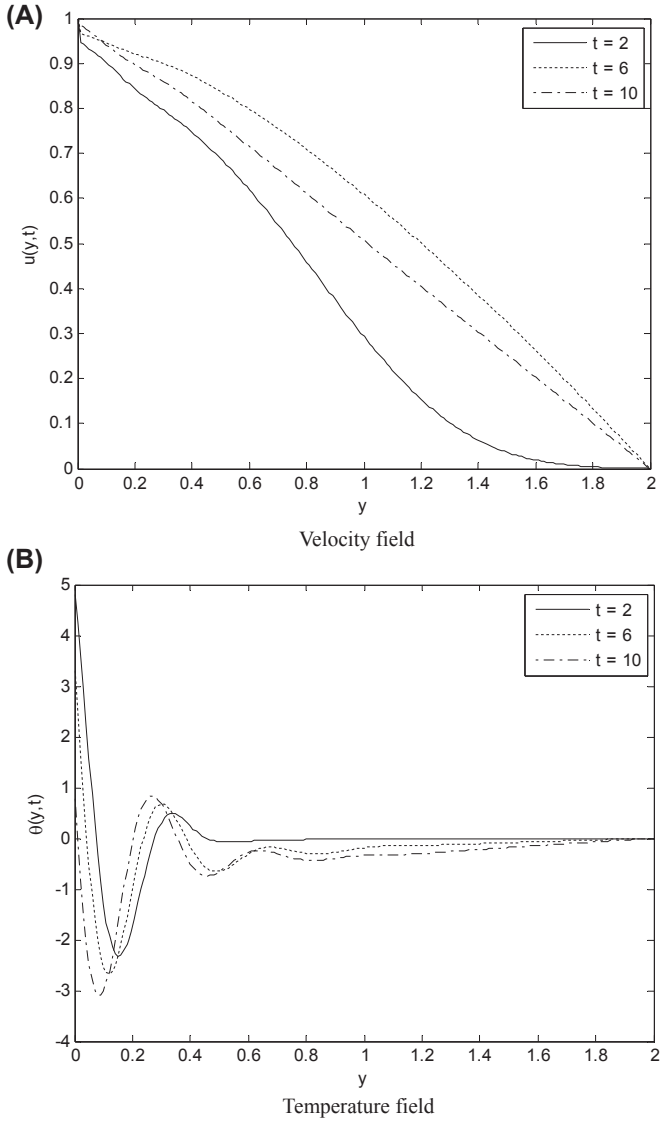

FIGURE 8.25 (A and B) Velocity and temperature profiles for values of time *t*.

figures that the transfer processes of velocity and heat transfer are accelerative with two parameters increasing, particularly near the boundary.

Fig. 8.30 displays the impact of porosity ϕ on velocity and temperature profiles. It can be seen that the velocity and temperature become bigger in the same position as the porosity decreases. On the contrary, Fig. 8.31 indicates

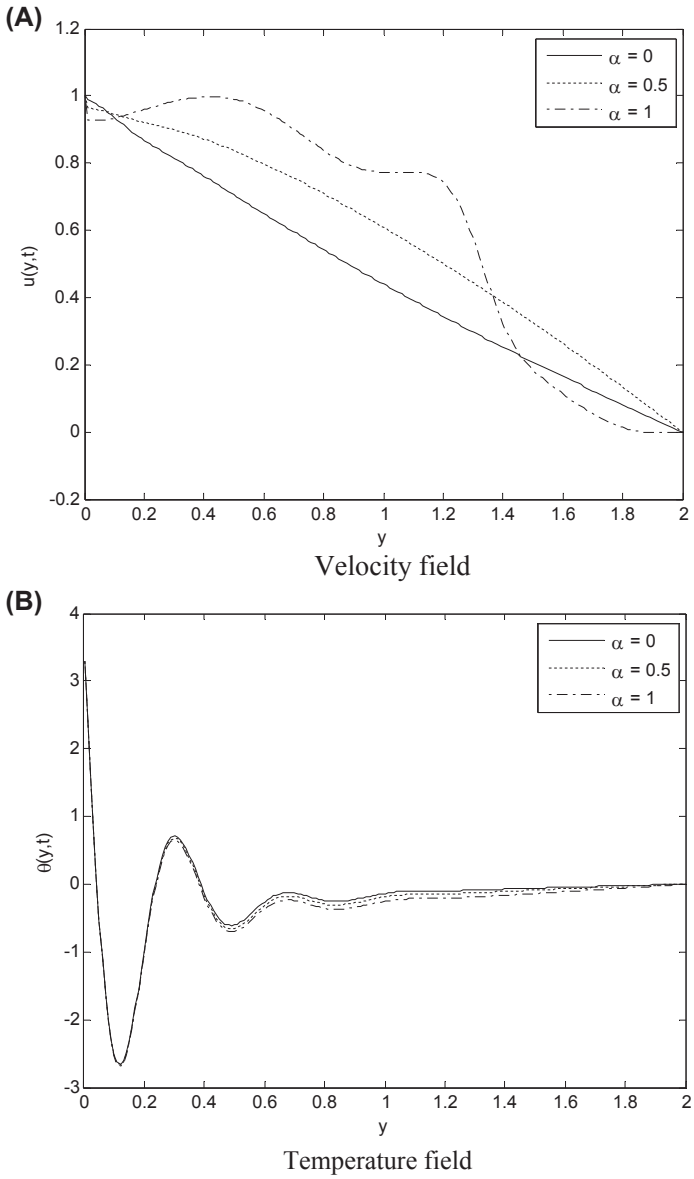

FIGURE 8.26 (A and B) Velocity and temperature profiles for values of fractional parameter α.

that the Darcy's parameter *Da* has an opposite effects on velocity and temperature profiles comparing with Fig. 8.30. It is seen from Fig. 8.32, comparing to the permeability, the Prandtl number has a similar but more pronounced effect on velocity and temperature distributions. Fig. 8.33 shows

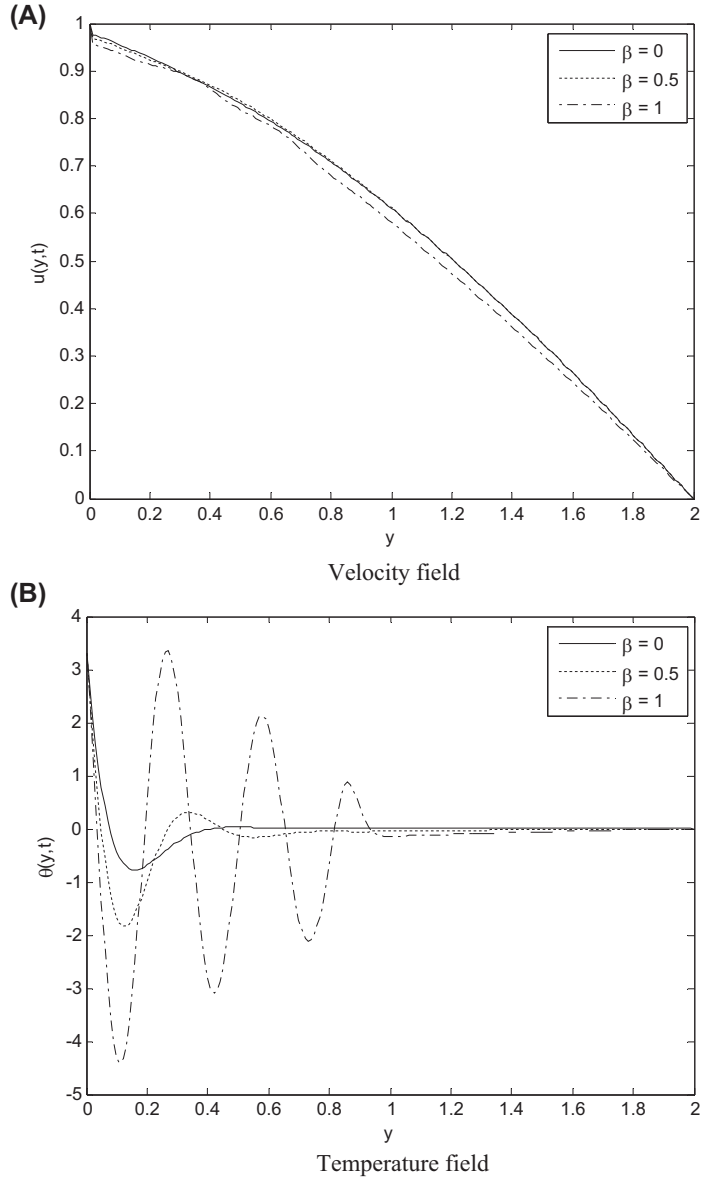

FIGURE 8.27 (A and B) Velocity and temperature profiles for values of fractional parameter β.

the effects of boundary temperature oscillations on velocity and temperature fields. With the frequency increases, the temperature fluctuations show an increasing fluctuation and the flow of fluid shows a more obvious jumping phenomenon.

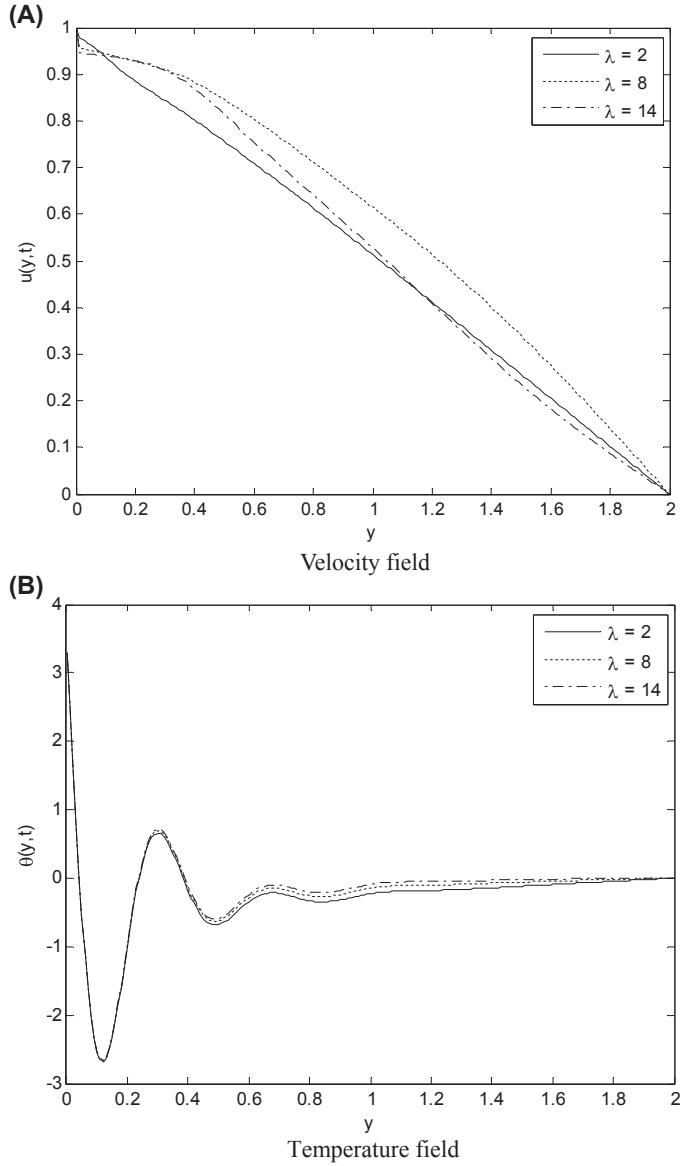

FIGURE 8.28 (A and B) Velocity and temperature fields for values parameter λ.

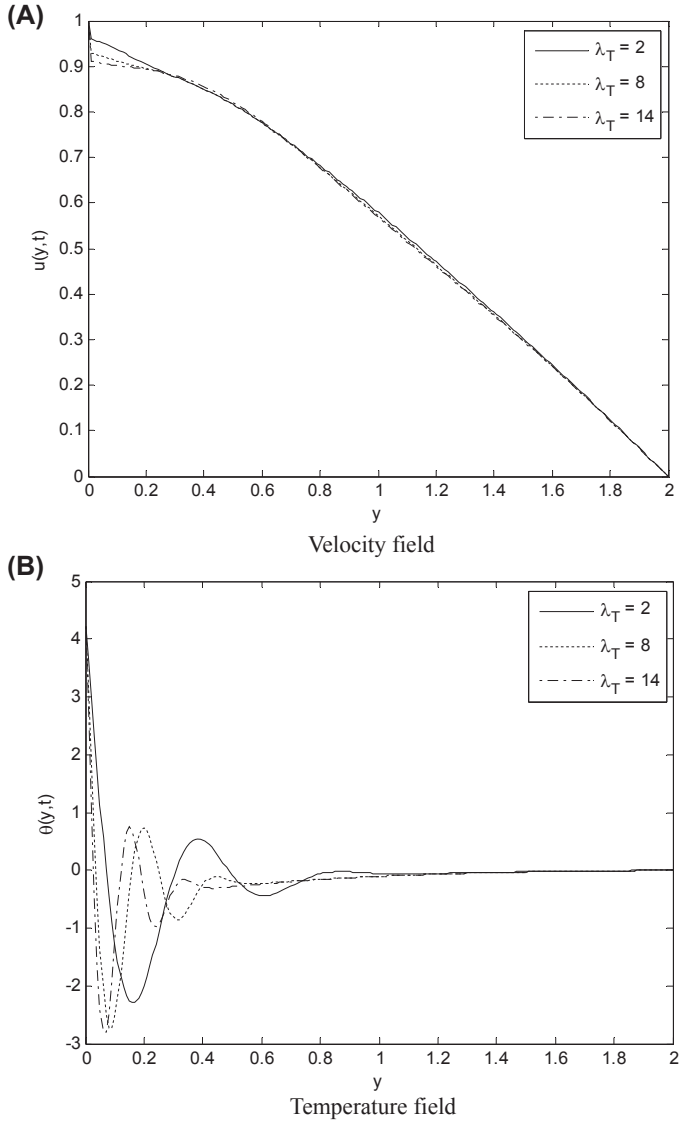

FIGURE 8.29 (A and B) Velocity and temperature profiles for values of parameter λ_T.

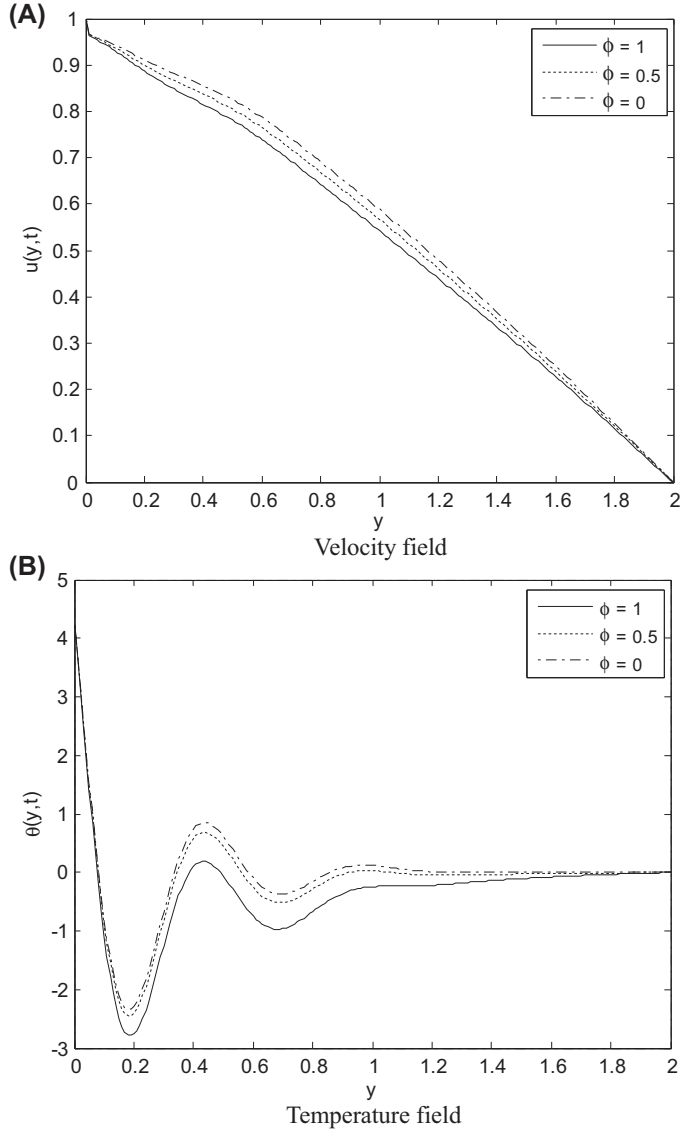

FIGURE 8.30 (A and B) Velocity and temperature profiles for different values of parameter ϕ.

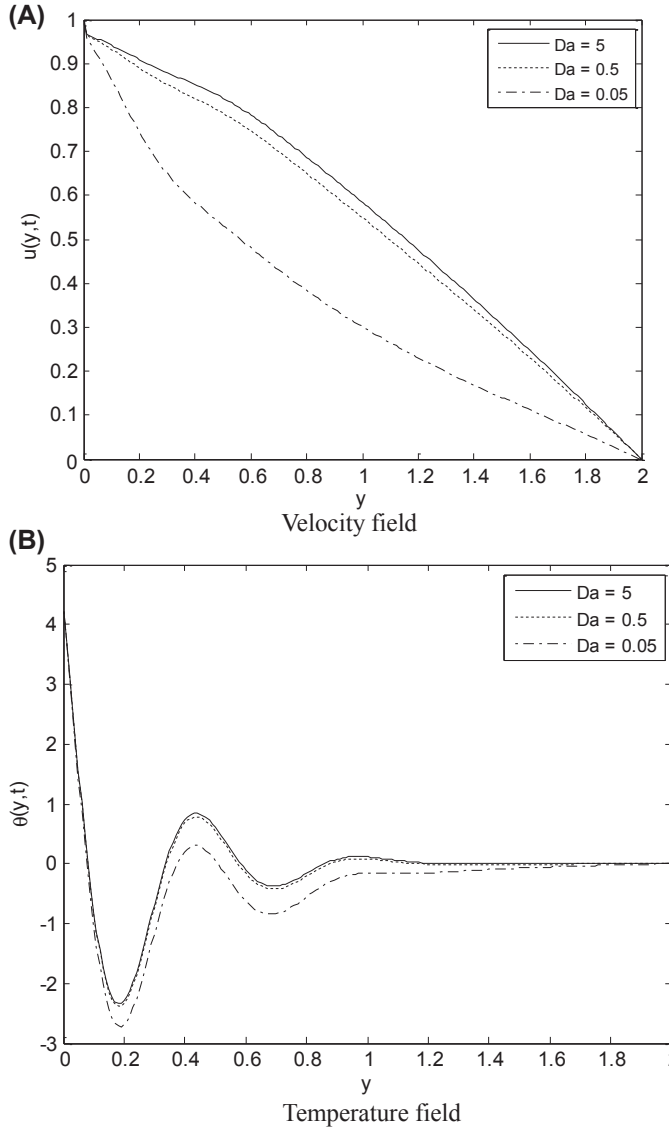

FIGURE 8.31 (A and B) Velocity and temperature profiles for different values of parameter *Da*.

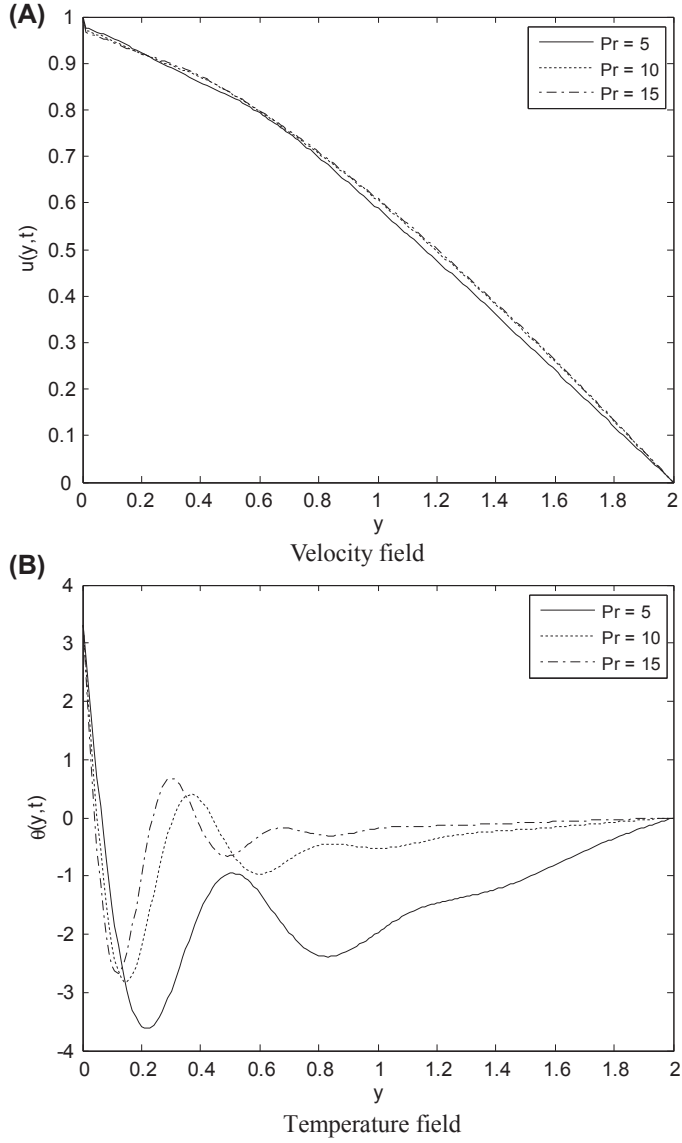

FIGURE 8.32 (A and B) Velocity and temperature profiles for different values of parameter Pr.

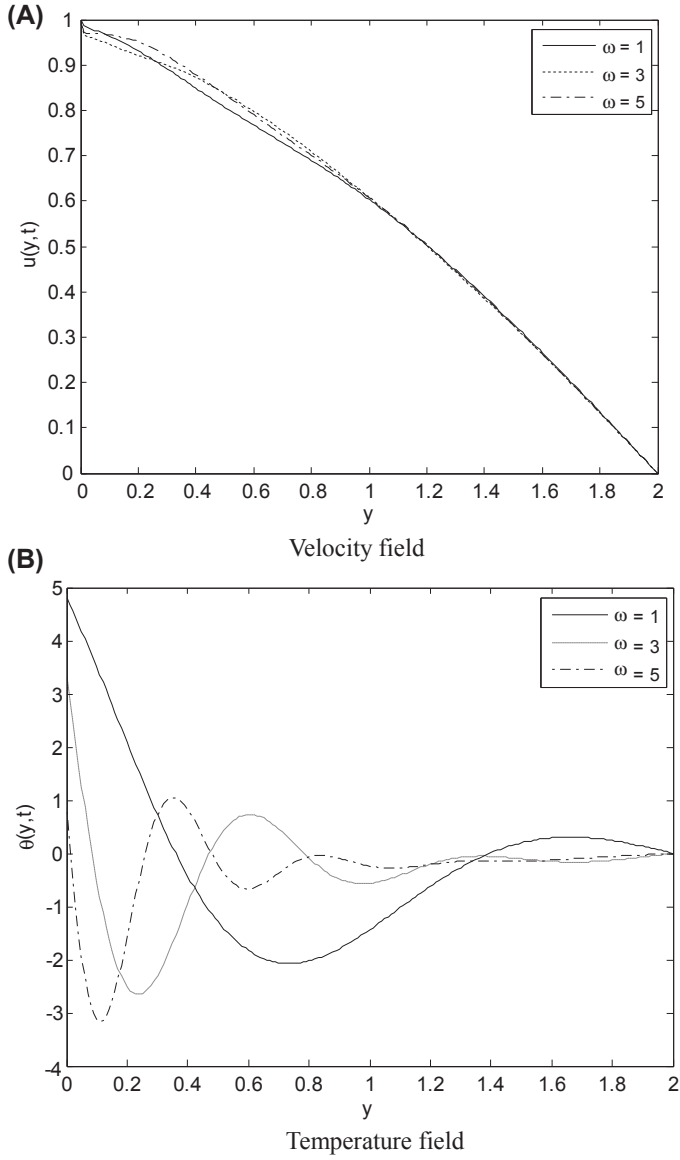

FIGURE 8.33 (A and B) Velocity and temperature profiles for different values of parameter ω.

8.5 UNSTEADY NATURAL CONVECTION HEAT TRANSFER OF FRACTIONAL MAXWELL FLUID

8.5.1 Background of the Problem

Natural convection is a mechanism of heat transportation in which the fluid motion is not generated by an external source. Instead the fluid motion is caused by buoyancy, the difference in fluid density occurring due to temperature gradients. Recently, natural convection has attracted much attentions from researchers because its wide applications both in nature and engineering technology.

In classical study on viscoelastic fluids, researchers commonly ignored the effects of nonlinear convection and dealt only with the cases when the governing equations are linear. In this research, we present an investigation for unsteady boundary layer natural convection heat transfer of Maxwell viscoelastic fluid over a vertical plate. The fractional boundary layer governing equations are first formulated and derived. From such derivation, the model constitutes nonlinear coupled equations with mixed time-space derivatives in the convection terms, which are solved by a newly developed finite difference method combined with an L1-algorithm. The effects of fractional derivative orders on velocity and temperature fields are graphically presented and analyzed in detail. Results show that both the velocity and temperature boundary layer manifest a short-term memory and basic relaxation time characteristics.

8.5.2 Mathematical Formulation

The constitutive equation of viscoelastic fluid with fractional Maxwell model is given by Podlubny (1999), Friedrich (1991), and Friedrich and Braun (1992):

$$\sigma + \lambda^{\alpha} \frac{d^{\alpha}\sigma}{dt^{\alpha}} = \mu \frac{d^{\gamma}\varepsilon}{dt^{\gamma}}, \quad 0 \le \alpha \le \gamma \le 1, \tag{8.123}$$

where σ, ε, λ, and μ are the shear stress, shear strain, relaxation time, and viscosity, respectively, and α and γ are fractional parameters. d^{α}/dt^{α} and d^{γ}/dt^{γ} are the Caputo fractional derivative operators and the fractional derivative of order α is defined as (Podlubny, 1999):

$$\frac{d^{\alpha}}{dt^{\alpha}} f(t) = \frac{1}{\Gamma(1-\alpha)} \int_0^t \frac{\partial f(\eta)}{\partial \eta} \frac{d\eta}{(t-\eta)^{\alpha}}, \tag{8.124}$$

where $\Gamma(\cdot)$ is the Gamma function. Friedrich and Braun (1992) proved that this kind of rheological constitutive equation shows fluid-like behavior only in the case of $\gamma = 1$ and α is variable, i.e.:

$$\sigma + \lambda^{\alpha} \frac{d^{\alpha}\sigma}{dt^{\alpha}} = \mu \frac{d\varepsilon}{dt}, \quad 0 \le \alpha \le 1. \tag{8.125}$$

Eq. (8.125) is known as the constitutive relation of fractional Maxwell fluid. It should be noted that while $\alpha = 0$ and $\alpha = 1$, it is simplified as the classical Newtonian fluid and ordinary Maxwell model, respectively.

We consider here the two-dimensional unsteady laminar boundary layer natural convection flow and heat transfer over a vertical plate, with x being the coordinate along the plate and y perpendicular to the plate. The viscous dissipation is assumed to be neglected. The constitutive relation becomes (Zhao et al., 2016):

$$\sigma_{xy} + \lambda^{\alpha}\frac{\partial^{\alpha}\sigma_{xy}}{\partial t^{\alpha}} = \mu\frac{\partial u}{\partial y}. \tag{8.126}$$

The momentum equation is:

$$\rho\frac{\partial u}{\partial t} + \rho u\frac{\partial u}{\partial x} + \rho v\frac{\partial u}{\partial y} = \frac{\partial \sigma_{xy}}{\partial y} + \rho g\beta_f(T - T_{\infty}). \tag{8.127}$$

Combining Eq. (8.126) and (8.127), we obtained the basic fractional boundary layer governing equation:

$$\begin{aligned}&\frac{\partial u}{\partial t} + u\frac{\partial u}{\partial x} + v\frac{\partial u}{\partial y} + \lambda_1^{\alpha}\frac{\partial^{\alpha+1}u}{\partial t^{\alpha+1}} + \lambda_1^{\alpha}\frac{\partial^{\alpha}}{\partial t^{\alpha}}\left(u\frac{\partial u}{\partial x}\right) + \lambda_1^{\alpha}\frac{\partial^{\alpha}}{\partial t^{\alpha}}\left(v\frac{\partial u}{\partial y}\right)\\ &\quad = \nu\frac{\partial^2 u}{\partial y^2} + \lambda_1^{\alpha}\frac{\partial^{\alpha}}{\partial t^{\alpha}}(\beta_f g(T - T_{\infty})) + \beta_f g(T - T_{\infty}).\end{aligned} \tag{8.128}$$

Similarly, the energy equation can be described with fractional derivatives as:

$$\frac{\partial T}{\partial t} + u\frac{\partial T}{\partial x} + v\frac{\partial T}{\partial y} + \lambda_2^{\beta}\frac{\partial^{\beta+1}T}{\partial t^{\beta+1}} + \lambda_2^{\beta}\frac{\partial^{\beta}}{\partial t^{\beta}}\left(u\frac{\partial T}{\partial x}\right) + \lambda_2^{\beta}\frac{\partial^{\beta}}{\partial t^{\beta}}\left(v\frac{\partial T}{\partial y}\right) = \alpha_f\frac{\partial^2 T}{\partial y^2}, \tag{8.129}$$

where variables u, v, and T are velocity components and temperature, respectively; β_f, ν, and α_f are the volumetric thermal expansion coefficient, dynamic viscosity, and thermal diffusion coefficient of the viscoelastic fluid, respectively; λ_2 is the relaxation time of heat conduction; and α and β are the velocity and temperature fractional derivative parameter, respectively.

The initial and boundary conditions are:

$$t \le 0: \ u = 0, \ v = 0, \ T = T_{\infty}; \ t > 0: \ u = 0, \ v = 0, \ T = T_w \ \text{at} \ x = 0;$$

$$u = 0, \ T = T_{\infty} \ \text{at} \ y = 0; \ u \to 0, \ T \to T_{\infty} \ \text{as} \ y \to \infty.$$

Introducing the following dimensionless variables:

$$x^* = \frac{x}{L},\ y^* = \frac{y}{L}Gr^{1/4},\ u^* = \frac{uL}{\nu}Gr^{-1/2},\ v^* = \frac{vL}{\nu}Gr^{-1/4},\ t^* = \frac{\nu t}{L^2}Gr^{1/2},\ \theta = \frac{T - T_\infty}{T_w - T_\infty},$$

$$Gr = \frac{gL^3\beta_f(T_w - T_\infty)}{\nu^2},\ \Pr = \frac{\nu}{\alpha_f},\ \lambda_1^* = \frac{\nu\lambda_1}{L^2}Gr^{1/2},\ \lambda_2^* = \frac{\nu\lambda_2}{L^2}Gr^{1/2},$$

where L is the length of the vertical plate.

We obtained the dimensionless governing equations (for brevity the dimensionless mart "*" is omitted hereafter):

$$\frac{\partial u}{\partial x} + \frac{\partial v}{\partial y} = 0, \tag{8.130}$$

$$\frac{\partial u}{\partial t} + u\frac{\partial u}{\partial x} + v\frac{\partial u}{\partial y} + \lambda_1^\alpha \frac{\partial^{\alpha+1}u}{\partial t^{\alpha+1}} + \lambda_1^\alpha \frac{\partial^\alpha}{\partial t^\alpha}\left(u\frac{\partial u}{\partial x}\right) + \lambda_1^\alpha \frac{\partial^\alpha}{\partial t^\alpha}\left(v\frac{\partial u}{\partial y}\right) = \frac{\partial^2 u}{\partial y^2} + \lambda_1^\alpha \frac{\partial^\alpha \theta}{\partial t^\alpha} + \theta. \tag{8.131}$$

$$\frac{\partial \theta}{\partial t} + u\frac{\partial \theta}{\partial x} + v\frac{\partial \theta}{\partial y} + \lambda_2^\beta \frac{\partial^{\beta+1}\theta}{\partial t^{\beta+1}} + \lambda_2^\beta \frac{\partial^\beta}{\partial t^\beta}\left(u\frac{\partial \theta}{\partial x}\right) + \lambda_2^\beta \frac{\partial^\beta}{\partial t^\beta}\left(v\frac{\partial \theta}{\partial y}\right) = \frac{1}{\Pr}\frac{\partial^2 \theta}{\partial y^2}. \tag{8.132}$$

The dimensionless initial and boundary conditions are:

$$t \le 0:\ u = 0,\ v = 0,\ \theta = 0;\ t > 0:\ u = 0,\ v = 0,\ \theta = 0 \text{ at } x = 0;$$

$$u = 0,\ v = 0,\ \theta = 1 \text{ at } y = 0;\ u \to 0,\ \theta = 0 \text{ as } y \to \infty.$$

It is seen that, when the fractional Maxwell model is introduced, the formulated boundary layer governing equations have nonlinear fractional mixed derivative in the convection terms, which are difficult to solve. We need to develop new numerical method and technique.

8.5.3 Numerical Algorithms

In this section we present the method to solve the nonlinear coupled equations with fractional mixed derivative and compare the particular cases derived from our model with classical results of Ostrach (1953).

8.5.3.1 Discretization Method

Define $x_i = i\Delta x,\ i = 0,\ 1,\ 2,\cdots,\ M,\ y_j = j\Delta y,\ j = 0,\ 1,\ 2,\cdots,\ N;\ t_k = k\Delta t,$ $k = 0, 1, 2,\cdots, R$, where $\Delta x = L/M$ and $\Delta y = Y_{max}/N$ are space steps, Δt is the time step. $u_{i,j}^k$ is the numerical solution of Eqs. (8.130)−(8.132) at the mesh point (x_i, y_j, t_k).

First, L1-algorithm is introduced to discretize the time fractional derivative ($0 < \alpha < 1$) as (Liu et al., 2007):

$$\begin{aligned}\frac{\partial^{\alpha} f(t_k)}{\partial t^{\alpha}} &= \frac{\Delta t^{-\alpha}}{\Gamma(2-\alpha)} \sum_{s=0}^{k-1} \alpha_s \left[f(t_{k-s}) - f(t_{k-s-1}) \right] + O\left(\Delta t^{2-\alpha}\right) \\ &= \frac{\Delta t^{-\alpha}}{\Gamma(2-\alpha)} \left[f(t_k) - \alpha_{k-1} f(t_0) - \sum_{s=1}^{k-1} (\alpha_{s-1} - \alpha_s) f(t_{k-s}) \right] \\ &\quad + O\left(\Delta t^{2-\alpha}\right),\end{aligned} \tag{8.133}$$

where $\alpha_s = (s+1)^{1-\alpha} - s^{1-\alpha}$, $s = 0, 1, 2, \ldots, R$.

Referring to properties of Caputo time fractional derivatives, the following relationship is established:

$$\partial^{\alpha+1} f(t_k) / \partial t^{\alpha+1} = \partial^{\alpha} f'(t_k) / \partial t^{\alpha}, \tag{8.134}$$

where $f'(t_k) = [f(t_k) - f(t_{k-1})]/\Delta t$ is the backward difference of time.

Second, the integer-order terms in the governing equations are discretized as (Ganesan and Palani, 2004):

$$\left.\frac{\partial u}{\partial t}\right|_{t=t_k} = \frac{u\left(x_i, y_j, t_k\right) - u\left(x_i, y_j, t_{k-1}\right)}{\Delta t} + O(\Delta t), \tag{8.135}$$

$$\left. u \frac{\partial u}{\partial x}\right|_{t=t_k} = u\left(x_i, y_j, t_{k-1}\right) \frac{u\left(x_i, y_j, t_k\right) - u\left(x_{i-1}, y_j, t_k\right)}{\Delta x} + O(\Delta x), \tag{8.136}$$

$$\left. v \frac{\partial u}{\partial y}\right|_{t=t_k} = v\left(x_i, y_j, t_{k-1}\right) \frac{u\left(x_i, y_j, t_k\right) - u\left(x_i, y_{j-1}, t_k\right)}{\Delta y} + O(\Delta y), \tag{8.137}$$

$$\left.\frac{\partial^2 u}{\partial y^2}\right|_{t=t_k} = \frac{u_{i,j+1}^{k} - 2u_{i,j}^{k} + u_{i,j-1}^{k} + u_{i,j+1}^{k-1} - 2u_{i,j}^{k-1} + u_{i,j-1}^{k-1}}{2\Delta y^2} + O\left(\Delta y^2\right), \tag{8.138}$$

Third, Eqs. (8.135)–(8.137) are substituted into the fractional derivatives (Lynch et al., 2003):

$$\frac{\partial^{\alpha+1} u\left(x_i, y_j, t_k\right)}{\partial t^{\alpha+1}} = \frac{\Delta t^{-1-\alpha}}{\Gamma(2-\alpha)} \left[u_{i,j}^{k} - u_{i,j}^{k-1} - \sum_{s=1}^{k-1} (\alpha_{s-1} - \alpha_s) \left(u_{i,j}^{k-s} - u_{i,j}^{k-s-1} \right) \right], \tag{8.139}$$

$$\frac{\partial^\alpha}{\partial t^\alpha}\left(u\frac{\partial u}{\partial x}\right)=\frac{\Delta t^{-\alpha}}{\Delta x\Gamma(2-\alpha)}\left[u_{i,j}^{k-1}\left(u_{i,j}^{k}-u_{i-1,j}^{k}\right)-\sum_{s=1}^{k-1}(\alpha_{s-1}-\alpha_s)u_{i,j}^{k-s-1}\left(u_{i,j}^{k-s}-u_{i-1,j}^{k-s}\right)\right], \tag{8.140}$$

where the truncation error is $O(\Delta t^{2-\alpha}+\Delta x)$.

$$\frac{\partial^\alpha}{\partial t^\alpha}\left(v\frac{\partial u}{\partial y}\right)=\frac{\Delta t^{-\alpha}}{\Delta y\Gamma(2-\alpha)}\left[v_{i,j}^{k-1}\left(u_{i,j}^{k}-u_{i,j-1}^{k}\right)-\sum_{s=1}^{k-1}(\alpha_{s-1}-\alpha_s)v_{i,j}^{k-s-1}\left(u_{i,j}^{k-s}-u_{i,j-1}^{k-s}\right)\right], \tag{8.141}$$

where the truncation error is $O(\Delta t^{2-\alpha}+\Delta y)$.

Similar difference process is dealt with dimensionless temperature terms. Note,

$$r_1=\frac{\lambda_1^\alpha\Delta t^{-\alpha}}{\Gamma(2-\alpha)},\ r_2=\frac{\Delta t}{2\Delta y^2},\ r_3=\frac{\lambda_2^\beta\Delta t^{-\beta}}{\Gamma(2-a)},\ r_4=\frac{\Delta t}{2\mathrm{Pr}\Delta y^2},$$

$$A_1=\sum_{s=1}^{k-1}(\alpha_{s-1}-\alpha_s)\left(u_{i,j}^{k-s}-u_{i,j}^{k-s-1}\right),\ A_2=\sum_{s=1}^{k-1}(\alpha_{s-1}-\alpha_s)u_{i,j}^{k-s-1}\left(u_{i,j}^{k-s}-u_{i-1,j}^{k-s}\right),$$

$$A_3=\sum_{s=1}^{k-1}(\alpha_{s-1}-\alpha_s)v_{i,j}^{k-s-1}\left(u_{i,j}^{k-s}-u_{i,j-1}^{k-s}\right),\ A_4=\theta_{i,j}^{k}-\sum_{s=1}^{k-1}(\alpha_{s-1}-\alpha_s)\theta_{i,j}^{k-s},$$

$$C_1=\sum_{q=1}^{k-1}(b_{q-1}-b_q)\left(\theta_{i,j}^{k-q}-\theta_{i,j}^{k-q-1}\right),\ C_2=\sum_{q=1}^{k-1}(b_{q-1}-b_q)u_{i,j}^{k-q-1}\left(\theta_{i,j}^{k-q}-\theta_{i-1,j}^{k-q}\right),$$

$$C_3=\sum_{q=1}^{k-1}(b_{q-1}-b_q)v_{i,j}^{k-q-1}\left(\theta_{i,j}^{k-q}-\theta_{i,j-1}^{k-q}\right),$$

where $b_q=(q+1)^{1-\beta}-q^{1-\beta}$, $q=0, 1, 2, \ldots, R$.

Thus, the iteration equations are achieved at last in the following form:

$$\begin{aligned}&-(1+r_3)\frac{\Delta t}{\Delta x}u_{i,j}^{k-1}\theta_{i-1,j}^{k}-\left[(1+r_3)\frac{\Delta t}{\Delta y}v_{i,j}^{k-1}+r_4\right]\theta_{i,j-1}^{k}\\&+\left[(1+r_3)\left(1+\frac{\Delta t}{\Delta x}u_{i,j}^{k-1}\right)+(1+r_3)\frac{\Delta t}{\Delta y}v_{i,j}^{k-1}+2r_4\right]\theta_{i,j}^{k}-r_4\theta_{i,j+1}^{k}\\&\quad=r_4\theta_{i,j-1}^{k-1}+(1+r_3-2r_4)\theta_{i,j}^{k-1}+r_4\theta_{i,j+1}^{k-1}+r_3C_1+\frac{\Delta t}{\Delta x}r_3C_2+\frac{\Delta t}{\Delta y}r_3C_3.\end{aligned} \tag{8.142}$$

$$
\begin{aligned}
&-(1+r_1)\frac{\Delta t}{\Delta x}u_{i,j}^{k-1}u_{i-1,j}^{k}-\left[(1+r_1)\frac{\Delta t}{\Delta y}v_{i,j}^{k-1}+r_2\right]u_{i,j-1}^{k}\\
&+\left[(1+r_1)\left(1+\frac{\Delta t}{\Delta x}u_{i,j}^{k-1}\right)-(1+r_1)\frac{\Delta t}{\Delta y}v_{i,j}^{k-1}+2r_2\right]u_{i,j}^{k}-r_2u_{i,j+1}^{k}\\
&\quad=r_2u_{i,j-1}^{k-1}+(1+r_1-2r_2)u_{i,j}^{k-1}+r_2u_{i,j+1}^{k-1}+r_1A_1+\frac{\Delta t}{\Delta x}r_1A_2\\
&\qquad+\frac{\Delta t}{\Delta y}r_1A_3+\Delta t r_1A_4+\frac{\Delta t\left(\theta_{i,j}^{k-1}+\theta_{i,j}^{k}\right)}{2},
\end{aligned}
\tag{8.143}
$$

$$
v_{i,j}^{k}=v_{i,j-1}^{k}+v_{i,j-1}^{k-1}-v_{i,j}^{k-1}+\frac{\Delta y}{2\Delta x}\begin{pmatrix}u_{i-1,j-1}^{k-1}-u_{i,j-1}^{k-1}+u_{i-1,j}^{k-1}-u_{i,j}^{k-1}\\+u_{i-1,j-1}^{k}-u_{i,j-1}^{k}+u_{i-1,j}^{k}-u_{i,j}^{k}\end{pmatrix}.
\tag{8.144}
$$

In the ordinary integer-order systems, the local skin friction coefficient and the Nusselt number, which can be used to measure the surface shear stress and heat transfer effect, respectively, are defined as (Pal and Mandal, 2015):

$$
C_f=\frac{\mu}{\rho u_m^2}\left(\frac{\partial u}{\partial y}\right)_{y=0},\quad Nu_x=-\frac{x}{T_w-T_\infty}\left(\frac{\partial T}{\partial y}\right)_{y=0}.
\tag{8.145}
$$

In the fractional Maxwell model, the local skin friction coefficient and the Nusselt number are derived from the fractional constitutive Eq. (8.125):

$$
C_f+\lambda_1^{\alpha}\frac{\partial^{\alpha}}{\partial t^{\alpha}}C_f=Gr^{-1/4}\left(\frac{\partial u}{\partial y}\right)_{y=0},\quad Nu+\lambda_2^{\beta}\frac{\partial^{\beta}}{\partial t^{\beta}}Nu=-xGr^{1/4}\left(\frac{\partial \theta}{\partial y}\right)_{y=0}.
\tag{8.146}
$$

By solving (8.146) at each time step, the local skin friction coefficient and the Nusselt number in steady state are obtained as t_k reaches the convergence time:

$$
C_f=\left[r_1\sum_{s=1}^{k-1}(\alpha_{s-1}-\alpha_s)C_f(t_{k-s})+Gr^{-1/4}\left(\frac{\partial u}{\partial y}\right)_{y=0}\right]\Big/(1+r_1).
\tag{8.147}
$$

$$
Nu=\left[r_3\sum_{q=1}^{k-1}(\beta_{q-1}-\beta_q)Nu(t_{k-q})-xGr^{1/4}\left(\frac{\partial \theta}{\partial y}\right)_{y=0}\right]\Big/(1+r_3).
\tag{8.148}
$$

Similarly, the average skin friction coefficient and Nusselt number satisfy:

$$
\overline{C_f}+\lambda_1^{\alpha}\frac{\partial^{\alpha}}{\partial t^{\alpha}}\overline{C_f}=Gr^{-1/4}\int_0^1\left(\frac{\partial u}{\partial y}\right)_{y=0}dx,\quad \overline{Nu}+\lambda_2^{\beta}\frac{\partial^{\beta}}{\partial t^{\beta}}\overline{Nu}=-Gr^{1/4}\int_0^1\left(\frac{\partial \theta}{\partial y}\right)_{y=0}dx,
\tag{8.149}
$$

$$\overline{C_f} = \left[r_1 \sum_{s=1}^{k-1} (\alpha_{s-1} - \alpha_s) \overline{C_f}(t_{k-s}) + Gr^{-1/4} \int_0^1 \left(\frac{\partial u}{\partial y} \right)_{y=0} dx \right] \Big/ (1 + r_1). \tag{8.150}$$

$$\overline{Nu} = \left[r_3 \sum_{q=1}^{k-1} (\beta_{q-1} - \beta_q) \overline{Nu}(t_{k-q}) - Gr^{1/4} \int_0^1 \left(\frac{\partial \theta}{\partial y} \right)_{y=0} dx \right] \Big/ (1 + r_3). \tag{8.151}$$

8.5.3.2 Iteration Algorithm

The values of u, v, and θ in the designated domain at time $t = 0$ are obtained from the initial conditions. During any one-time step, the variables of previous time levels, which appear as coefficients or in summation, are treated as constants. The calculations of u, v, and θ at each time level k are conducted in the following order:

Eq. (8.142) at each internal nodal point on a particular i-level, which constitutes a tri-diagonal system of equations, is solved by Thomas algorithm (Carnahan et al., 1969). The (i-1)-level makes a contribution to the right side of the linear equations, where the starting point is from the plate. The values of θ are obtained at each internal nodal point on a particular i at the kth time level. Utilizing the values of θ at the kth time level, together with θ and u in the previous time levels tracing back to the initial time, the values of u at the kth time level are acquired. Then the values of v are solved from Eq. (8.144) at each internal nodal point on a particular i-level. This process is repeated until the designated boundary is reached. Thus, the values of u, v, and θ are obtained at all grid points in the computational domain. The values of C_f, Nu, $\overline{C_f}$, and $\overline{Nu}$ are evaluated in a similar manner, where the integrals are calculated using compound trapezoidal rule. The time process is also repeated until the steady state is reached when the absolute differences between values of velocity u and temperature θ at two consecutive time steps are less than 10^{-4} at all grid points.

8.5.3.3 Reliability Comparison

The computational region is treated as a rectangle with sides $X_{max} = 1$ and $Y_{max} = 12$ (Y_{max} corresponds to $y \to \infty$, which lies very well outside the momentum and thermal boundary layers). The solution matrix is $M \times N$ during one time step, but the whole storage matrix is $M \times N \times R$. As time iteration goes on, the running time increases by geometric ratio for the existence of fractional derivative summations. In comprehensive consideration of solution accuracy and calculation time, the mesh sizes are fixed as

$\Delta x = 0.05$, $\Delta y = 0.1$, and $\Delta t = 0.1$. It has been tested that the finite difference method in this research is conditionally stable, but solutions in the selected mesh sizes are factually stable and convergent.

Fig. 8.34 shows three-dimensional distributions of temperature and velocity by one set of parameters, which demonstrate good stability and convergence in space and time. The special case as $\lambda_1 = \lambda_2 = 0$ is compared with steady integer-order natural convection in Ostrach (1953). The solutions, for three values of Prandtl numbers, are showed in Fig. 8.35. At $X_{max} = 1$, the dimensionless variable u is double the similarity transformation variables f' while the ratio of y/η is $\sqrt[4]{4}$, which is actually assigned to 1.5 in the graphic. The results are in good agreement, which proves that the chosen mesh sizes are relatively reliable and can be utilized in the following computations.

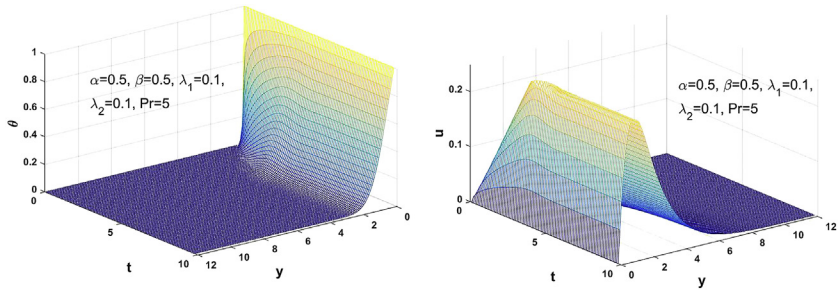

FIGURE 8.34 Three-dimensional distributions of temperature and velocity.

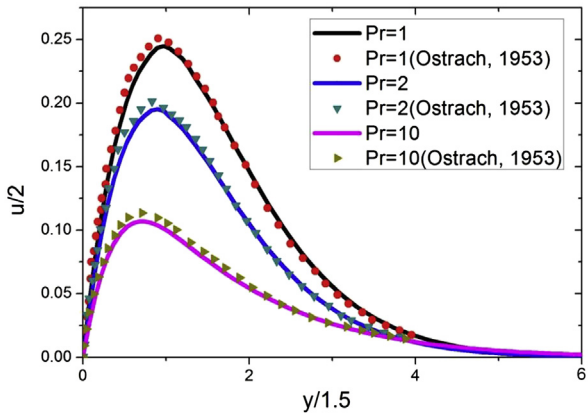

FIGURE 8.35 Comparison with classical solutions of steady natural convection.

8.5.4 Results and Discussion

Without loss of generality, the involved parameters are given as follows: the fractional order α and β are 0, 0.1, 0.2, 0.3, 0.5, and 1, respectively; the relaxation times λ_1 and λ_2 are 0.1, the Prandtl number is fixed to 5, and the Grashof number doesn't take part in the computation and is ignored. The results are compared with classical Newtonian fluid and ordinary Maxwell model when the fractional orders equal 0 and 1, respectively.

8.5.4.1 Effects on Temperature Field

Dimensionless temperature is firstly taken into consideration because the natural convection is driven by temperature gradient. Fig. 8.36 illustrates the temperature profiles at $X_{max} = 1$ in steady state with different values of fractional derivative parameter α. The monotonic decreasing smooth profile can be used to establish the thickness of the thermal boundary layer. It indicates that with the increase of α, the temperature rises and the difference between two adjacent profiles decreases remarkably, while the thermal boundary layer becomes thicker.

The effect of fractional derivative parameter β on temperature field is similar to α, which is shown in Fig. 8.37. It is found that the classical Newtonian fluid has the thinnest thermal boundary layer, while ordinary Maxwell fluid behaves in its weakest capacity in heat conduction. These results demonstrate that fractional order weakens the effect of heat conduction because viscoelasticity strengthens the heat transfer resistance.

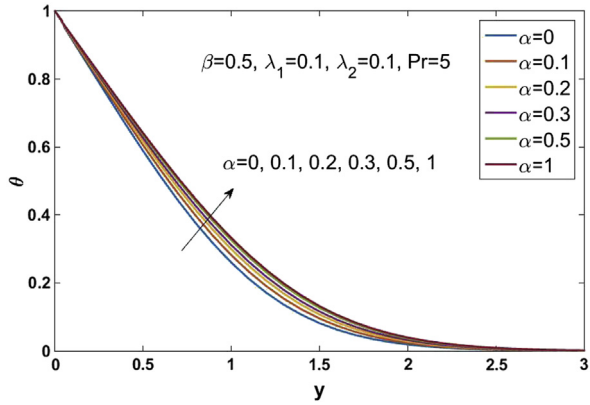

FIGURE 8.36 Temperature distributions for different α.

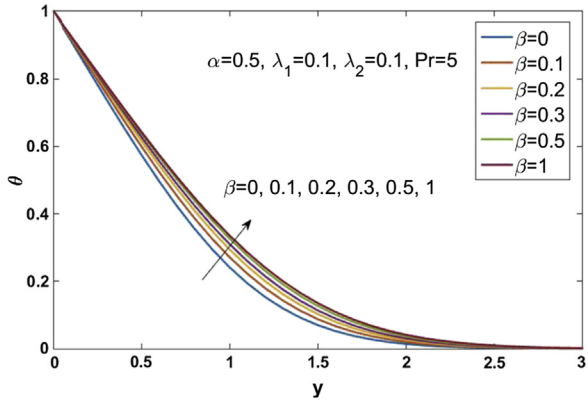

FIGURE 8.37 Temperature distributions for different β.

8.5.4.2 *Effects on Velocity Field*

Fig. 8.38 shows the effects of fractional derivative parameter α on velocity profiles. It indicates that the velocity profile is not a monotonic function of fractional derivative parameter. For each fractional derivative parameter, the velocity profile has a maximum, which is strongly depended on the parameter, i.e., the smaller parameter the fractional derivative parameter is, the bigger peak value of velocity profile is, and the left position to the vertical plate goes. We can also find that the velocity profiles intersect each other for different values of fractional derivative parameter, and the intersection point moves from a far-field region to the vertical plate, which implies that the thickness of the velocity boundary layer rises as the velocity fractional derivative parameter α increases.

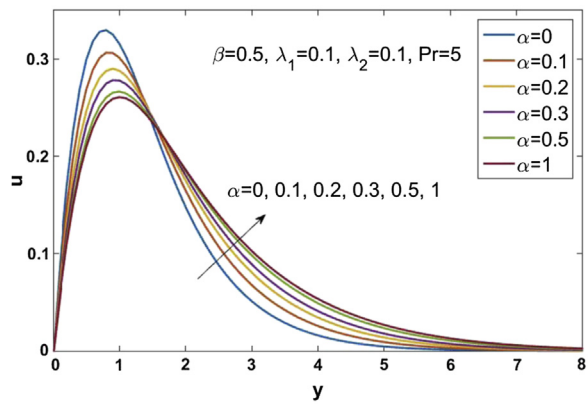

FIGURE 8.38 Velocity distributions for different α.

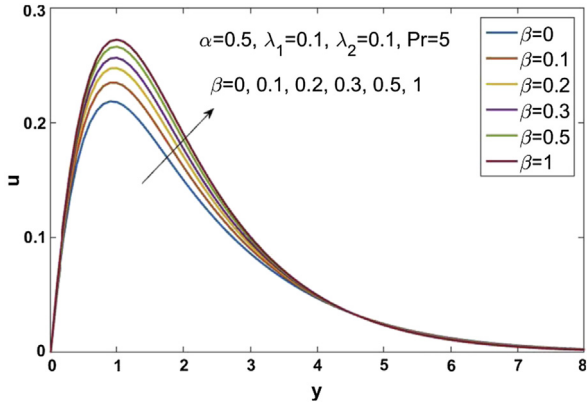

FIGURE 8.39 Velocity distributions for different β.

Fig. 8.39 shows the velocity profiles for different values of temperature fractional derivative parameter β. Similar to Fig. 8.38, it is found that for each β, the velocity profile has a maximum and strongly depends on β. However, the behavior is opposite to cases of the velocity fractional derivative parameter α. It indicates that the smaller parameter β is, the lower the velocity profile is, and the left position to vertical plate goes, which implies the loss of thickness of the velocity boundary layer as the parameter β decreases. Moreover, no intersection points exist for different temperature fractional derivative parameter β.

It is found that the ordinary Maxwell fluid velocity boundary layer has largest thickness, while the classical Newtonian fluid performs best in the natural convection. These results demonstrate that the fractional order weakens the effect of natural convection because viscoelasticity enhances the dynamic viscosity. The effects of α also imply that the fractional equation with relaxation time has a short memory of obvious states and responds slowly to external body force.

8.5.4.3 Effects on Skin Friction Coefficient

Figs. 8.40 and 8.41 illustrate the effects of α and β on average skin friction coefficient, respectively. Results indicate that, for each fractional derivative α, the average skin friction coefficient profile is monotonic increasing. The local skin friction coefficient at $X_{max} = 1$ for different α and β is presented in Tables 8.5 and 8.6. It is found that local and average skin friction coefficient rise with the increase of fractional order α and β. The effect of fractional order is irrelevant with the velocity gradient near the plate in steady state because Figs. 8.38 and 8.39 present contradictory tendency. Actually, from Eqs. (8.147) and (8.150), we know that the skin friction is a comprehensive function of velocity gradient.

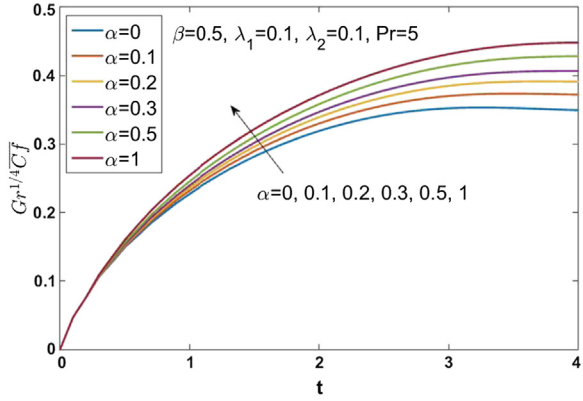

FIGURE 8.40 Average skin friction distributions for different α.

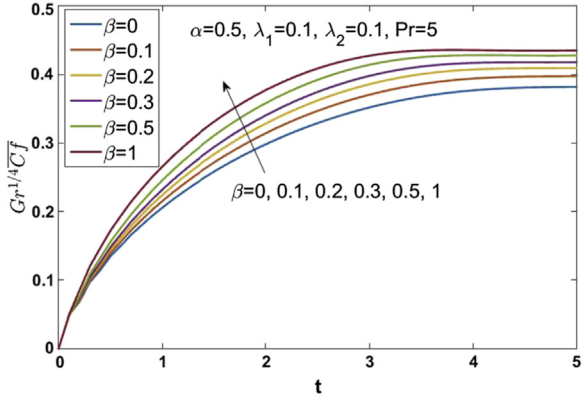

FIGURE 8.41 Average skin friction distributions for different β.

TABLE 8.5 Local Skin Friction Coefficient and Nusselt Number for Different α at $X_{max} = 1$

α	**0**	**0.1**	**0.2**	**0.3**	**0.5**	**1**
$Gr^{1/4}Cf$	0.4648	0.5019	0.5316	0.5531	0.5777	0.5903
$Nu/Gr^{1/4}$	0.7834	0.7556	0.7318	0.7144	0.6951	0.6833

TABLE 8.6 Local Skin Friction Coefficient and Nusselt Number for Different β at $X_{max} = 1$

β	0	0.1	0.2	0.3	0.5	1
$Gr^{1/4}Cf$	0.5126	0.5360	0.5533	0.5652	0.5777	0.5852
$Nu/Gr^{1/4}$	0.4344	0.5144	0.5821	0.6342	0.6951	0.7230

8.5.4.4 *Effects on Nusselt Number*

Figs. 8.42 and 8.43 illustrate the effects of α and β on average Nusselt number, respectively. Similarly, it is seen that, for each fractional derivative β, the average Nusselt number is monotonic decreasing, while for each fractional derivative α is not monotone, declining in early time and increasing until the steady state. The local Nusselt number at $X_{max} = 1$ for different α and β is presented in Tables 8.5 and 8.6. Results demonstrate that the local and average Nusselt number reduce with the increase of fractional derivative parameter α, but rises with the increase of β. This contrary effect of α and β showed that average Nusselt number is no more relevant with the temperature gradient near the plate in Figs. 8.36 and 8.37, but a comprehensive function of temperature gradient tracing back to initial conditions. Moreover, Figs. 8.42 and 8.43 demonstrate that fractional order α has a slight memory of heat conduction and attempts to recover in obvious states, but β degenerates this effect.

Here we study unsteady boundary layer natural convection flow and heat transfer of Maxwell viscoelastic fluid over a vertical plate. The fractional derivative is introduced in Maxwell constitutive model. The fractional

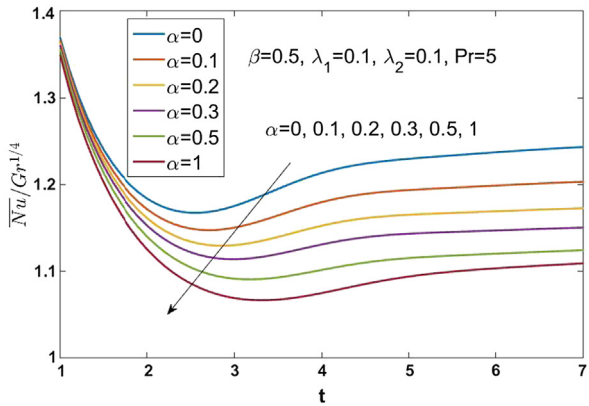

FIGURE 8.42 Average Nusselt number for different α.

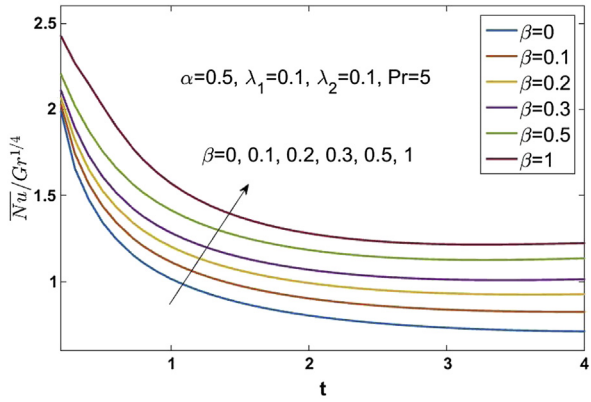

FIGURE 8.43 Average Nusselt number for different β.

boundary layer governing equations are firstly formulated and solved by a newly developed finite difference method combined with an L1-algorithm. The effects of fractional orders α and β are discussed in detail on temperature, velocity, skin friction coefficient, and Nusselt number. Results indicate that the fractional order increases the thickness of velocity and thermal boundary layer and weakens the effect of natural convection and heat conduction. Besides, skin friction coefficient and Nusselt number rise with the augment of α. As β increases, skin friction coefficient rises, but Nusselt number declines.

8.6 FRACTIONAL CONVECTION DIFFUSION WITH CATTANEO–CHRISTOV FLUX

This section presents an investigation for fractional anomalous transport of particles in a comb-like structure. The effects of Cattaneo–Christov flux are taken into account. Formulated fractional governing equation displays a parabolic character for α in (0, 0.5) and the coexisting characteristics of the parabolic and hyperbolic for $\alpha \to 1$ with relaxation parameter effect. When the relaxing parameter equals to zero, the equation reduces a parabolic equation, which is derived from the classical Fick's first law of diffusion. Solutions are obtained numerically by using L1-and L2-approximations for fractional derivative. The effects of the involved parameters on particles distribution behavior are shown graphically and analyzed. Results indicate that the anomalous transport of particles possesses both diffusion and wave characteristics with the existence of relaxation time. Meanwhile, the formation of cusps has been discussed in detail.

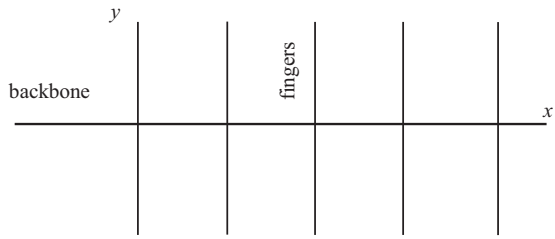

FIGURE 8.44 The sketch framework of comb model.

8.6.1 Fractional Anomalous Diffusion

The research of anomalous diffusion of particles with new constitutive relations has attracted much attention in recent years. A large number of mathematical models have been proposed, among them, the comb structure model (Arkhincheev, 2007; Iomin, 2013) shown in Fig. 8.44 is one of the most significant models that can be used to simulate the transport process of particles well. The model displays two special characteristics: one is that the migration (particles transport) and proliferation (the increase or decrease of particles number) are independent of each other, namely the migration-proliferation dichotomy (Fedotov and Iomin, 2007) is considered; the other is that the diffusion and convection velocity in the x-direction only happen along the x-axis and the diffusion in the y-direction is perpendicular to the x-axis. The comb structure is a widely used model to simulate various pertinent situations, such as cell transport (Iomin, 2005), spiny dendrites (Iomin and Méndez, 2013), percolation clusters (Arkhincheev and Baskin, 1991), and so on.

The anomalous transport of particles in comb structure can be seen as a special case of continuous time random walk and the 1-D diffusion in comb model is described by the time fractional Fokker–Planck equation (Iomin, 2006) with the time fractional derivative of order α—the classical one corresponds to the time fractional derivative of order 1/2. Iomin (2006) discussed the fractional transport of cancer cells due to self-entrapping. His work indicated that the distribution function of the fractional transport depends on the scaled proliferation rate and the order of the fractional derivative. Baskin and Iomin (2004) studied specific properties of particles transported by comb model and the diffusive transport of particles leads to subdiffusion, which corresponds $0 < \beta < 1$ in the relationship between the mean square displacement and parameter t: $\langle x^2(t)\rangle \sim t^{\beta}$. Moreover, the log-normal distribution with exponentially fast spreading was obtained for the cases that transport exponent μ in $< x^2(t) > \sim t^{\mu}$ approaches infinity. Lenzi et al. (2013) investigated a diffusive process in the comb model by considering the effects of drift terms, which represents an external force acting on the system; their results showed that an anomalous spreading may present different diffusive regimes connected to anomalous diffusion and stationary states. For more

papers about the comb model, see Refs. (Arkhincheev, 2010; Arkhincheev et al., 2011; Iomin and Baskin, 2005).

The 1-D constitutive relationship (Méndeza and Iomin, 2013) to describe the comb model is derived by the Fick's first law of diffusion:

$$j = -D\frac{\partial P(x,t)}{\partial x}, \tag{8.152}$$

the corresponding time fractional continuity equation is:

$$\frac{\partial^{\alpha} P(x,t)}{\partial t^{\alpha}} = -div\, j, \tag{8.153}$$

where j refers to the diffusion flux, D denotes the diffusion coefficient, and $\alpha = 1/2$ corresponds to the classical comb model. $P(x,t)$ is the distribution function defined by $P(x,t) = \int_{-\infty}^{\infty} P_1(x,y,t)dy$ where $P_1(x,y,t)$ refers to the particles distribution at the special location (x,y) and time t. The symbol $\frac{\partial^{\alpha}}{\partial t^{\alpha}}$ stands for the time fractional derivative based on the Caputo's definition (Podlubny, 1999), given by:

$$\frac{\partial^{\alpha} j}{\partial t^{\alpha}} = \frac{1}{\Gamma(1-\alpha)} \int_0^t \frac{1}{(t-\tau)^{\alpha}} \frac{\partial j(x,\tau)}{\partial \tau} d\tau, \tag{8.154}$$

The classical Fick's first law of diffusion has been the most successful law for studying diffusion problem in various pertinent situations. However, an unphysical property is that it issues an infinite velocity of propagation due to the fact that there is a finite amount of particles at larger distances from the origin even for very small times.

Cattaneo model (Cattaneo, 1948; Gómez et al., 2007) overcomes the shortcoming of the Fick's first law of diffusion well by introducing the relaxation time term. The modified Fick's first law of diffusion is as follows:

$$j + \xi\frac{\partial j}{\partial t} = -D\frac{\partial P(x,t)}{\partial x}, \tag{8.155}$$

where the propagation velocity (Compte and Metzler, 1997) $v = (D/\xi)^{1/2}$, ξ is a nonnegative constant and refers particularly to the relaxation time of diffusion. The limit $\xi \to 0$ corresponds to the classical Fick's first law of diffusion with an infinite velocity of propagation.

Compte and Metzler (1997) proposed three possible generalized Cattaneo equations, each one supported by a different scheme, and the properties of these generalizations are studied in both the long-time and the short-time regimes. One generalized Cattaneo constitutive relationship is as follows:

$$j + \xi\frac{\partial^{\alpha} j}{\partial t^{\alpha}} = -D\frac{\partial P(x,t)}{\partial x}. \tag{8.156}$$

Qi and Jiang (2011) presented exact solution for the space fractional Cattaneo diffusion equation:

$$j+\xi\frac{\partial^{\alpha}j}{\partial t^{\alpha}}=-D\frac{\partial^{\mu-1}P(x,t)}{\partial|x|^{\mu-1}},\quad 1<\mu\leq 2. \tag{8.157}$$

Here, the symbol $\frac{\partial^{\mu-1}}{\partial|x|^{\mu-1}}$ stands for the space Riesz fractional operator and the corresponding definition is given in Ref. (Qi and Jiang, 2011). For more recent studies about the Cattaneo models, see Refs. (Atanackovic et al., 2007; Liu et al., 2013b; Xu et al., 2013; Qi and Guo, 2014).

However, the model only involves the partial time derivative and is considered only as a "place holder" for a more complete formulation. The frame-indifferent generalization of Cattaneo's law was developed by Christov (2009) by the implementation of the Oldroyd upper-convective derivative. Christov (2007) proposed a generalized Fourier's law model by incorporating spatial memory into the constitutive relation; the integral and differential versions of the memory terms in the constitutive relation are discussed. The model also considers the material invariance and has been applied well in analyzing the flow and heat transfer of various fluids (Han et al., 2014; Mustafa, 2015).

Motivated by the previously mentioned works, we study fractional anomalous diffusion in comb structure; the higher spatial gradient is introduced in the constitutive relation between the flux and particles distribution. In addition, the effects of Cattaneo−Christov flux diffusion and convection are also taken into consideration. The new constitutive relation is described by:

$$j+\xi\left[\frac{\partial j}{\partial t}+u\cdot\nabla j-j\cdot\nabla u+(\nabla\cdot u)j\right]=-D\frac{\partial P(x,t)}{\partial x} \tag{8.158}$$

The numerical discretization method with the L1-and L2-approxiamations for fractional derivative is used to obtain the numerical solution. The effects of the involved parameters on the particles distribution are analyzed and discussed in detail.

8.6.2 Mathematical Formulation

We consider convection velocity as a constant for simplicity and introduce the time fractional operator into the Cattaneo−Christov constitutive relation, Eq. (8.158), and the modified model is given by Liu et al. (2016):

$$j+\xi\left(\tau_1^{\alpha-1}\frac{\partial^{\alpha}j}{\partial t^{\alpha}}+u\frac{\partial j}{\partial x}\right)=-D\frac{\partial P(x,t)}{\partial x}, \tag{8.159}$$

where $0<\alpha\leq 1$ and τ_1 is a newly introduced quantity whose dimension is s.

The corresponding fractional mass conservation equation is given by:

$$\tau_1^{\alpha-1}\frac{\partial^\alpha P(x,t)}{\partial t^\alpha}+u\frac{\partial P(x,t)}{\partial x}=-div\ j. \tag{8.160}$$

Combining Eqs. (8.159) and (8.160), we obtain the time fractional Cattaneo−Christov convection-diffusion equation:

$$\xi\tau_1^{2\alpha-2}\frac{\partial^{2\alpha}P}{\partial t^{2\alpha}}+\tau_1^{\alpha-1}\frac{\partial^\alpha P}{\partial t^\alpha}+2u\xi\tau_1^{\alpha-1}\frac{\partial^{\alpha+1}P}{\partial x\partial t^\alpha}+u\frac{\partial P}{\partial x}+\left(u^2\xi-D\right)\frac{\partial^2 P}{\partial x^2}=0, \tag{8.161}$$

subject to the initial and boundary conditions:

$$P(x,0)=\delta(x),\ \left.\frac{\partial P(x,t)}{\partial t}\right|_{t=0}=0, \tag{8.162}$$

and

$$P(\pm\infty,t)=0, \tag{8.163}$$

where $\delta(x)$ refers to the Dirac distribution.

Changing the involved coefficients of Eq. (8.161), we can get various kinds of equations. By setting $\xi\neq 0$ and $u=0$, Eq. (8.161) reduces to the time fractional Cattaneo diffusion equation (Langlands and Henry, 2005). By setting $\xi=0$ and $u\neq 0$, Eq. (8.161) reduces to the time fractional convection-diffusion equation. By setting $\xi=0$ and $u=0$, Eq. (8.161) reduces to the time fractional diffusion equation, which has been analyzed and discussed by Iomin (2006).

8.6.3 Numerical Algorithms

Firstly, we define h as the space step and $x_i=-\frac{L}{2}+ih$ $(i=0,1,2,\ldots,M)$, while τ is the time step and $t_j=j\tau$ $(j=0,1,2,\ldots,N)$, where $L=Mh$ is a sufficiently large number. In this research, we replace the infinite boundary by $\left[-\frac{L}{2},\frac{L}{2}\right]$.

The nondimensional quantities are introduced for simplicity:

$$t\to\tau_1 t^*,\ \ x\to\sqrt{D\tau_1}x^*,\ \ \xi\to\tau_1\xi^*,\ \ u\to\sqrt{\frac{D}{\tau_1}}u^*,\ \ L=\sqrt{D\tau_1}L^*, \tag{8.164}$$

Eq. (8.161) and the corresponding initial and boundary conditions can be rewritten in the dimensionless forms (here we omitted the superscript * for simplicity):

$$\xi\frac{\partial^{2\alpha}P}{\partial t^{2\alpha}}+\frac{\partial^\alpha P}{\partial t^\alpha}+2u\xi\frac{\partial^{\alpha+1}P}{\partial x\partial t^\alpha}+u\frac{\partial P}{\partial x}+\left(u^2\xi-1\right)\frac{\partial^2 P}{\partial x^2}=0, \tag{8.165}$$

$$P(x,0)=\delta(x),\quad \left.\frac{\partial P(x,t)}{\partial t}\right|_{t=0}=0, \tag{8.166}$$

$$P(\pm L,t)=0. \tag{8.167}$$

Some useful definitions of the difference schemes are given as follows:

Definition 1. The first-order time and space derivatives can be approximated by the backward difference scheme, i.e.,

$$\frac{\partial P(x_i,t_j)}{\partial t}=\frac{P_i^j-P_i^{j-1}}{\tau}, \tag{8.168}$$

and

$$\frac{\partial P(x_i,t_j)}{\partial x}=\frac{P_i^j-P_{i-1}^j}{h}, \tag{8.169}$$

respectively.

Definition 2. The second-order space derivative can be approximated by the central difference scheme, i.e.,

$$\frac{\partial^2 P(x_i,t_j)}{\partial x^2}=\frac{P_{i+1}^j-2P_i^j+P_{i-1}^j}{h^2}, \tag{8.170}$$

Definition 3. The L1-approximation ($0<\alpha\le 1$) (Du et al., 2010) and L2-approximation ($1\le\beta\le 2$) (Huang and Liu, 2005; Sun and Wu, 2006) for the Caputo fractional derivative can be derived by:

$$\frac{\partial^\alpha P(x_i,t_j)}{\partial t^\alpha}=\frac{1}{\tau^\alpha\Gamma(2-\alpha)}\left(P_i^j+\sum_{k=1}^{j-1}(c_{j-k}-c_{j-k-1})P_i^k-c_{j-1}P_i^0\right), \tag{8.171}$$

and

$$\frac{\partial^\beta P(x_i,t_j)}{\partial t^\beta}=\frac{1}{\tau^\beta\Gamma(3-\beta)}\left[a_0\left(P_i^j-P_i^{j-1}\right)-\sum_{l=1}^{j-1}(a_{j-l-1}-a_{j-l})\left(P_i^l-P_i^{l-1}\right)\right], \tag{8.172}$$

respectively, where $c_0=1$, $c_k=(k+1)^{1-\alpha}-k^{1-\alpha}$ $(k>0)$, $a_0=1$, $a_l=(l+1)^{2-\beta}-l^{2-\beta}$ $(l>0)$.

For $\beta=2\alpha$, the definition of the L2-approximation can be changed as:

$$\frac{\partial^{2\alpha} P(x_i,t_j)}{\partial t^{2\alpha}}=\frac{1}{\tau^{2\alpha}\Gamma(3-2\alpha)}\left[a_0\left(P_i^j-P_i^{j-1}\right)-\sum_{l=1}^{j-1}(a_{j-l-1}-a_{j-l})\left(P_i^l-P_i^{l-1}\right)\right], \tag{8.173}$$

where $a_0=1$, $a_k=(k+1)^{2-2\alpha}-k^{2-2\alpha}$, $(k>0)$.

Through the difference schemes mentioned herein, for $0.5 \leq \alpha \leq 1$, the final discrete scheme of Eq. (8.165) can be expressed by:

$$\begin{aligned}
&\left(\frac{\xi u^2-1}{h^2}\right)P_{i+1}^{j}+\left[r_1+r_2+r_3-2\frac{\xi u^2-1}{h^2}+\frac{u}{h}\right]P_i^j+\left[\frac{\xi u^2-1}{h^2}-\frac{u}{h}-r_1\right]P_{i-1}^{j}\\
&\quad=r_1\left[\sum_{k=1}^{j-1}(c_{j-k-1}-c_{j-k})\left(P_i^k-P_{i-1}^k\right)+c_{j-1}\left(P_i^0-P_{i-1}^0\right)\right]\\
&\qquad+r_2\left[\sum_{k=1}^{j-1}(c_{j-k-1}-c_{j-k})P_i^k+c_{j-1}P_i^0\right]\\
&\qquad+r_3\left[P_i^{j-1}+\sum_{l=1}^{j-1}(a_{j-l-1}-a_{j-l})\left(P_i^l-P_i^{l-1}\right)\right],
\end{aligned} \tag{8.174}$$

where $r_1=\frac{2u\xi}{\tau^{\alpha}\Gamma(2-\alpha)h}$, $r_2=\frac{1}{\tau^{\alpha}\Gamma(2-\alpha)}$, $r_3=\frac{\xi}{\tau^{2\alpha}\Gamma(3-2\alpha)}$.

By defining a new matrix G with the coefficients of the previous equation:

$$G_{il}=\begin{cases}\dfrac{\xi u^2-1}{h^2} & l=i+1,\\ r_1+r_2+r_3-2\dfrac{\xi u^2-1}{h^2}+\dfrac{u}{h} & l=i,\quad,\\ \dfrac{\xi u^2-1}{h^2}-\dfrac{u}{h}-r_1 & l=i-1,\end{cases} \tag{8.175}$$

Eq. (8.174) can be simplified as:

$$\begin{aligned}
GP_i^j&=r_1\left[\sum_{k=1}^{j-1}(c_{j-k-1}-c_{j-k})\left(P_i^k-P_{i-1}^k\right)+c_{j-1}\left(P_i^0-P_{i-1}^0\right)\right]\\
&\quad+r_2\left[\sum_{k=1}^{j-1}(c_{j-k-1}-c_{j-k})P_i^k+c_{j-1}P_i^0\right]\\
&\quad+r_3\left[P_i^{j-1}+\sum_{l=1}^{j-1}(a_{j-l-1}-a_{j-l})\left(P_i^l-P_i^{l-1}\right)\right],
\end{aligned} \tag{8.176}$$

The discrete schemes of the initial and boundary conditions are given by:

$$p_i^0=\delta(x_i),\quad p_i^0=p_i^1\quad\text{for}\quad i=0,1,2,\ldots,M, \tag{8.177}$$

and

$$p_0^j=0,\quad p_M^j=0,\quad\text{for}\quad j=1,2,\ldots,N, \tag{8.178}$$

respectively.

By defining $r_4 = \frac{u^2\xi - 1}{h^2}$, $r_5 = \frac{\xi}{\tau^{2\alpha}\Gamma(2-2\alpha)}$ $r_6 = \frac{1}{\tau^{\alpha}\Gamma(2-\alpha)}$, $r_7 = \frac{2u\xi}{h\tau^{\alpha}\Gamma(2-\alpha)}$, for $0 < \alpha \leq 0.5$, Eq. (8.165) can be simplified as:

$$\begin{aligned} & r_4 P_{i+1}^j + \left[r_5 + r_6 + r_7 + \frac{u}{h} - 2r_4\right] P_i^j + \left[r_4 - r_7 - \frac{u}{h}\right] P_{i-1}^j \\ & = -r_5 \left[\sum_{k=1}^{j-1} (b_{j-k} - b_{j-k-1}) P_i^k - b_{j-1} P_i^0\right] - r_6 \left[\sum_{k=1}^{j-1} (c_{j-k} - c_{j-k-1}) P_i^k - c_{j-1} P_i^0\right], \\ & -r_7 \left[\sum_{k=1}^{j-1} (c_{j-k} - c_{j-k-1}) \left(P_i^k - P_{i-1}^k\right) - c_{j-1}\left(P_i^0 - P_{i-1}^0\right)\right], \end{aligned} \tag{8.179}$$

where $b_0 = 1$, $b_k = (k+1)^{1-2\alpha} - k^{1-2\alpha}$.

By defining a new matrix G^1 with the coefficients of the previous equation:

$$G_{il}^1 = \begin{cases} r_4 & l = i+1, \\ r_5 + r_6 + r_7 + \dfrac{u}{h} - 2r_4 & l = i, \\ r_4 - r_7 - \dfrac{u}{h} & l = i-1, \end{cases}, \tag{8.180}$$

Eq. (8.174) can be simplified as:

$$\begin{aligned} G^1 P_i^j = & -r_5 \left[\sum_{k=1}^{j-1} (b_{j-k} - b_{j-k-1}) P_i^k - b_{j-1} P_i^0\right] - r_6 \left[\sum_{k=1}^{j-1} (c_{j-k} - c_{j-k-1}) P_i^k - c_{j-1} P_i^0\right] \\ & -r_7 \left[\sum_{k=1}^{j-1} (c_{j-k} - c_{j-k-1}) \left(P_i^k - P_{i-1}^k\right) - c_{j-1}\left(P_i^0 - P_{i-1}^0\right)\right], \end{aligned} \tag{8.181}$$

The discrete schemes of the initial and boundary conditions are given by:

$$p_i^0 = \delta(x_i) \quad \text{for} \quad i = 0, 1, 2, \ldots, M \tag{8.182}$$

and

$$p_0^j = 0, \quad p_M^j = 0 \quad \text{for} \quad j = 1, 2, \ldots, N, \tag{8.183}$$

respectively.

8.6.4 Comparison of Numerical and Analytical Solutions

By considering the parameter u as $u = 0$, Eq. (8.165) can be changed as the following form:

$$\xi \frac{\partial^{2\alpha} P}{\partial t^{2\alpha}} + \frac{\partial^{\alpha} P}{\partial t^{\alpha}} - \frac{\partial^2 P}{\partial x^2} = 0, \tag{8.184}$$

By using variable transformation, Laplace and Fourier transforms, and properties of H-function, the analytical solution of Eq. (8.184) for $t = 1$ and $\xi = 1$ was obtained by Qi and Jiang (2011):

$$P(x,1) = \frac{1}{\mu|x|\sqrt{\pi}} \sum_{n=0}^{\infty} \frac{(-1)^n}{n!} \frac{1}{\xi^n} \left\{ \frac{1}{\xi} A + B \right\}, \tag{8.185}$$

where $A = H_{2,3}^{2,1}\left[\frac{\sqrt{\xi}|x|}{2} \middle| \begin{matrix} \left(1, \frac{1}{2}\right), (1 + n\alpha + \alpha, \alpha) \\ \left(\frac{1}{2}, \frac{1}{2}\right), \left(1 + n, \frac{1}{2}\right), \left(1, \frac{1}{2}\right) \end{matrix} \right]$ and

$B = H_{2,3}^{2,1}\left[\frac{\sqrt{\xi}|x|}{2} \middle| \begin{matrix} \left(1, \frac{1}{2}\right), (1 + n\alpha, \alpha) \\ \left(\frac{1}{2}, \frac{1}{2}\right), \left(1 + n, \frac{1}{2}\right), \left(1, \frac{1}{2}\right) \end{matrix} \right]$.

Moreover, by considering the relaxation time parameter ξ as $\xi = 0$, Eq. (8.165) can be simplified as:

$$\frac{\partial^{\alpha} P}{\partial t^{\alpha}} + u \frac{\partial P}{\partial x} - \frac{\partial^2 P}{\partial x^2} = 0. \tag{8.186}$$

Using variable transformation, Mellin and Laplace transforms, and properties of H-function, Huang and Liu (2005) obtained the analytical solution of Eq. (8.186) for $t = 1$ and $\alpha = 0.5$, given by:

$$P(x,1) = \frac{\exp\left(\frac{x}{2}\right)}{2\sqrt{\pi}} \int_{-\infty}^{\infty} e^{-\frac{1}{4}\sigma - x^2/(4\sigma)} H_{11}^{10}\left(\sigma \middle| \begin{matrix} \left(\frac{1}{4}, \frac{1}{2}\right) \\ \left(-\frac{1}{2}, 1\right) \end{matrix} \right) d\sigma \tag{8.187}$$

The curves of the comparison between the analytical solution and the numerical one of the previous two special cases are shown in Fig. 8.45. We can see that the curves of the analytical and numerical solutions are in very good agreement, which validates the correctness of the numerical one.

8.6.5 Results and Discussion

In this section, the nonlinear fractional differential Eq. (8.165) subject to the boundary and initial conditions is solved using the numerical discretization

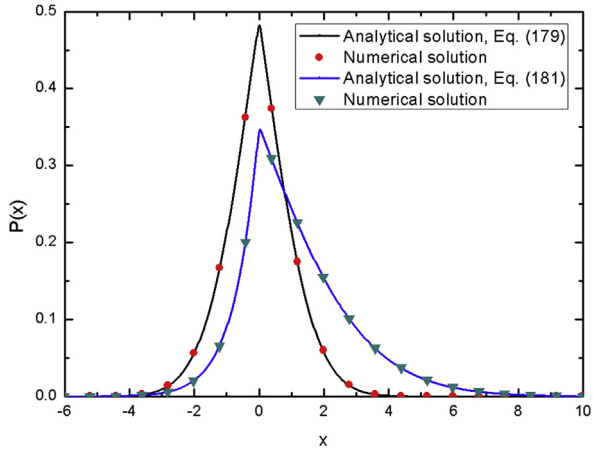

FIGURE 8.45 The comparison of the analytical and numerical solutions in the special case that $\alpha = 0.5$, $\xi = 1$, $u = 0$, and $t = 1$ for Eq. (8.179) and $\alpha = 0.5$, $\xi = 0$, $u = 1$, and $t = 1$ for Eq. (8.181).

method. The influences of different values of time, time fractional parameter, relaxation time, and convection velocity on the particles distribution are also discussed.

Figs. 8.45–8.48 show the particles distribution with different values of parameter t when $\xi = 1$ and $u = 0$ at the condition that the fractional parameters $\alpha = 0.5$, $\alpha = 0.7$, and $\alpha = 1$, respectively. For the time fractional parameter $\alpha = 0.5$, Eq. (8.165) corresponds a diffusion equation, which has a

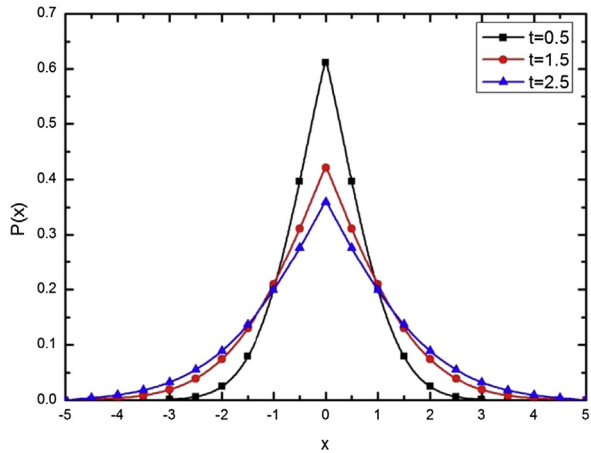

FIGURE 8.46 Distribution curves with different values of parameter t when $\alpha = 0.5$, $\xi = 1$, and $u = 0$.

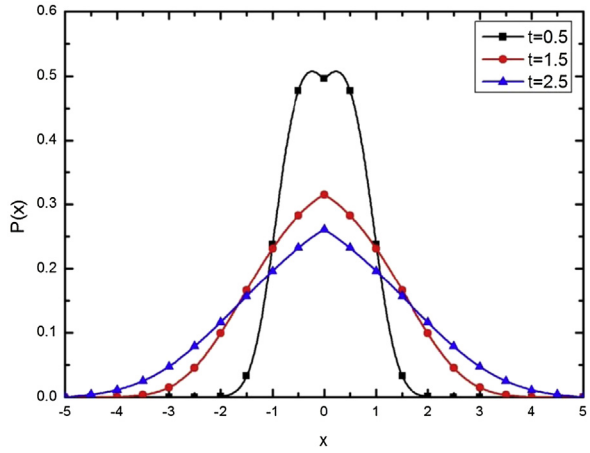

FIGURE 8.47 Distribution curves with different values of parameter t when $\alpha = 0.7$, $\xi = 1$, and $u = 0$.

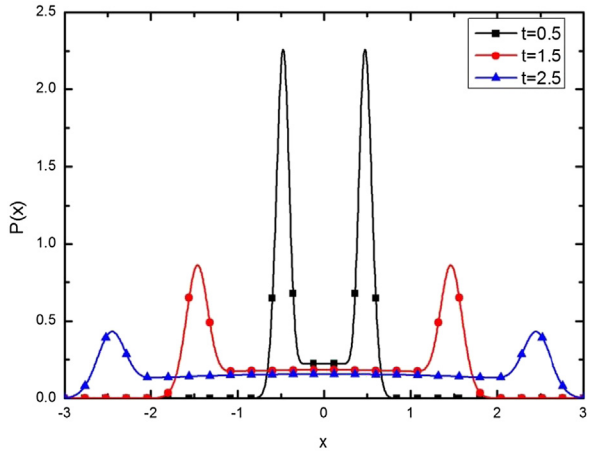

FIGURE 8.48 Distribution curves with different values of parameter t when $\alpha = 1.0$, $\xi = 1$, and $u = 0$.

parabolic character. Fig. 8.46 shows that the peaks of distribution curves become lower while both sides of distribution curves become higher with time increases, that is to say, the particles diffuse along both sides of x-axis gradually.

For the time fractional parameter $\alpha = 0.7$, the highest order of time derivative in differential Eq. (8.165) is 1.4, which coexists the characteristics of parabolic and hyperbolic. Fig. 8.47 shows that the distribution appears to be a hyperbolic curve at the parameter $t = 0.5$ and degenerates to the parabolic

curves with time increase. We can conclude that the hyperbolic character weakens while the parabolic character enhances with the increase of time. For the time fractional parameter $\alpha = 1$, Eq. (8.165) corresponds a diffusion-wave equation. Fig. 8.48 shows that the particles propagate as wave form along the positive and negative directions of x-axis and the peaks of distribution curves become lower with time increase. Meanwhile, the value of the distribution between the two peaks is not zero and becomes smaller with time increases for the existence of diffusion.

Figs. 8.49 and 8.50 show the particles distribution with different values of fractional parameter α when $\xi = 1$ and $u = 0$ at the early time $t = 0.1$ and later time $t = 1$, respectively. The time fractional parameter refers to the memory of particles movement. It can be seen from the figures, with the increasing of the fractional parameter α, the peak of the particles distribution becomes higher at the early time $t = 0.1$ but this trend reverses at the later time $t = 1$ for the parabolic curves. The results indicate, for a larger fractional parameter, the diffusion velocity is slower at the early time but faster at the later time. In other words, the initial diffusion velocity is slower and actually the diffusion acceleration is larger. The results are important for addressing the electrotonic significance of decreasing spine densities (Liu et al., 2011; Henry and Langlands, 2008). For a larger fractional parameter, the distribution starts to appear with a hyperbolic character. With the increasing of the fractional parameter α, the peaks become higher for the hyperbolic curves at any time, namely the volatility of the curves becomes stronger.

Figs. 8.51–8.53 show the influence of different values of relaxation time ξ on particles distribution when $\alpha = 0.5$, $\alpha = 0.7$, and $\alpha = 1.0$, respectively. For the parameter $\alpha = 0.5$, the peak of the distribution curve becomes higher with

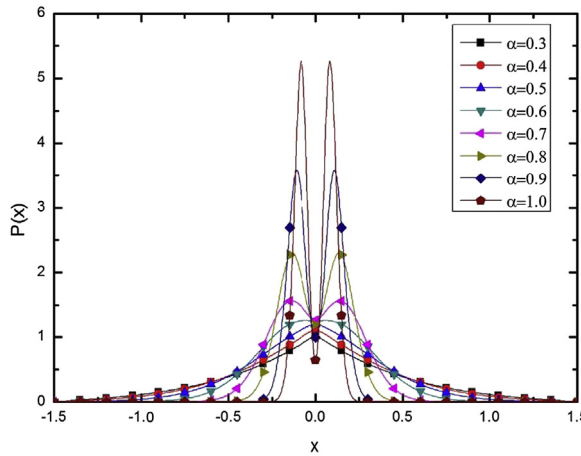

FIGURE 8.49 Distribution curves with different values of parameter α at the early time $t = 0.1$ when $\xi = 1$ and $u = 0$.

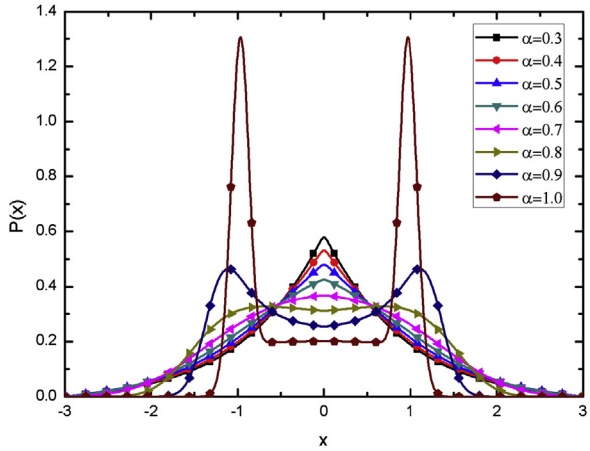

FIGURE 8.50 Distribution curves with different values of parameter α at the later time $t = 1$ when $\xi = 1$ and $u = 0$.

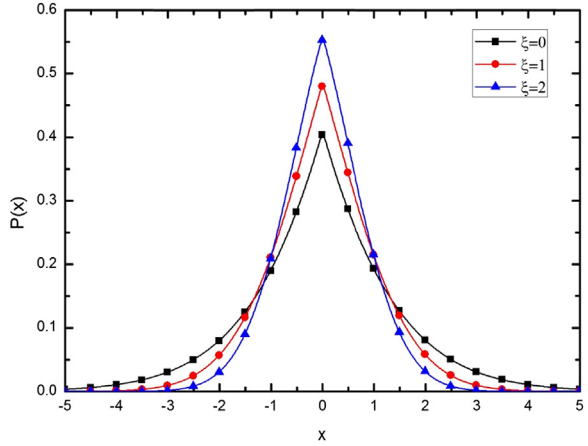

FIGURE 8.51 Distribution curves with different values of parameter ξ when $\alpha = 0.5$, $u = 0$, and $t = 1$.

the increasing of the parameter ξ. For the parameter $\alpha = 0.7$, the distribution curve appears hyperbolic character for a larger parameter ξ. For the parameter $\alpha = 1.0$, the peaks become higher and the distance between the two peaks becomes shorter with the increasing of parameter ξ. Comparing with the Figs. 8.46–8.48, we can conclude that the constant ξ has delay effect. The larger the coefficient ξ is, the stronger the delay effect will be, and vice versa.

The convection velocity has significant effects on particles distribution, which is shown in Figs. 8.54–8.57. Here we only discuss the convection velocity along the positive direction of x-axis. For the negative direction, its

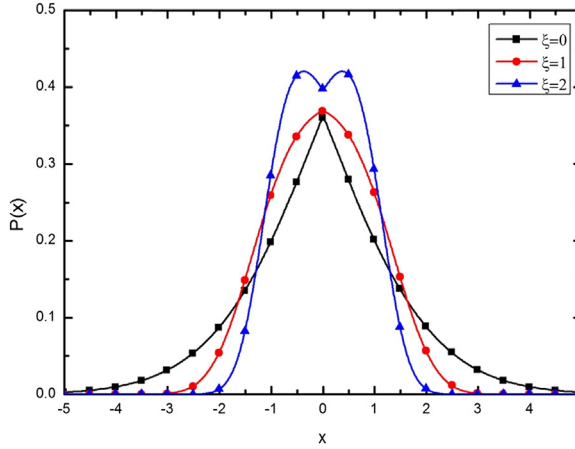

FIGURE 8.52 Distribution curves with different values of parameter ξ when $\alpha = 0.7$, $u = 0$, and $t = 1$.

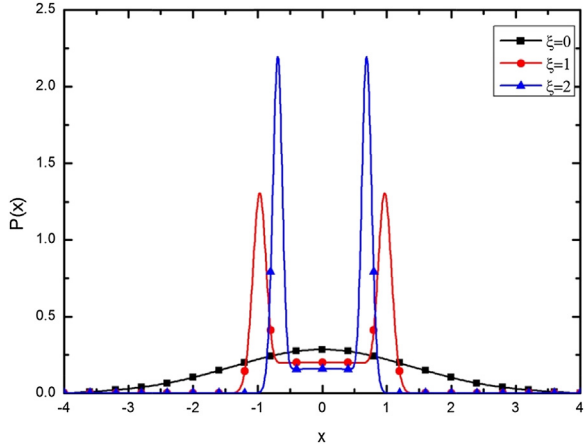

FIGURE 8.53 Distribution curves with different values of parameter ξ when $\alpha = 1.0$, $u = 0$, and $t = 1$.

influence on particles distribution can be obtained by similar analysis. It can be seen from the four figures that the convection velocity can influence the symmetry of the distribution curves.

For parameters $\xi = 0$ and $\alpha = 1.0$, Eq. (8.165) reduces to the convection-diffusion equation that is derived from Fick's law. Fig. 8.54 shows that the distribution curves move along the direction of convection velocity and the greater the velocity is, the father the peak will deviate from the initial position. Moreover, the peak becomes lower but not obvious for a greater velocity u. Fig. 8.55 shows the influences of different values of velocity u on the particles

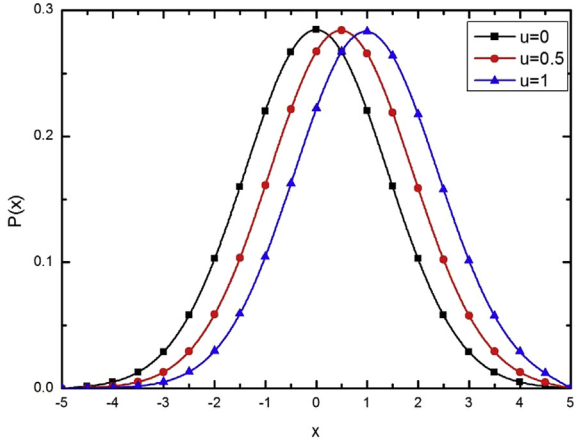

FIGURE 8.54 Distribution curves with different values of velocity u when $\alpha = 1.0$, $\xi = 0$, and $t = 1$.

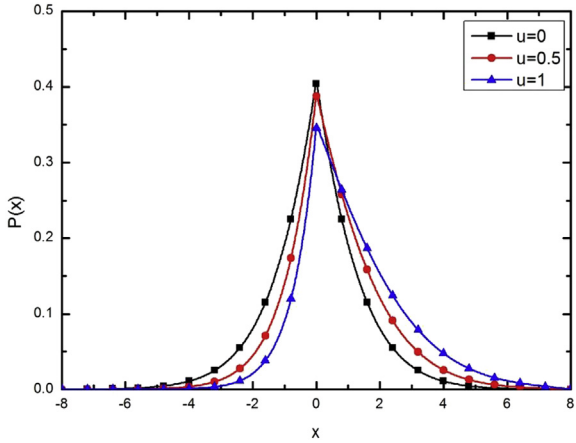

FIGURE 8.55 Distribution curves with different values of velocity u when $\alpha = 0.5$, $\xi = 0$, and $t = 1$.

distribution in the condition of the time fractional derivative of order 1/2, which corresponds to a parabolic equation. The greater the convection velocity is, the lower the peak of distribution curve will be. In addition, the particles diffuse faster along the positive direction but slower along the negative direction for a greater convection velocity. It is noteworthy that the peak does not move even when the convection velocity changes. Moreover, the distribution curves have sharp peaks because of the existence of time fractional operator.

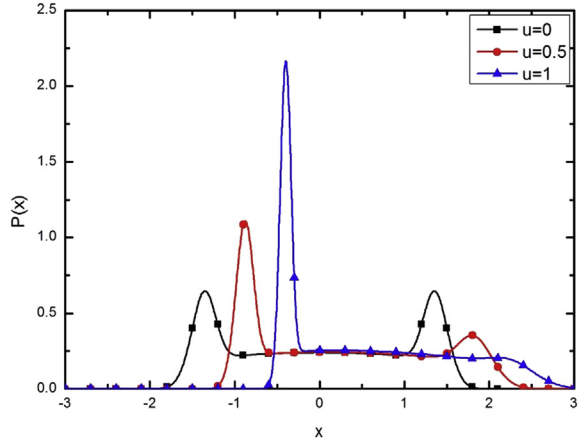

FIGURE 8.56 Distribution curves with different values of velocity u when $\alpha = 1.0$, $\xi = 0.5$, and $t = 1$.

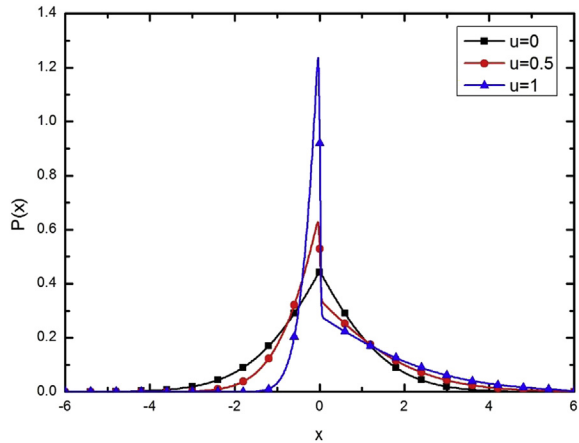

FIGURE 8.57 Distribution curves with different values of velocity u when $\alpha = 0.5$, $\xi = 0.5$, and $t = 1$.

The importance of time fractional operator is verified because of the largest difference at the initial position and time.

Figs. 8.56 and 8.57 show that the particles distribution presents as diffusion wave form and the governing equation has the coexisting characteristics of parabolic and hyperbolic due to the fact of the existence of relaxation parameter ξ and fractional parameter α. Fig. 8.56 shows the influence of convection velocity on particles distribution when $\alpha = 1.0$, $\xi = 0.5$, and $t = 1$. The larger the convection velocity is, the higher the left peak and the lower the right one will be. In other words, the curve peak becomes higher for the same

directions of the convection velocity and wave propagation while lower for opposite directions. Moreover, the peak moves along the direction of convection velocity. Fig. 8.57 shows the particles distribution with different values of parameter u when $\alpha = 0.5$, $\xi = 0.5$, and $t = 1$. The cusps that are similar to the inflection points in Fig. 8.56 appear in the curves. They are the result of the existence of relaxation time ξ and fractional parameter α, which make the particles transport have the coexisting characters of parabolic and hyperbolic. For the existences of convection velocity, the peak becomes higher for a greater convection velocity. The right side of particles distribution appears in a general diffusion form and the particles diffuse faster for a greater convection velocity.

8.7 SUMMARY

We study some complex flow, heat, and mass transfer problems arising in non-Newtonian fluids. Four types of Fourier's heat conduction models are investigated for power law non-Newtonian fluids: Flow and heat transfer of power law non-Newtonian fluids over a rotating disk with modified Fourier's heat conduction law and fractional Maxwell fluid with modified Fourier's heat conduction law and modified Darcy's diffusion law; fractional Maxwell fluid unsteady natural convection boundary layer heat transfer over a vertical plate with modified Newtonian friction law and Fourier's heat conduction law; and the fractional convection diffusion in a comb-like structure with Cattaneo–Christov flux. The solutions are obtained numerically and the influences of pertinent parameters on the velocity and temperature fields are discussed in detail.

REFERENCES

Abel, M.S., Siddheshwar, P.G., Mahesha, N., 2009. Effects of thermal buoyancy and variable thermal conductivity on the MHD flow and heat transfer in a power-law fluid past a vertical stretching sheet in the presence of a non-uniform heat source. International Journal of Non-Linear Mechanics 44, 1–12.

Acrivos, A., Shah, M.J., Petersen, E.E., 1960. Momentum and heat transfer in laminar boundary-layer flows of non-Newtonian fluids past external surfaces. American Institute of Chemical Engineers Journal 6, 312–317.

Ames, W.F., 1977. Numerical Methods for Partial Differential Equations, second ed. Academic, New York.

Andersson, H.I., Korte, E., Meland, R., 2001. Flow of a power-law fluid over a rotating disk revisited. Fluid Dynamics Research vol. 28, 75–88.

Arkhincheev, V.E., 2007. Random walks on the comb model and its generalizations. Chaos 17, 043102.

Arkhincheev, V.E., 2010. Unified continuum description for sub-diffusion random walks on multi-dimensional comb model. Physica A 389, 1–6.

Arkhincheev, V.E., Kunnen, E., Baklanov, M.R., 2011. Active species in porous media: random walk and capture in traps. Microelectronic Engineering 88, 694–696.

Arkhincheev, V.E., Baskin, E.M., 1991. Anomalous diffusion and drift in a comb model of percolation clusters. Journal of Experimental and Theoretical Physics 73, 161−165.

Arunachalam, M., Rajappa, N.R., 1978. Thermal boundary layer in liquid metals with variable thermal conductivity. Applied Sciences Research 34, 179−187.

Atanackovic, T.M., Pilipovic, S., Zorica, D., 2007. A diffusion wave equation with two fractional derivatives of different order. Journal of Physics A: Mathematical and Theoretical 40, 5319−5333.

Attia, H.A., 2008. Rotating disk flow and heat transfer through a porous medium of a non-Newtonian fluid with suction and injection. Communications in Nonlinear Science and Numerical Simulation 13, 1571−1580.

Barletta, A., 1997. Fully developed laminar forced convection in circular ducts for power-law fluids with viscous dissipation. International Journal of Heat and Mass Transfer 40, 15−26.

Baskin, E., Iomin, A., 2004. Superdiffusion on a comb structure. Physical Review Letters 93, 120603.

Benton, E.R., 1966. On the flow due to a rotating disk. Journal of Fluid Mechanics 24, 781−800.

Carnahan, B., Luther, H.A., Wilkes, J.O., 1969. Applied Numerical Methods. John Wiley and Sons, New York.

Cattaneo, C., 1948. Sulla conduzione del calore, Some aspects in Diffusion Theory.

Chaim, T.C., 1998. Heat transfer in a fluid with variable thermal conductivity over a linearly stretching sheet. Acta Mechanica 129, 63−72.

Chen, C., Liu, F., Anh, V., Turner, I., 2010. Numerical schemes with high spatial accuracy for a variable-order anomalous subdiffusion equation. SIAM Journal on Scientific Computing 32, 1740−1760.

Cheng, C.Y., 2009. Nonsimilar boundary layer analysis of double-diffusive convection from a vertical truncated cone in a porous medium with variable viscosity. Applied Mathematics and Computation 212, 185−193.

Christov, C.I., 2009. On frame indifferent formulation of the Maxwell−Cattaneo model of finite-speed heat conduction. Mechanics Research Communications 36, 481−486.

Christov, C.I., 2007. On a higher-gradient generalization of Fourier's law of heat conduction. AIP Conference Proceedings 946, 11−22.

Ciarlet, P.G., 1978. The Finite Element Method for Elliptic Problems. North-Holland Publishing Company, Amsterdam.

Cochran, W.G., Goldstein, S., 1934. The flow due to a rotating disk. Mathematical Proceedings of the Cambridge Philosophical Society 30, 365−375.

Compte, A., Metzler, R., 1997. The generalized Cattaneo equation for the description of anomalous transport processes. Journal of Physics A: Mathematical and General 30, 7277−7289.

Crosan, T., Pop, I., 2001. Free convection over a vertical flat plate with a variable wall temperature and internal heat generation in a porous medium saturated with a non-Newtonian fluid. Technische Mechanik 4, 313−318.

Du, R., Cao, W.R., Sun, Z.Z., 2010. A compact difference scheme for the fractional diffusion-wave equation. Applied Mathematical Modelling 34, 2998−3007.

Ece, M.C., Buyuk, E., 2002. Similarity solutions for free convection to power-law fluids from a heated vertical plate. Applied Mathematics Letters 15, 1−5.

Ezzat, M.A., 2010. Thermoelectric MHD non-Newtonian fluid with fractional derivative heat transfer. Physica B 405, 4188−4194.

Fedotov, S., Iomin, A., 2007. Migration and proliferation dichotomy in tumor-cell invasion. Physical Review Letters 98, 118101.

Fetecau, C., Fetecau, C., Kamran, M., Vieru, D., 2009. Exact solution for the flow of a generalized Oldroyd-B fluid induced by a constantly accelerating plate between side walls perpendicular to the plate. Journal of Non-Newtonian Fluid Mechanics 156, 189−201.

Fletcher, C.A.J., 1988. Computationl Techniques for Fluid Dynamics 1. Spring-Verlag, New York.
Friedrich, C., 1991. Relaxation and retardation functions of the Maxwell model with fractional derivatives. Rheologica Acta 30, 151−158.
Friedrich, C., Braun, H., 1992. Generalised Cole-Cole behavior and its rheological relevance. Rheologica Acta 31, 309−322.
Ganesan, P., Palani, G., 2004. Finite difference analysis of unsteady natural convection MHD flow past an inclined plate with variable surface heat and mass flux. International Journal of Heat and Mass Transfer 47, 4449−4457.
Gómez, H., Colominas, I., Navarrina, F., Casteleiro, M., 2007. A finite element formulation for a convection−diffusion equation based on Cattaneo's law. Computer Methods in Applied Mechanics and Engineering 196, 1757−1766.
Gorla, R.S.R., Pop, I., Lee, J.K., 1992. Convective wall plume in power-law fluid: second-order correction for the adiabatic wall. Warme-und Stoffubertragung 27, 473−479.
Hady, F.M., 1995. Mixed convection boundary-layer flow of non-Newtonian fluids on a horizontal plate. Applied mathematics and Computation 68, 105−112.
Han, S.H., Zheng, L.C., Li, C.R., Zhang, X.X., 2014. Coupled flow and heat transfer in viscoelastic fluid with Cattaneo−Christov heat flux model. Applied Mathematics Letters 38, 87−93.
Henry, B.I., Langlands, T.A.M., 2008. Fractional cable models for spiny neuronal dendrites. Physical Review Letters 100, 128103.
Hossain, M.A., Munir, M.S., Pop, I., 2001. Natural convection with variable viscosity and thermal conductivity from a vertical wavy cone. International Journal of Thermal Science 40, 437−443.
Hossain, M.A., Munir, M.S., Rees, D.A.S., 2000a. Flow of viscous incompressible fluid with temperature dependent viscosity and thermal conductivity past a permeable wedge with uniform surface heat flux. International Journal of Thermal Science 39, 635−644.
Hossain, M.A., Munir, M.S., Takhar, H.S., 2000b. Natural convection flow of a viscous fluid about a truncated cone with temperature dependent viscosity and thermal conductivity. Acta Mechanica 140, 171−181.
Howell, T.G., Jeng, D.R., De Witt, K.J., 1997. Momentum and heat transfer on a continuous moving surface in power law fluid. International Journal of Heat and Mass Transfer 40, 1853−1861.
Huang, F., Liu, F., 2005. The time fractional diffusion equation and the advection-dispersion equation. The Anziam Journal 46, 317−330.
Iomin, A., 2005. Superdiffusion of cancer on a comb structure. Journal of Physics: Conference Series 7, 57−67.
Iomin, A., 2006. Toy model of fractional transport of cancer cells due to self-entrapping. Physical Review E 73, 061918.
Iomin, A., 2013. Fractional kinetics of glioma treatment by a radio-frequency electric field. The European Physical Special Topics 222, 1875−1884.
Iomin, A., Baskin, E., 2005. Negative superdiffusion due to inhomogeneous convection. Physical Review E 71, 061101.
Iomin, A., Méndez, V., 2013. Reaction-subdiffusion front propagation in a comblike model of spiny dendrites. Physical Review E 88, 012706.
Irvine, T.F.J., et al., 1988. Symposium on Fundamentals of Forced Convection Heat Transfer, vol. 101. ASME Publ. HTD, pp. 123−127.
Jamil, M., Zafar, A.A., Rauf, A., Khan, N.A., 2012. New exact analytical solutions for helical flows of second grade fluids. Communications in Nonlinear Science and Numerical Simulation 17, 141−153.

Jayanthi, S., Kumari, M., 2007. Effect of variable viscosity on non-Darcy free or mixed convection flow on a vertical surface in a non-Newtonian fluid saturated porous medium. Applied Mathematics and Computation 186, 1643–1659.

Kármán, T., 1921. Uber laminare und turbulente reibung. ZAMM-Zeitschrift fur Angewandte Mathematik und Mechanik 1, 233–252.

Kays, W.M., 1966. Convective Heat and Mass Transfer. McGraw-Hill, New York.

Khan, M., Ali, S.H., Qi, H.T., 2009. Exact solutions for some oscillating flows of a second grade fluid with a fractional derivative model. Mathematical and Computer Modelling 49, 1519–1530.

Khan, M., Arshad, M., Aujum, A., 2012. On exact solutions of Stokes second problem for MHD Oldroyd-B fluid. Nuclear Engineering and Design 243, 20–32.

Kim, S.C., 1995. Graetz problem solutions for a modified power law fluid over a wide range of shear rate. The Korean Journal of Rheology 7, 35–41.

Kumari, K., Pop, I., Takhar, H.S., 1997. Free-convection boundary-layer flow of a non-Newtonian fluid along a vertical wavy surface. International Journal of Heat and Fluid Flow 18, 625–631.

Langlands, T.A.M., Henry, B.I., 2005. The accuracy and stability of an implicit solution method for the fractional diffusion equation. Journal of Computational Physics 205, 719–736.

Lenzi, E.K., Silva, L.R., Tateishi, A.A., Lenzi, M.K., Ribeiro, H.V., 2013. Diffusive process on a backbone structure with drift terms. Physical Review E 87, 012121.

Li, B.T., Zheng, L.C., Zhang, X.X., 2010a. Numerical methods for solving energy equations of dilatant fluid flow. In: The Third International Conference on Computational Sciences and Optimization, Huangshan, Anhui, China, vol. 1, pp. 11–14.

Li, B.T., Zheng, L.C., Zhang, X.X., 2010b. Numerical investigation on heat transfer of power law fluids in a pipe with constant wall temperature. World Congress on Engineering 3, 1864–1866.

Li, B.T., Zheng, L.C., Zhang, X.X., 2010c. Unsteady forced convection heat transfer for power law fluids in a pipe. In: The International Heat Transfer Conference, Washington, DC, USA.

Li, C.R., Zheng, L.C., Zhang, Y., Ma, L.X., Zhang, X.X., 2012. Helical flows of a heated generalized Oldroyd-B fluid subject to a time-dependent shear stress in porous medium. Communications in Nonlinear Science and Numerical Simulations 17, 5026–5041.

Liu, F., Meerschaert, M.M., McGough, R., Zhuang, P., Liu, Q., 2013a. Numerical methods for solving the multi-term time fractional wave equations. Fractional Calculus & Applied Analysis 16, 9–25.

Liu, F., Turner, I., Anh, V., Yang, Q., Burrage, K., 2013b. A numerical method for the fractional Fitzhugh–Nagumo monodomain model. ANZIAM Journal 54, 608–629.

Liu, F., Yang, C., Burrage, K., 2009. Numerical method and analytical technique of the modified anomalous subdiffusion equation with a nonlinear source term. Journal of Computational and Applied Mathematics 231, 160–176.

Liu, F., Zhuang, P., Anh, V., Turner, I., Burrage, K., 2007. Stability and convergence of the difference methods for the space–time fractional advection–diffusion equation. Applied Mathematics and Computation 191, 12–20.

Liu, F., Zhuang, P., Liu, Q., 2015. Numerical Methods of Fractional Partial Differential Equations and Applications. Science Press, China.

Liu, F.W., Yang, Q.Q., Turner, I., 2011. Two new implicit numerical methods for the fractional cable equation. Journal of Computational and Nonlinear Dynamics 6, 1–7.

Liu, L., Zheng, L.C., Liu, F.W., Zhang, X.X., 2016. Anomalous convection diffusion and wave coupling transport of cells on comb frame with fractional Cattaneo-Christov flux. Communications in Nonlinear Science and Numerical Simulations 38, 45–58.

Lynch, V.E., Carreras, B.A., del-Castillo-Negrete, D., Ferreira-Mejias, K.M., Hicks, H.R., 2003. Numerical methods for the solution of partial differential equations of fractional order. Journal of Computational Physics 192, 406–421.

Makinde, O.D., Onyejekwe, O.O., 2011. A numerical study of MHD generalized Couette flow and heat transfer with variable viscosity and electrical conductivity. Journal of Magnetism and Magnetic Materials 323, 2757–2763.

Malekzadeh, P., Moghimi, M.A., Nickaeen, M., 2011. The radiation and variable viscosity eddects on electrically conducting fluid over a vertically moving plate subjuected to suction and heat flux. Energy Conversion and Management 52, 2040–2047.

Malik, M.Y., Hussain, A., Nadeem, S.B., 2013. Layer flow of an Eyring-Powell model fluid due to a stretching cylinder with variable viscosity. Scientia Iranica B 20, 313–321.

Méndeza, V., Iomin, A., 2013. Comb-like models for transport along spiny dendrites. Chaos, Solitons & Fractals 53, 46–51.

Milsaps, K., Polhausen, K., 1952. Heat transfer by laminar flow from a rotating plate. Journal of Aeronautical Sciences 19, 120–126.

Ming, C.Y., Zheng, L.C., Zhang, X.X., 2009. The flow and heat transfer of power-law fluid over a rotating disk. In: Proceedings of the 3rd International Conference on Mechanical Engineering and Mechanics, pp. 1242–1246.

Mitschka, P., 1964. Nicht-Newtonsche Flüssigkeiten II. Drehstromungen Ostwald-de Waelescher Nicht-Newtonscher Flüssigkeiten. Collection of Czechoslovak Chemical Communications 29, 2892–2905.

Mustafa, M., 2015. Cattaneo-Christov heat flux model for rotating flow and heat transfer of upperconvected Maxwell fluid. AIP Advances 5, 047109.

Nazar, M., Fetecau, C., Awan, A.U., 2010. A note on the unsteady flow of a generalized second-grade fluid through a circular cylinder subject to a time dependent shear stress. Nonlinear Analysis-Real World Applications 11, 2207–2214.

Osalusi, E., Side, J., Harris, R., Johnston, B., 2007. On the effectiveness of viscous dissipation and Joule heating on steady MHD flow and heat transfer of a Bingham fluid over a porous rotating disk in the presence of Hall and ion-slip currents. International Communications in Heat and Mass Transfer 34, 1030–1040.

Ostrach, S., 1953. An Analysis of Laminar Free Convection Flow and Heat Transfer about a Flat Plate Parallel to the Direction of the Generating Body Force. NACA Technical Reports Server, 1111.

Pal, D., Mandal, G., 2015. Hydromagnetic convective–radiative boundary layer flow of nanofluids induced by a non-linear vertical stretching/shrinking sheet with viscous–Ohmic dissipation. Powder Technology 279, 61–74.

Podlubny, I., 1999. Fractional Differential Equations. Academic Press, San Diego.

Pop, I., 1993. Boundary layer flow at a three-dimensional stagnation point in power-law non-Newtonian fluids. International Journal of Heat and Fluid Flow 14, 408–412.

Pop, I., Rashidi, M., Gorla, R.S.R., 1991. Mixed convection to power-law type non-Newtonian fluids from a vertical wall. Polymer-Plastics Technology and Engineering Journal 30, 47–66.

Qi, H.T., Guo, X.W., 2014. Transient fractional heat conduction with generalized Cattaneo model. International Journal of Heat and Mass Transfer 76, 535–539.

Qi, H.T., Jiang, X.Y., 2011. Solutions of the space-time fractional Cattaneo diffusion equation. Physica A 390, 1876–1883.

Rao, J.H., Jeng, D.R., De Witt, K.J., 1999. Momentum and heat transfer in a power-law fluid with arbitrary injection/suction at a moving wall. International Journal of Heat and Mass Transfer 42, 2837–2847.

Rashaida, A.A., 2005. Flow of a Non-Newtonian Bingham Plastic Fluid over a Rotating Disk (Ph.D. thesis). University of Saskatchewan.

Rogers, M.H., Lance, G.N., 1960. The rotationally symmetric flow of a viscous fluid in the presence of an infinite rotating disk. Journal of Fluid Mechanics 7, 617–631.

Rundora, L., Makinde, O.D., 2013. Effects of suction/injection on unsteady reactive variable viscosity non-Newtonian fluid flow in a channel filled with porous medium and convective boundary conditions. Journal of Petroleum Science and Engineering 108, 328–335.

Sahoo, B., 2009. Effects of partial slip, viscous dissipation and Joule heating on Von Kármán flow and heat transfer of an electrically conducting non-Newtonian fluid. Communications in Nonlinear Science and Numerical Simulation 14, 2982–2998.

Salem, A.M., 2007. Variable viscosity and thermal conductivity effects on MHD flow and heat transfer in viscoelastic fluid over a stretching sheet. Physics Letters A 369, 315–322.

Samarskii, A.A., 2001. The Theory of Difference Schemes. Marcel Dekker, New York.

Schowalter, W.R., 1960. The application of boundary-layer theory to power-law pseudoplastic fluids: similar solutions. American Institute of Chemical Engineers Journal 6, 24–28.

Seddeek, M.A., 2002. Effects of radiation and variable viscosity on a MHD free convection flow past a semi-infinite flat plate with an aligned magnetic field in the case of unsteady flow. International Journal of Heat and Mass Transfer 45, 931–935.

Smith, G.D., 1985. Numerical Solution of Partial Differential Equations: Finite Difference Methods. Clarendon Press, Oxford.

Sparrow, E.M., Gregg, G.L., 1959. Heat transfer from a rotating disk to fluid of any Prandtl number. Journal of Heat Transfer-Transactions of the ASME 81, 249–251.

Srinivasa, A.H., Eswara, A.T., 2013. Unsteady free convection flow and heat transfer from an isothermal truncated cone with variable viscosity. International Journal of Heat and Mass Transfer 57, 411–420.

Sun, Z.Z., Wu, X.N., 2006. A fully discrete difference scheme for a diffusion-wave system. Applied Numerical Mathematics 56, 193–209.

Tan, W.C., Masuoka, T., 2005a. Stokes' first problem for a second grade fluid in a porous half-space with heated boundary. International Journal of Non-Linear Mechanics 40, 515–522.

Tan, W.C., Masuoka, T., 2005b. Stokes' first problem for an Oldroyd-B fluid in a porous half-space. Physics of Fluids 17, 023101–023107.

Tan, W.C., Masuoka, T., 2007. Stability analysis of a Maxwell fluid in a porous medium heated from below. Physics Letters A 360, 454–460.

Vieru, D., Fetecau, C., Fetecau, C., 2008. Flow of a viscoelastic fluid with the fractional Maxwell model between two side walls perpendicular to a plate. Applied Mathematics and Computation 200, 459–464.

Wang, T.Y., 1995a. Mixed convection from a vertical plate to non-Newtonian fluids with uniform surface heat flux. International Communication in Heat and Mass Transfer 22, 369–380.

Wang, T.Y., 1995b. Mixed convection heat transfer from a vertical plate to non-Newtonian fluids. International Journal of Heat and Fluid Flow 16, 56–61.

Xu, H.Y., Qi, H.T., Jiang, X.Y., 2013. Fractional Cattaneo heat equation in a semi-infinite medium. Chinese Physics B 22, 014401.

Xue, C.F., Nie, J.X., 2009. Exact solutions of the Rayleigh-Stokes problem for a heated generalized second grade fluid in a porous half-space. Applied Mathematical Modelling 33, 524–531.

Zhao, J.H., Zheng, L.C., Zhang, X.X., Liu, F.W., 2016. Unsteady boundary layer natural convection heat transfer of fractional Maxwell viscoelastic fluid over a vertical plate. International Journal of Heat and Mass Transfer 97, 760–766.

Zandbergen, P.J., Dijkstra, D., 1987. Von Karman Swirling flows. Annual Review of Fluid Mechanics 19, 465–491.

Zheng, L.C., Liu, Y.Q., Zhang, X.X., 2011. Exact solutions for MHD flow of generalized Oldroyd-B fluid due to an infinite accelerating plate. Mathematical and Computer Modelling 54, 780–788.

Zheng, L.C., Liu, Y.Q., Zhang, X.X., 2012. Slip effects on MHD flow of a generalized Oldroyd-B fluid with fractional derivative. Nonlinear Analysis RWA 13, 513–523.

Zheng, L.C., Zhang, X.X., Lu, C.Q., 2006. Heat transfer of power law non-Newtonian. Chinese Physics Letters 23, 3301–3304.

Zheng, L.C., Zhang, X.X., Ma, L.X., 2008. Fully developed convective heat transfer for power law fluids in a circular tube. Chinese Physics Letters 25, 195–197.